



Provided by the author(s) and University of Galway in accordance with publisher policies. Please cite the published version when available.

Title	Contributions to practical iris biometrics on smartphones
Author(s)	Thavalengal, Shejin
Publication Date	2016-05-12
Item record	http://hdl.handle.net/10379/5775

Downloaded 2024-05-10T06:03:05Z

Some rights reserved. For more information, please see the item record link above.



Contributions to Practical Iris Biometrics on Smartphones



Shejin Thavalengal

College of Engineering and Informatics
National University of Ireland, Galway

This dissertation is submitted for the degree of
Doctor of Philosophy

Supervisor: Prof. Peter Corcoran

May 2016

“Let every eye negotiate for itself and trust no agent.”

~William Shakespeare, *Much Ado About Nothing*

Table of contents

List of figures	xv
List of tables	xix
Nomenclature	xxi
1 Introduction to Iris Recognition on Smartphones	1
1.1 Smartphones in Our Life	1
1.2 Secure Authentication in Smartphones	2
1.2.1 Biometrics	2
1.3 Objective and Scope of the Work	4
1.4 Contributions of the thesis	4
1.5 Organization of the Thesis	6
2 Background	7
2.1 The Human Eye	7
2.1.1 The Iris of the Human Eye	7
2.2 Iris Recognition	9
2.2.1 Iris Recognition - Baseline system	11
2.3 Mobile Biometrics - How Iris Comes in to the Picture	15
2.3.1 Something User Knows	15
2.3.2 Something User Has	16
2.3.3 Something User Is	16
2.3.4 Why Iris Recognition?	17
2.4 Iris Recognition: Challenges	18
2.5 Iris Recognition on Smartphones: A Literature Review	22
2.6 Summary	26

3	Current Smartphones and Iris Recognition	29
3.1	Smartphone Case Study	29
3.1.1	Optical Analysis	30
3.1.2	Equivalent Pixel Dimensions and Optical Resolution	32
3.1.3	Diffraction Limit Calculation	32
3.1.4	Considerations for Infrared Imaging	33
3.2	Smartphone Visible Iris Recognition	34
3.2.1	MICHE Database	34
3.2.2	Evaluation of Existing Smartphone Iris Recognition Techniques	34
3.3	Discussion and Conclusions	38
4	Iris Authentication in Smartphones: Considerations for Constraint Free Acquisition	39
4.1	Iris Image Quality Requirements	40
4.1.1	Iris Image Size and Quality	40
4.1.2	Other Relevant Image Quality Parameters	40
4.2	Proof-of-Concept Tests	41
4.2.1	Test Databases	42
4.2.2	Test Algorithm	44
4.2.3	Impact of Spatial Resolution	44
4.2.4	Impact of Blur Induced by the Acquisition Device	48
4.3	Acquisition System Requirements	52
4.3.1	Acquisition Process: Wavelength and Illumination	54
4.3.2	Acquisition Process: Camera	55
4.3.3	Face and Eye Tracking, Focus and Exposure	59
4.3.4	Iris Analysis and Authentication: Preprocessing	59
4.3.5	Iris Analysis and Authentication: Main Processing	60
4.3.6	Iris Analysis and Authentication: Security	60
4.4	Discussions and Conclusions	60
5	Proof-of-Concept and Evaluation of a Dual Function Visible/NIR Camera for Iris Authentication on Smartphones	63
5.1	Dual Function RGB NIR Camera for Smartphones	64
5.1.1	Sensor	64
5.1.2	Filters	65
5.1.3	Illumination	66
5.2	System Dataflow	67

5.2.1	Frame Grabber	67
5.2.2	Image Resampling Module	69
5.2.3	RGB ISP	69
5.2.4	Iris Recognition Module	70
5.3	Optical Analysis of the Prototype Device	70
5.3.1	Equivalent Pixel Dimensions and Optical Resolution	71
5.3.2	Modulation Transfer Function of Diffraction Limited System	72
5.3.3	Diffraction Limit Calculation	74
5.4	Data Acquisition and Iris Recognition Experiments	75
5.4.1	Analyses and Observations	75
5.5	Summary and Conclusions	80
6	Iris Liveness Detection for Next Generation Smartphone Biometrics	83
6.1	Iris Liveness Detection: A Brief Overview	83
6.2	Liveness Detection on Smartphones	84
6.3	Proposed Liveness Detection Process	85
6.3.1	RGB-NIR image acquisition	85
6.3.2	Multispectral Feature Extraction	87
6.3.3	Intermediate Decision Making	87
6.3.4	Multi-Frame Pupil Localization	91
6.3.5	Pupil Analysis	92
6.3.6	Decision Making	93
6.4	Conclusions	95
7	Iris Pattern Obfuscation in Digital Images	97
7.1	Introduction	97
7.1.1	Next Generation Camera in our life	99
7.1.2	The Elephant in the Room - Personal Images	100
7.2	Iris Pattern Obfuscation	101
7.2.1	Vertical Flipping	101
7.2.2	Radial Blurring	102
7.2.3	Sector Swapping	103
7.2.4	Quadrant Interchanging	104
7.2.5	Iris Replacing	105
7.3	Experiments and Analysis	108
7.4	Challenges in Implementing Iris Pattern Obfuscation	110
7.4.1	Undetectable modification of Eye Regions	112

7.4.2	Robust detection of ‘At-Risk’ Eye Regions	112
7.4.3	Real Time Implementation	114
7.5	Conclusion	114
8	Conclusions and Future Work	115
8.1	Conclusions	115
8.2	Future Work	117
	References	119
	Appendix A Performance Metrics of Biometric Systems	133
A.1	Functions of a General Biometric Systems	133
A.2	Biometric Performance Metrics	133
A.3	Performance Evaluation of Liveness Detection System	136

Declaration

I hereby declare that except where specific reference is made to the work of others, the contents of this dissertation are original and have not been submitted in whole or in part for consideration for any other degree or qualification in this, or any other university. This dissertation is my own work and contains nothing which is the outcome of work done in collaboration with others, except as specified in the text and Acknowledgements. This dissertation contains fewer than 80,000 words including appendices, bibliography, footnotes, tables and equations and has fewer than 150 figures.

Shejin Thavalengal
May 2016

Acknowledgements

Somewhere I read that it would be better to eschew an acknowledgments page altogether and give the people I want to thank a bottle of wine and a copy of the thesis. But, I think, it is fair to write a comprehensive acknowledgement here rather than buying a plethora of wine bottles and cutting down a lot of trees to print this thesis.

I have been lucky to have a wonderful PhD advisor Prof. Peter Corcoran, who made my path smooth, fruitful and memorable. He influenced my graduate career in an ineffably positive way. He has been supportive since the day I sent him an email about PhD opportunities with him. He is funny, lively, enthusiastic, energetic, and a great company. Thanks Peter, for all the help, all the fun and for not letting ‘the schooling interfere with my education’.

My heartfelt gratitude to Alexandru Drimborean, my manager at FotoNation, for taking me as a part of the FotoNation family and involving me in some exciting projects. Alex’s thoughtful guidance and constructive criticism played a very important role in my work.

I am forever indebted to Professor Christopher Dainty for his constant feedback on my work and proof reading my thesis. Also, I gained a lot from his vast knowledge in the field of optics. Chris was a patient listener even when I went to him with the craziest ideas one can imagine.

I would like to thank Dr Petronel Bigioi for his feedback on my work. I also had the privilege of serving as a teaching assistant for him. Thanks to Dr. Alexander Goncharov for the Advanced Optics lecture at NUIG.

A vote of gratitude to Sharon Cheevers, for making my transition from India to Ireland very smooth and helping me settle down here. I have no idea how I would manage all that without her help.

Thanks to Sudhi Sathyavathi for being a friend. All the jokes we shared, all the discussions we had in Malayalam, made me feel home. I would like to thank Sathish Mangapuram for his tips and tricks, throughout his time in FotoNation. A special thanks to Colm Lynch, for being a great colleague and for introducing me to the Indian community in NUIG.

I thank the many colleagues and friends I have in FotoNation: Gavin McGranaghan, Istvan Andorko, Pat Fortune, Serghei Carateev, Paweł Filipczuk, Mariusz Mądry, Dan East, Anne Rumpf, Cormac Britton, Rafael Campos, Raphael Teyseyre, Ilariu (Lale) Raducan,

Ruxandra Vranceanu and Razvan G. Condorovici. Sorry Pat, I could not come to the majority of your gigs.

I would be remiss if I did not thank my friends at C3I - Hossein Javednia, Claudia Costache, Adrian Unguranu, Anuradha Kar, Asma Khatoon, Niamh Fitzgerald, and Timothee Cognard.

I am thankful for having two wonderful housemates - Dean Mitchell and Olina Štěpánková. You guys are amazing. A special thanks to Daniel Czerwiec for all his help during my first few days in Galway.

I am blessed to have created a diverse and adorable circle of friends. Special thanks to Antonino Vespoli, Tudor Nedelcu and Shabab Bazrafkan for all the parties and the good time. Without you, the lunchtime will be irksome. Thanks Tudor for all the help with various tests I carried out at FotoNation.

A big thank you to Pinaki DasGupta, Prathamesh Dhanpalwar and Roshan Dsouza. Those times we cooked together, played cards and went bowling were some of the best times I had here. The numerous trips we had both inside and outside of Ireland were truly incredible. A vote of gratitude to Arun Thirumaran, Anish Kumar, Vijay Ragavan and Chansha Dawood, the Christmas of 2013 could have been depressing without you guys.

I must also acknowledge all my lovely friends in Galway, especially Ananya Shivanand, Edha Jain, Sandesh Rao, Dilip Thomas, Mangesh Morey and Migle Makelyte. Thank you guys!

I am extremely grateful to Leonie Esters, for making me appreciate my life, for the long walks, for the coffee evenings, for the dinners and movie nights. If I list all the wonderful things we had, this space will not be enough.

Special thanks to Ana Filipa for the wonderful time we spent together, for some of the best trips I had in my life, for introducing me to ‘francesinha’ and for trying to teach me Portuguese, *minha linda*.

And above everything, throughout the entire journey, I have benefitted immensely from the support of my family. Thanks to my mom, for her unconditional love, and for not emotionally blackmailing me in to a big fat Indian wedding, yet.

I would like to acknowledge Irish Research Council’s employment based PhD program for the generous funding for my PhD.



Abstract

This thesis investigates the practical adaption of iris biometrics on smartphones. Iris recognition is a mature and widely deployed technology which will be able to provide the high security demanded by next generation smartphones. Practical challenges in widely adopting this technology on smartphones are identified. Based on this, a number of design strategies are presented for constraint free, high performing iris biometrics on smartphones. A prototype, smartphone form factor device is presented to be used as a front-facing camera. Analysis of its optical properties and iris imaging capabilities shows that such a device with improved optics and sensors could be used for implementing iris recognition in the next generation of smartphones. A novel iris liveness detection is presented to prevent spoofing attacks on such a system. Also, the social impact of wider adoption of this technology is discussed. Iris pattern obfuscation is presented to address various security and privacy concerns which may arise when iris recognition will be a part of our daily life.

List of figures

1.1	Various biometric modalities	3
1.2	Example of an iris of the human eye.	3
2.1	Schematic of the human eye: tranverse section os the left eyeball	8
2.2	Human iris: Front view and composite drawing of the surfaces and layers of the iris.	10
2.3	Overview of an iris recognition system following Daugman’s approach. . .	11
2.4	Example of RGB and NIR iris image pairs	12
2.5	Summary of Clarke <i>et al.</i> ’s work	16
2.6	Which combination of authentication techniques users prefer.	17
2.7	Example of traditional iris acquisition device.	19
2.8	Examples of image acquisition using middle distance device	20
2.9	Iris On the Move System	21
2.10	Examples of long range iris acquisition devices	22
2.11	Samsung SPH-S2300 mobile phone	23
2.12	Samsung SPH-S2300 mobile phone used in Park <i>et al.</i> ’s work	24
2.13	OKI iris solution	24
2.14	‘Eye cup’ with a luminous diode attached to a Sony Ericsson P800 to capture iris images with uniform illumination and stand-off distance	25
2.15	AOptix Stratus	26
2.16	World’s first smartphone with iris recognition	27
3.1	A typical smartphone user authentication scenario	30
3.2	Optical analysis parameters	31
3.3	Smartphone case study: Modulation transfer function at 250mm stand off distance.	33
3.4	Examples of images from the MICHE database.	34
4.1	Examples of images from CASIA v4 Distance and MMU1 databases. . . .	43

4.2	Outline of OSIRIS reference system.	45
4.3	ROC Curves for CASIA v4 interval and MMU1 databases for different number of pixels across iris diameter.	46
4.4	Iris recognition performance for different databases as a function of effective number of pixels across iris diameter.	47
4.5	Performance Curves for CASIA v4 interval and MMU1 databases for different defocus blur.	49
4.6	Examples of images with different defocus blur.	50
4.7	Examples of images with different motion blur.	50
4.8	Performance curves for CASIA v4 interval and MMU1 databases for different length of camera motion.	51
4.9	Performance curves for CASIA v4 interval and MMU1 databases for different levels of blur during enrollment and authentication.	53
4.10	Flow diagram of the proposed smartphone iris recognition system.	54
4.11	Wilde's iris image acquisition device.	56
4.12	Iris image acquisition device presented by Cambier and Siedlarz.	57
4.13	Iris acquisition on smartphones: Dual camera system - one camera for general purpose use such as video call and one dedicated iris camera for iris acquisition; and hybrid front facing camera	58
4.14	Summary of primary design considerations for smartphone iris acquisition device.	61
5.1	Example for colour filter arrays	64
5.2	Transmittance curve of the filter used in the proof-of-concept device.	66
5.3	A typical eye image captured using the prototype device.	67
5.4	The prototype device	68
5.5	System overview of the proof-of-concept device.	69
5.6	Ideal system modulation transfer function plot for 200mm stand-off distance.	73
5.7	Modulation transfer function plot for 200mm stand-off distance.	74
5.8	Examples of iris images captured using the prototype device	75
5.9	ROC curves for 15cm and 20cm stand-off distances.	76
5.10	Score distribution for 15cm and 20cm stand-off distances.	76
5.11	Performance comparison between full image set and image set with improved iris segmentation for 15cm and 20cm stand-off distance.	77
5.12	Score distribution comparison for 15cm stand-off distance.	78
5.13	Score distribution comparison for 20cm stand-off distance.	78

6.1	Workflow of the proposed liveness detection technique.	86
6.2	Different test scenarios on the proposed liveness detection system	89
6.3	RGB-NIR image pairs in the database	90
6.4	Pupil localization Process	93
6.5	Pupil analysis	94
6.6	Binary decision tree used for classifying the input image	95
7.1	Example for vertical flipping technique for iris pattern obfuscation	102
7.2	Example of radial blurring for iris pattern obfuscation	102
7.3	Example for Sector Swapping technique for iris pattern obfuscation	103
7.4	Various stages of quadrant interchanging technique for iris pattern obfuscation	105
7.5	Example for iris detail images for a particular scale.	106
7.6	Example for quadrant interchanging technique	106
7.7	Example for iris replace technique for iris pattern obfuscation	107
7.8	Example for different iris obfuscation techniques on CASIA database.	109
7.9	Results of iris pattern obfuscation experiments.	111
7.10	Examples for obfuscation	113
A.1	An overview of enrollment, verification, and identification tasks of a biometric system.	134
A.2	An overview of the outcome of a biometric verification system.	135
A.3	Receiver operating characteristics curve	136

List of tables

2.1	ISO image acquisition requirements.	19
3.1	Camera specifications.	30
3.2	Summary of various acquisition parameters of the MICHE subset.	35
3.3	Equal error rate (%) for various iris recognition schemes on MICHE subset.	37
3.4	Comparison of segmentation accuracy (in %) in MICHE subset.	37
5.1	System parameters.	66
5.2	Summary of optical analysis for different stand-off distances.	74
5.3	Comparison of iris image quality scores on different databases. Larger the score, better the quality of the image.	79
7.1	An example for quadrant interchange operator for different scales.	105
7.2	An example for w^k, w_s^k selection for different scales.	106
7.3	Comparison results of images shown in Figure 7.8.	108

Nomenclature

Acronyms / Abbreviations

APCER Attack Presentation Classification Error Rate

CCD Charge Coupled Device

CFA Colour Filter Array

CMOS Complementary Metal-Oxide Semiconductor

eDoF extended Depth of Field

EER Equal Error Rate

FAR False Acceptance Rate

FN False Negatives

FoV Field of View

FP False Positives

FRR False Rejection Rate

HD Hamming Distance

HDR High Dynamic Range

IEC International Electrotechnical Commission

IOM Iris on the Move

IR Infra-Red

ISO International Organization for Standardization

ISP Image Signal Processor

MID-BPR Mobile ID Device-Best Practice Recommendation

MTF Modulation Transfer Function

NIR Near Infra-Red

NIST National Institute of Standards and Technology

NPCER Normal Presentation Classification Error Rate

PCB Printed Circuit Board

PIN Personal Identification Number

RGB Red Green Blue (visible spectrum)

ROC Receiver Operating Characteristics

TAR True Acceptance Rate

TN True Negatives

TP True Positives

Chapter 1

Introduction to Iris Recognition on Smartphones

1.1 Smartphones in Our Life

A ‘Smartphone’ is defined as *a mobile phone that can be used as a small computer and that connects to the internet* [1]. Even though the first smartphone - IBM Simon - was introduced more than two decades ago, the world witnessed an immense evolution of smartphones after the introduction of the first iPhone in 2007 [2]. The current smartphones we carry in our pocket are not only a computer, a phone, a database, an infinite jukebox, a camera, a locator and have all the information in the world at our fingertips, but also a personal companion which is a part of our daily life [3]. It is speculated that the smartphone’s role as a constant companion, helper, coach and guardian has only just begun [4].

Two-thirds of U.S. adults own a smartphone in the year 2015. Among these users, 46% noted that they cannot live without a smartphone [5], which makes these devices truly a national obsession [6]. The world population is also following a similar pattern in smartphone use. It is predicted that approximately 2 billion people will be using smartphones in 2016. This number is expected to grow to a third of the world’s population in 2018 [7].

It may not be surprising to note that, for U.K. smartphone users, making phone calls is only the fifth most popular use of the device [8]. The majority of smartphones are connected to the internet all the time. Fifty seven percent of U.S. smartphone users are reported to do online banking through these devices [5]. Unlike the PCs and laptops, the smartphone is a very personal device, where users store their personal data, passwords, health information, financial transactions, daily calendars and to do list and much more [9]. Hence, secure authentication of a smartphone user’s identity is crucial.

1.2 Secure Authentication in Smartphones

Smartphones are an important part of our daily life, and carry very sensitive information. This raises a haunting question: how secure are these devices? The European Union Agency for Network and Information Security (ENISA) reported a number of smartphone security risks which includes data leakage and financial malware attacks [10]. The two most common user authentication techniques in smartphones are touch screen pattern and passwords. While touch screen patterns are convenient, oily residues (or smudges) on the screen can be used for inferring the pattern successfully [11, 12]. On the other hand, the usual 4 character password with a 90 character U.S. keyboard will have only 90^4 combinations. Remembering a large number of strong passwords and entering them several times a day whenever the user has to access his smartphone or related services is tiresome. This led to a situation where three in ten smartphone users do not keep a password on their smartphones or reuse the same password for various other applications [13, 14]. Reusing the password opens up to the vulnerabilities of causing catastrophic damages when password at one location is compromised. Hence, in order to balance the security needed by these smartphones with the user convenience, there should be a mechanism to authenticate the users continuously with something which the user is or what user does. This trait should be unique to each individual and should not be easy to steal or mimic. 'Biometrics' could be ideal for this purpose.

1.2.1 Biometrics

Biometrics can be defined as the process of recognizing individuals based on their physiological or behavioral traits [15]. Any physiological or behavioral traits which satisfy a number of requirements such as universality, distinctiveness, permanence, collectibility, performance, acceptability, and circumvention can be classified as a practical biometric trait [15]. Face, voice, fingerprint, iris, palm geometry are some of the most common examples. A brief comparison of these modalities is shown in Figure 1.1 [15].

Iris Recognition

Iris recognition is the method of recognizing individuals based on their iris pattern. Iris of the human eye is the annular region between the pupil and sclera, and controls the amount of incident light on retina. An example of an iris image is shown in Fig. 1.2.

As it can be observed from the Figure 1.1, iris is a biometric modality with high distinctiveness, permanence and performance. There are a number of other characteristics which make iris a promising candidate for a biometric solution in next generation smartphones:





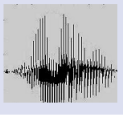
BIOMETRIC	FINGERPRINT	FACE	HAND GEOMETRY	IRIS	VOICE
					
Barriers to universality	Worn ridges; hand or finger impairment	None	Hand impairment	Visual impairment	Speech impairment
Distinctiveness	High	Low	Medium	High	Low
Permanence	High	Medium	Medium	High	Low
Collectibility	Medium	High	High	Medium	Medium
Performance	High	Low	Medium	High	Low
Acceptability	Medium	High	Medium	Low	High
Potential for circumvention	Low	High	Medium	Low	High

Fig. 1.1 Various biometric modalities [15]. Copyright ©2003, IEEE.

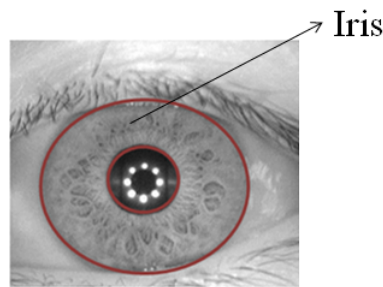


Fig. 1.2 Example of an iris of the human eye. Image is from CASIA V4 iris database [16].

1. The iris pattern consists of complex and distinctive ligaments, furrows, ridges, rings, corona, freckles and collarette, which makes it rich in texture [17].
2. Iris is relatively stable during adulthood of a person [17–20].
3. Irises have high pattern variability, even for identical twins and between the left and right eye of the same person [17].
4. Iris is an internal, yet externally visible organ.
5. It is extremely difficult to surgically spoof the iris.
6. Iris recognition is a widely deployed and a mature technology in specialist recognition system.

1.3 Objective and Scope of the Work

The objective of this work is to provide a practical iris recognition solution for user authentication in next generation smartphones. Being a contact-less, near ideal biometric, iris recognition is an appealing candidate for providing the security required by these devices. Even though iris recognition technology is mature and widely deployed- especially in access control, national-ID programs and border control, iris recognition on smartphones did not make an impact yet. This is partly due to the market demand for an unconstrained and easy to use iris recognition system and the challenging nature of acquiring suitable high quality images using current smartphones. This work is in pursuit of quantifying and addressing some of these challenges and providing the consumer industry with smartphones equipped with an easy to use, highly sophisticated user authentication by iris recognition.

1.4 Contributions of the thesis

The main contributions of this thesis can be summarized as follows:

1. A state of the art literature review and a detailed analysis on the use of existing smartphones for iris recognition is carried out to provide context for the main work presented in this thesis.
2. Various design considerations for a practical iris recognition solution on smartphones were proposed. These are more holistic than the existing works, taking account of system optics, required image quality, and multi-wavelength acquisitions, and address the potential use of hybrid visible/NIR sensors.
3. A proof-of-concept smartphone form factor device is presented and analysed as a practical solution. This proof-of-concept has been further developed by a team of engineers in the industry sponsor to realize a pre-commercial prototype.
4. A novel iris liveness detection technique is proposed to be used with the presented device. The approach presented here incorporates liveness detection into the acquisition work-flow. A patent application has been filed on this technique.
5. Iris pattern obfuscation in digital images is introduced as a preventive measure to address various privacy related concerns which may arise with a wider adoption of this technology in consumer market. This technology could be applied to all images 'in-camera' during the acquisition process in the same way that today's digital images are automatically corrected for red-eye effect when a flash is used.

List of Publications Related to the thesis

The work presented in this thesis resulted in the following journal papers:

1. Shejin Thavalengal, Istvan Andorko, Alexandru Drimbarean, Petronel Bigioi and Peter Corcoran, “Proof-of-concept and evaluation of a dual function visible/NIR camera for iris authentication in smartphones”, *IEEE Transactions on Consumer Electronics*, vol.61, no.2, pp.137,143, May 2015.
2. Shejin Thavalengal, Petronel Bigioi and Peter Corcoran, “Iris authentication in hand-held devices - considerations for constraint-free acquisition”, *IEEE Transactions on Consumer Electronics*, vol.61, no.2, pp.245,253, May 2015.
3. Shejin Thavalengal and Peter Corcoran, “Iris Liveness Detection for Smartphones”, *under review*.

Two conference papers were published in high impact biometrics conference proceedings and one of them was referenced in IEEE biometrics virtual journal - *IEEE Biometrics Compendium*:

1. Shejin Thavalengal, Petronel Bigioi and Peter Corcoran, “Evaluation of Combined Visible/NIR Camera for Iris Authentication on Smartphones”, in Proceedings of the *2015 Computer Vision and Pattern Recognition (CVPR 2015) Biometric Workshop*, Jun.2015, Boston, USA.
2. Shejin Thavalengal, Ruxandra Vranceanu, Razvan G. Condorovici and Peter Corcoran, “Iris Pattern Obfuscation in Digital Images”, in Proceedings of the *International Joint Conference on Biometrics (IJCB 2014)*, Sept.2014, Florida, USA. (Referenced in *IEEE Biometrics Compendium*, issue 20, July 2015.)

A number of conference papers are also published based on this work:

1. Peter Corcoran, Petronel Bigioi and Shejin Thavalengal, “Feasibility and Design Consideration for an Iris Acquisition System for Smartphones”, in Proceedings of the *4th IEEE International Conference on Consumer Electronics - Berlin (ICCE-Berlin 2014)*, Sept.2014, Berlin, Germany.
2. Shejin Thavalengal, Petronel Bigioi and Peter Corcoran, “Efficient Segmentation for Multi-frame Iris Acquisition on Smartphones”, in Proceedings of the *2016 IEEE International Conference on Consumer Electronics (ICCE)*, Jan.2016, Las Vegas, USA.

3. Shejin Thavalengal and Peter Corcoran, “A Practical Challenge for Iris Authentication on Handheld Imaging Devices”, in Proceedings of the *2015 IEEE International Conference on Consumer Electronics (ICCE)*, Jan.2015, Las Vegas, USA.
4. Shejin Thavalengal and Peter Corcoran, “Iris Recognition on Consumer Devices - Challenges and Progress”, in Proceedings of the *2015 IEEE International Symposium on Technology in Society (ISTAS)*, Nov.2015, Dublin, Ireland.

Also, a patent disclosure is filed on the topic “Iris Liveness Detection for Next Generation Smartphone Biometrics. ”

1.5 Organization of the Thesis

The rest of the thesis is organized as follows: **Chapter 2** presents an extensive overview of iris authentication on smartphones and related literature.

In **Chapter 3**, feasibility of the existing smartphones for iris recognition is analysed. A state of the art smartphone camera is analysed both in terms of its optical quality and spatial resolution. Also, performance of the existing state of the art iris recognition algorithms on an iris image database captured using smartphones are evaluated.

Chapter 4 presents various challenges that directly affect the design of an unconstrained iris recognition system on smartphones, especially the acquisition device. The acquisition framework, associated workflows and key challenges in successfully implementing iris authentication in the unconstrained use case for a handheld imaging device were outlined here along with various prospective design strategies.

Based on the analyses in Chapter 4, **Chapter 5** introduces a hybrid camera for smartphone iris authentication. The feasibility of this device to provide a high performing iris recognition on smartphones is examined.

A novel iris liveness detection is presented in **Chapter 6**. This technique is designed to determine if the biometric being captured by the device presented in Chapter 5 is an actual measurement from a live person who is present at the time of image acquisition.

Chapter 7 considers the problem of theft of iris features from personal photographs and videos that may come in to play when iris recognition is widely adopted on consumer devices. A potential solution - iris pattern obfuscation is presented. Various iris pattern obfuscation techniques are presented and challenges in practical implementation are analysed.

Summary and conclusion of the thesis is presented in **Chapter 8** with a discussion of further directions for work in this area. Also, **Appendix A** gives an overview of the various performance metrics used in this thesis.

Chapter 2

Background

This chapter provides background information on iris recognition on smartphones and a review of related research. The initial section briefly describes the anatomy of the human eye and structure of the human iris. An introduction to iris recognition is given in the next section. A detailed description on existing smartphone user authentication techniques and how iris recognition fits in there is given. This is followed by the challenges in adapting the existing iris recognition techniques for smartphones and other consumer devices. Literature on iris recognition in smartphones are highlighted.

2.1 The Human Eye

The human eye - a very remarkable sensory organ - is that globular part of the human body through which we gather visual information about the external environment. A schematic drawing of the human eye is shown in Figure 2.1. The anterior portion of the eye consists of cornea, iris, pupil and crystalline lens. While the pupil acts as an aperture, iris serves as a diaphragm which regulates the amount of light entering the eye. The cornea is a transparent, convex region which covers iris and pupil. The crystalline lens and cornea are responsible for the formation of optical image on the retina [22].

2.1.1 The Iris of the Human Eye

Iris of the human eye is located behind the cornea and aqueous humour and in front of the crystalline lens. Iris is the only internal organ which is externally visible normally [23]. Iris is generally composed of four different layers [22]:

1. *The anterior border layer*: This layer consist of fibroblasts and crypts of Fuchs. For individuals with dark coloured iris, this layer contains pigment granules.

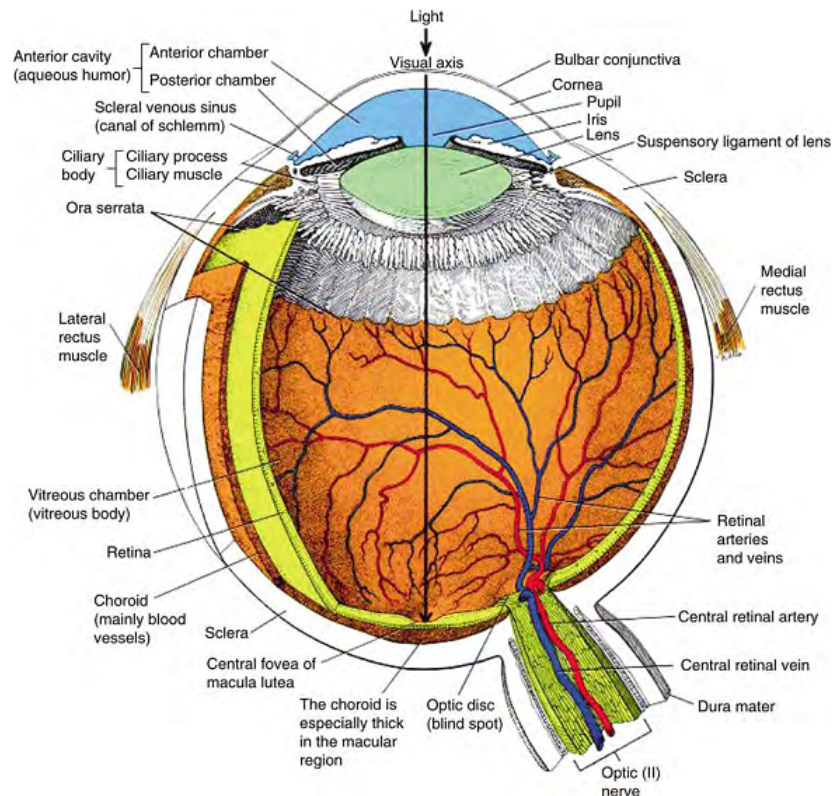


Fig. 2.1 Schematic of the human eye: A transverse section of the left eyeball. Adapted from [21].

2. *The stroma iridis* consists of collagen fibers. The majority of these fibers radiate towards pupil which forms an interwoven structure. The sphincter pupillae muscles in the stromal layer near pupil regulate pupil constrictions. These muscles cause the contraction furrows in the iris.
3. *The anterior epithelium* contains the dilator pupillae muscles which are arranged in a radial pattern.
4. *The posterior epithelium* surface is covered by two layers of pigmented columnar epithelium. This layer is the main light absorber in the iris.

The colour of the iris is defined by the number and the situation of the pigment cells. In the albino, pigment is absent. Various shades of blue irises have pigment cells confined to the posterior epithelium, while gray, brown and black eyes have pigment cells in the stroma iridis and the anterior border layer [24].

The iris surface is divided into two zones - (i) inner pupillary zone and (ii) outer ciliary zone. These two layers are separated by a sinuous structure called collarette [22]. The

pigment related iris features includes Wöflin spots, iris freckles, pigment frill, crypts of Fuchs and small crypts in the periphery of iris, iris sphincter, contraction furrows, radial furrows and Schwalbe's contraction folds. These complex iris features are depicted in Figure 2.2.

The structural features of iris contribute to a highly detailed iris pattern with high pattern variability -even between the left and right eye of the same individual. Also, iris is an epigenetic trait, that is, the iris pattern is not genetically determined. Even monozygotic twins have uncorrelated iris patterns, at least from the algorithmic point of view [23, 25].

2.2 Iris Recognition

Iris recognition is the process of recognising a person by analysing his complex iris pattern presented in section 2.1.1. Compared to other biometric traits such as face or fingerprints, the use of iris recognition is relatively new. Major iris recognition milestones can be summarized as follows:

- Iris as a biometric trait was originally proposed by the ophthalmologist Burch in 1936 [22].
- Flom and Safir patented the general concept of iris recognition in 1987 [26].
- In 1989 John Daugman developed an efficient algorithm for analyzing iris pattern for biometrics. The patent was granted in 1994 [27].
- 1995 witnessed first commercial iris recognition systems [28].
- In 2003, UAE border system began using iris recognition for verifying passenger identity [29].
- In 2005, Iris on the Move - an unconstrained iris recognition system which is capable of carrying out iris recognition even when the users are walking at a steady pace through the system - was introduced by Sarnoff [30]. The same year witnessed first National Institute of Standards and Technology (NIST) iris evaluation.
- In 2009, India initialized AADHAAR program aiming to provide Unique ID (UID) for its citizens. Iris is one of the primary biometric modalities being used in this large scale project [31].
- In 2011 Daugman's patent expired, which opened up the iris recognition market.

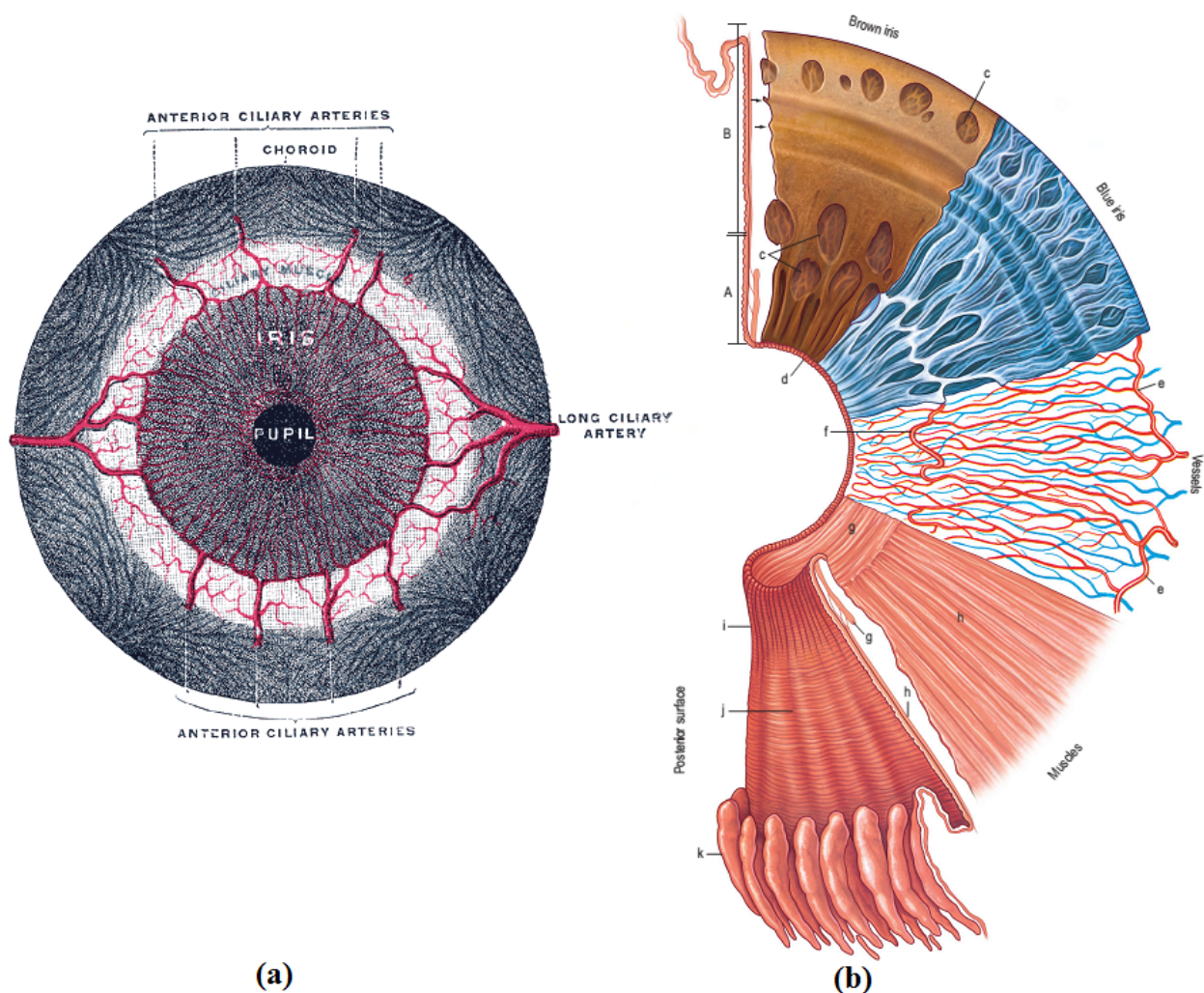


Fig. 2.2 Human iris: (a) Iris front view. (b) Composite drawing of the surfaces and layers of the iris. Beginning at the upper left and proceeding clockwise, the iris cross section shows the pupillary (A) and ciliary portions (B), and the surface view shows a brown iris with its dense, matted anterior border layer. Circular contraction furrows are shown (arrows) in the ciliary portion of the iris. Fuchs' crypts (c) are seen at either side of the collarette in the pupillary and ciliary portion and peripherally near the iris root. The pigment ruff is seen at the pupillary edge (d). A blue iris surface shows a less dense anterior border layer and more prominent trabeculae. The iris vessels are shown beginning at the major arterial circle in the ciliary body (e). Radial branches of the arteries and veins extend toward the pupillary region. The arteries form the incomplete minor arterial circle (f), from which branches extend toward the pupil, forming capillary arcades. The sector below it demonstrates the circular arrangement of the sphincter muscle (g) and the radial processes of the dilator muscle (h). The posterior surface of the iris shows the radial contraction furrows (i) and the structural folds (j) of Schwalbe. Circular contraction folds are also present in the ciliary portion. The pars plicata of the ciliary body is at k. Reprinted with permission from Gray's Anatomy [24].

- Mobile Iris Challenge Evaluation (MICHE) started in 2013 [32] to provide a forum for comparative research on the contributions to the mobile iris recognition field.
- In 2015 NTT DoCoMo introduced first smartphone with iris recognition technology [33].

2.2.1 Iris Recognition - Baseline system

An iris recognition system following Daugman's approach can be described as in Figure 2.3. This system follows the process pipeline as: (i) In the image acquisition step, an iris image is

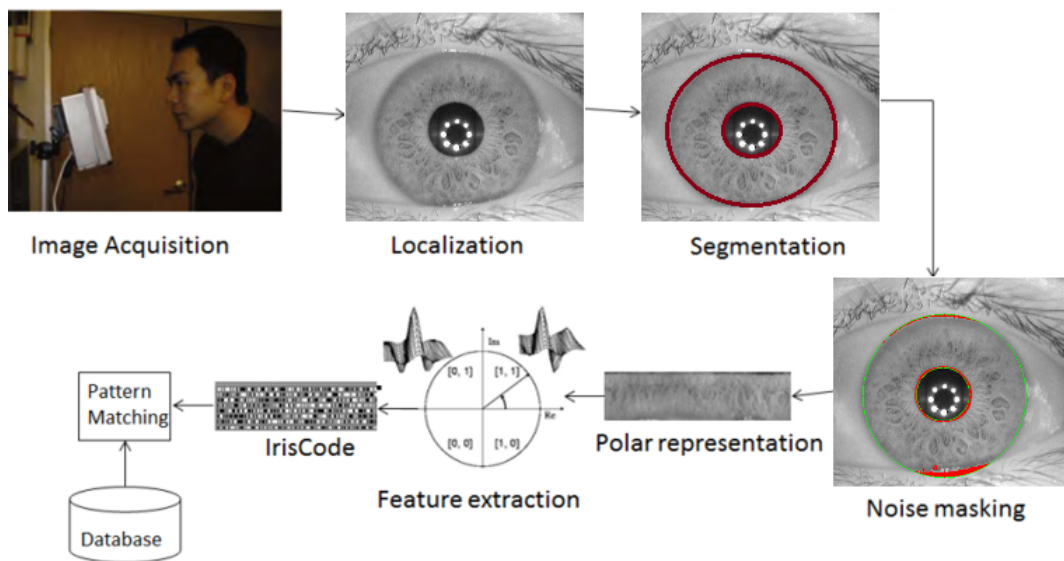


Fig. 2.3 Overview of an iris recognition system following Daugman's approach [17].

acquired using a camera. (ii) Eye/iris region is located in this image followed by isolating the region representing iris. Various noises such as reflections and occlusions due to eyelids and eye lashes were masked. (iii) The iris region is converted in to a doubly dimensionless polar coordinate system. (iv) The feature extraction step derive a representation (a binary representation called IrisCode [17]) of the iris texture that can be used to match two irises. (v) The similarity of two iris representations is evaluated by pattern matching techniques. For a better understanding, each of these stages in a Daugman based system is explained in the following subsections,

Image acquisition

One has to note that, all the commercially deployed iris recognition systems use near infra-red (NIR) imaging (images captured in a wavelength of 700nm-900nm) for iris acquisition [17].

Imaging in NIR region improves identification in individuals with heavily pigmented irises. This can be observed in Figure 2.4, where both light and heavily pigmented iris shows clear iris pattern when image is acquired in NIR illumination.

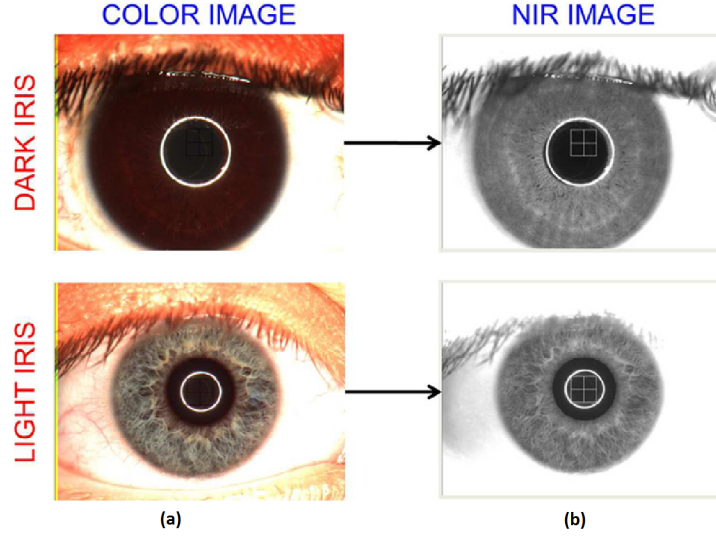


Fig. 2.4 Example of RGB and NIR iris image pairs: (a) RGB eye image, (b) the same eye image captured at NIR wavelength [34]. Copyright ©2015, IEEE.

Also, NIR imaging makes the system robust to anomalous features related to change in pigmentation due to melanomas or tumors, eye drops for glaucoma treatment, which may lead to colouration changes or pigment spots [22]. However, melanin is relatively transparent to near-infrared light, which makes NIR iris acquisition robust to pigment related effects.

Iris Segmentation

Once the eye image is obtained, it has to be segmented to isolate the iris region. Here, the exact iris boundaries at pupil and sclera have to be obtained, the occluding eyelids have to be detected and reflections have to be removed. Daugman's technique uses an integro-differential operator for iris segmentation [17], which is,

$$\max_{(r,x_0,y_0)} \left| G_\sigma(r) * \frac{\partial}{\partial r} \oint_{(r,x_0,y_0)} \frac{I(x,y)}{2\pi r} ds \right|, \quad (2.1)$$

where $I(x,y)$ is the eye image. This integro-differential operator searches over the image domain (x,y) for the maximum in the blurred partial derivative with increasing radius r , of the normalized contour integral of $I(x,y)$ along a circular arc ds of radius r and center coordinates (x_0,y_0) [17]. $G_\sigma(r)$ is the smoothing function and '*' denotes convolution operation. The

whole operator can be considered as ‘exploding circles’. Applying this operator twice, one can obtain the two circular boundaries of iris. After this step, the occluding eyelashes are detected with the help of curvilinear edge detection [17].

There have been several similar techniques for iris segmentation such as the algorithm proposed by Wildes *et al.* [35], Kong *et al.* [36], Tisse *et al.* [37] and Ma *et al.* [38]. (All of these use circular Hough transform for ‘finding the circles’). Another segmentation technique proposed by He *et al.* [39] uses an Adaboost-cascade iris detector and an elastic model named ‘pulling and pushing method’.

Further studies revealed that iris and pupil boundaries are not circular always, and modeling this properly improves the iris recognition performance [40]. Daugman’s follow up work [40] incorporates active contours or ‘snakes’ to model the iris accurately. A similar approach proposed by Shah and Ross [41] uses ‘geodesic active contours’ for accurate iris segmentation.

Once the iris is segmented, the reflections arising due to camera flash, spectacle or lenses and superimposing eyelashes were masked. Daugman approached this by statistically estimating whether the iris pixels follow a multimodal distribution and removing the values in this distribution which are caused by eyelashes [40].

Iris Normalization

Once the iris boundaries are determined, the points between the inner and outer boundary regions are interpolated into a doubly-dimensionless coordinate system. This is done to maintain reference to the same regions of iris tissue regardless of overall iris image size and pupillary constriction. This can be represented as

$$I(x(r, \theta), y(r, \theta)) \rightarrow I(r, \theta), \quad (2.2)$$

with $r \in [0, 1]$ and $\theta \in [0, 2\pi]$. Also, $x(r, \theta)$ and $y(r, \theta)$ are defined as

$$x(r, \theta) = (1 - r)x_p(\theta) + rx_s(\theta), \quad (2.3)$$

$$y(r, \theta) = (1 - r)y_p(\theta) + ry_s(\theta). \quad (2.4)$$

where $(x_p(\theta), y_p(\theta))$ and $(x_s(\theta), y_s(\theta))$ are the set of points between inner and outer boundary of iris respectively.

Feature Extraction

Following normalization, features are extracted from the iris image, which will represent the discriminative texture present in them. The most popular feature extraction technique for the iris images is the use of Gabor filters with different wavelet sizes, frequencies, and orientations on the iris image. This is followed by a phase-quadrant quantization [17] to produce a 2048 bit iris code. This feature extraction technique can be explained mathematically as,

$$h_{\{Re,Im\}} = sgn_{\{Re,Im\}} \int_{\rho} \int_{\phi} I(\rho, \phi) e^{-i\omega(\theta_0-\phi)} e^{-(r_0-\rho)^2/\alpha^2} e^{-(\theta_0-\phi)^2/\beta^2} \rho d\rho d\phi, \quad (2.5)$$

where $h_{\{Re,Im\}}$ is the complex valued bit depending on the sign ($sgn_{\{Re,Im\}}$) of the integral on the right hand side of the Equation 2.5. $I(\rho, \phi)$ is the normalized iris image and α, β, ω are the parameters of the Gabor filter. (r_0, θ_0) is the window in the normalized image where the Gabor filters are applied.

Other methods for feature extraction includes the use of zero crossings of 1-D wavelet [42], Haar wavelets [43], Laplacian of Gaussian [35] and the use of correlation filters [44].

An iris mask is also generated as the same size of iris code. This iris mask indicates which part of the iris code is iris texture and which part is the occlusion due to eyelids, eyelashes and reflections.

Pattern Matching

The last step in an iris recognition system is the pattern matching stage, here the iris pattern (the binary IrisCode [17]) of the person in question is matched with the iris patterns stored in a database previously. The most common method in pattern matching is the computation of a fractional Hamming distance as the measure of dissimilarity between two irises [17], which can be obtained as,

$$HD = \frac{\|(code A \otimes code B) \cap mask A \cap mask B\|}{\|mask A \cap mask B\|}, \quad (2.6)$$

where $code A$ and $mask A$ are the iris code and corresponding mask of the iris A; and $code B$ and $mask B$ are those of iris B. Here, \otimes represents the XOR operator and \cap represents the AND operator. Ideally, irises from the same class should produce $HD = 0$. This HD is normalized to account the different level of occlusions that may present in different iris

images by

$$HD_{norm} = \frac{1}{2} - \left(\frac{1}{2} - HD \right) \sqrt{\frac{n}{911}}. \quad (2.7)$$

Here, n is the number of bits that were actually compared between the two IrisCodes. This HD_{norm} is used to determine the similarity or dissimilarity between two iris images.

2.3 Mobile Biometrics - How Iris Comes in to the Picture

‘Mobile biometric system’ can be broadly viewed as *any portable biometric system, which is not intended to be stationary and hardwired to a larger system* [45]. The main focus of this thesis is on smartphones and other closely related consumer devices which fit in to the definition of such a system. Current smartphones come with state of the art sensing technologies and processing power, which makes them truly a handheld work station. Moreover, smartphones are being omnipresent and it is expected to have 2 billion people using smartphones in 2016 [7]. This is predicted to grow to a third of the world’s population in 2018. Reliable assessment of the smartphone user’s identity will be crucial as data such as sensitive personal information, financial transactions and user generated content will be generated and transmitted via these devices. Some researchers have even postulated that smartphones may become mandatory to identify their owner [46]. Various levels of authentication on smartphone can be carried out by exploiting one of the following,

2.3.1 Something User Knows

The current Personal Identification Number (PIN), typed in password or graphical pattern relies on a secret knowledge authentication approach [47, 48], i.e., ‘What user knows and remembers’. These authentication approaches come with vulnerabilities such as storing the password/PIN, sharing it, choosing weak passwords for easiness to remember and input, writing down them, reusing the same password across multiple devices and services, never changing the passwords etc. These characteristics make the password easy to compromise and put the contents of the smartphone at risk which may end up causing personal and financial damage to the owner.

Also, typing in a strong alpha-numeric password is cumbersome. The user will have to change the keyboard layouts multiple times. While, an eight letter alphanumeric password can be typed in a desktop computer at a speed of 17 words per minute, it reduces to 6 words per minute on a smartphone [48]. This even makes the user uncomfortable in accessing

business data on such devices [48]. A survey on 297 smartphone users on their use of current smartphone authentication methods revealed that one third of them do not use any password at all [47]. 30% of the users noted PIN is inconvenient and other 38% mentioned that they have difficulties in remembering their PIN. Almost all of the users noted that they either never changed their PIN, or re-used the PIN for some other purposes or forgotten or shared their PIN with someone else.

2.3.2 Something User Has

The second approach of user authentication is using something ‘user possesses’, i.e., use of tokens such as a smart card [49]. This could not be an ideal solution as these tokens can be misplaced or stolen. Also, these methods stress user to remember to pick up and carry the token with them whenever they want to use their device. For convenience, user may attach the token to the device [47]. This will nullify the security efforts as any one with this token can access these devices, hence a stolen device with the token attached is the worst thing that could happen to one’s device.

2.3.3 Something User Is

The third approach is to use biometrics - which is ‘something that the user is’. In this case, the user will not be forced to remember long complex passwords or asked to carry a token with them. Biometric authentication will be natural and easy to use at the same time providing high security required by next generation devices [46]. A series of surveys carried out by Clarke *et al.* during 2002-2005 says that 83% of the users think biometrics is a good option as an authentication method on smartphones and 61% of users support continuous non-intrusive authentication [47]. A similar study [50] indicates that 93% of young smartphone users expect biometrics in their devices in near future. Also, 43% of the users mentioned they prefer biometrics over PIN. The summary of Clarke’s work can be shown in Figure 2.5. A recent survey asked the users which combination of authentication techniques they preferred in their device [51]. The results are summarized in Figure 2.6. The majority of the users preferred a combination of fingerprint and password. The combination of iris recognition and password is ranked second.

It can be noted from these studies that smartphone users are expecting biometric authentication in their devices in the near future. Fingerprints and iris are the most preferred modalities, while face and other related biometrics are not preferred [51, 47, 48].

Potential biometric techniques for mobile devices				
Biometric technique	User preference from survey	Sample acquisition capability as standard?	Accuracy	Non-intrusive?
Ear shape recognition	NA	×	High	✓
Facial recognition	Medium	✓	High	✓
Fingerprint recognition	High	×	Very high	×
Hand geometry	Medium	×	Very high	×
Handwriting recognition	NA	✓	Medium	✓
Iris scanning	Medium	×	Very high	×
Keystroke analysis	Low	✓	Medium	✓
Service utilization	NA	✓	Low	✓
Voiceprint verification	High	✓	High	✓

Fig. 2.5 Summary of Clarke *et al.* [47] work. It can be noted that iris recognition is ranked with high accuracy, but medium user preference. Reprinted with permission from Elsevier, Copyright ©2005 Elsevier.

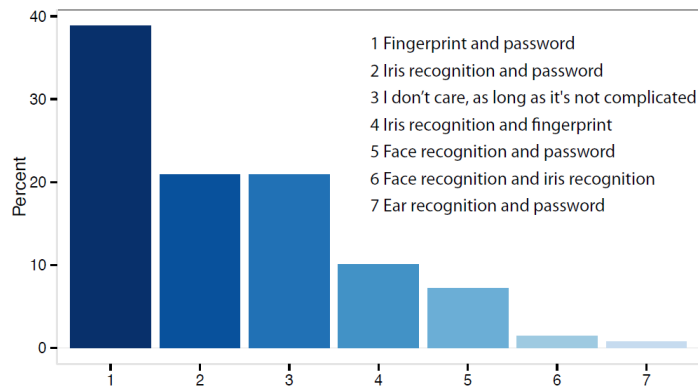


Fig. 2.6 Which combination of authentication techniques users prefer [51]. Copyright ©2015, IEEE.

2.3.4 Why Iris Recognition?

While users expect fingerprint to be a common biometrics in smartphones, this may be skewed by the recent introduction of smartphones enabled with fingerprint recognition (NTT DoCoMo F505i in 2004 and iPhone 5s in 2014 to name a few). Iris recognition has some inherent advantages over fingerprint recognition:

1. High pattern variability with 250 degrees of freedom - the uniqueness of every iris parallels the uniqueness of every fingerprint irrespective of the genotype [17].
2. Higher coverage over large population India's unique ID experience suggests that, for their population at least, iris gives better coverage than fingerprint [28].
3. Contactless acquisition of iris image from a distance is easy, while fingerprint generally need sensors which require contact and alignment.

4. Iris is an internally protected, yet externally visible organ. Hence, unlike fingerprint, surgically modifying iris is impossible without risking vision.
5. Iris is relatively stable over time, age and occupation may cause some sensors difficulty in capturing a complete and accurate fingerprint image [52].
6. Iris is more robust against spoofing attacks [53]. Unlike fingerprint, individuals do not leave the traces of their iris behind which could be a potential source of lifting and copying the pattern.
7. Public perception toward fingerprint- users have privacy concerns of criminal implications [52]. Iris does not have any such criminal connotation.

2.4 Iris Recognition: Challenges

While iris recognition has some advantages over other biometric techniques, there are a number of challenges to be addressed for an unconstrained and easy to use iris recognition system which may be widely adopted by the consumer market. The main challenges are related to a good quality iris image acquisition. Some of them can be listed as,

1. Iris is a relatively small object (approximately 11mm physical size) located in a wet, curved, reflecting surface.
2. Iris is a moving target, in another moving target -the eye, which itself is located in another moving target -head.
3. Iris could be obscured by eyelashes, eyelides, lenses and reflections.
4. Iris images are best captured in NIR illumination - both in terms of recognition performance and non-intrusive, non-disturbing image acquisition.

A detailed review on iris image acquisition devices can be found at [54]. The traditional, commercially deployed iris recognition systems typically acquire iris images by a dedicated infrared imaging system and the eye is pre-aligned with the acquisition camera. The NIST study on iris quality provides a range of useful information on the required size and resolution of an iris region, in pixels [55]. In addition, many different aspects of the acquisition system can affect the quality of the iris pattern that is extracted from the raw image. There are also a number of International Organization for Standardization (ISO) standards for dedicated iris imaging systems [56, 57]. The ISO requirements for iris image capture can be summarized in Table 2.1.

Table 2.1 ISO image acquisition requirements.

Property	Value
Modulation Transfer Function	>0.6 at 2 cycles/mm spatial frequency
Visible Iris	>70% of the iris
Gray Scale Density	dynamic range of 256 gray levels
Contrast	Pupil to Iris - 50 levels Iris to Sclera - 90 levels
Iris Diameter (pixels)	>100
Illumination	NIR wavelength (700 nm - 900 nm)

Iris acquisition devices can be broadly classified into three groups based on their user-friendliness and image acquisition distances [58]: (i) traditional, (ii) medium distance and (iii) long range acquisition devices.

The traditional acquisition devices result in high quality iris images, they are highly constrained systems which use specialized lens set up on a fixed stand along with chin/head rest for users. Such devices minimize subtle movement of the head and keep the distance of iris to acquisition devices constant. Example of such a device is shown in Figure 2.7.

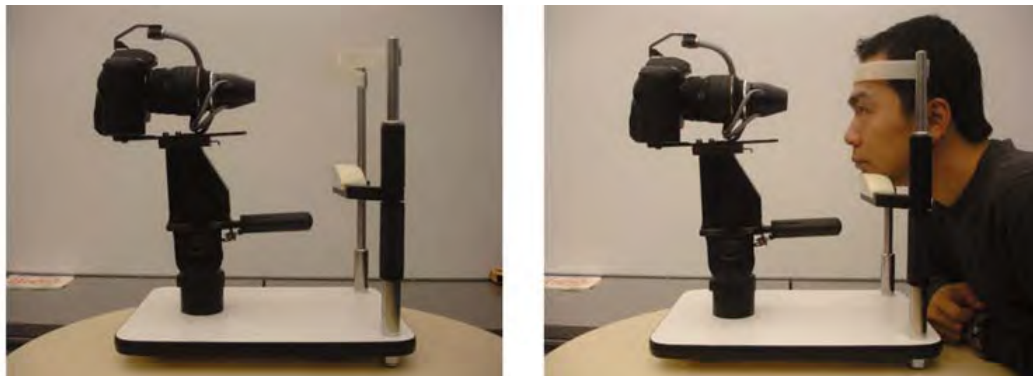


Fig. 2.7 Example of traditional iris acquisition device. A head rest and chin rest can be seen [54]. Reprinted with permission of Springer.

Middle distance iris image acquisition devices are less constrained systems as compared to the traditional ones. The images are acquired at around 50cm standoff distances and users are not required to put their head against the rack. LG 2200 and VistaFA2 Biocam are examples of such systems.

The long distance iris recognition systems are generally considered to be less constrained and work at a stand-off distance beyond 1m. 'Iris on the Move' (IOM) system by Sarnoff is one of the best known [30]. The system is proposed for airports where iris information is being used increasingly to verify passenger identity. Such a system is shown in Figure 2.9.

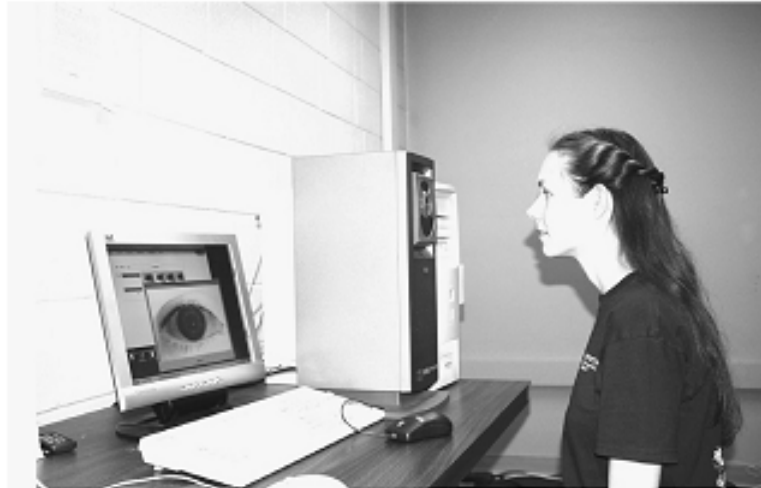


Fig. 2.8 Examples of image acquisition using middle distance device [59]. Adapted with permission from Elsevier. Copyright ©2007 Elsevier Inc.



Fig. 2.9 Iris On the Move System. The panels behind the subject are the sides of a commercial metal detector. The stanchions just in front of the subject support. An array of NIR illuminators can be seen along with the camera package at the far right of the subject [30, 59]. Reprinted with permission from IEEE and Elsevier, Copyright ©2006 IEEE, Copyright ©2007 Elsevier Inc.

Very long range iris recognition is also explored in the iris recognition industry. The typical long range iris recognition devices which work beyond 1m generally use advanced optics (such as the ones used in astronomy [60]) and strong directional illumination. Examples of such systems are given in Figure 2.10. A detailed review is given in [60].

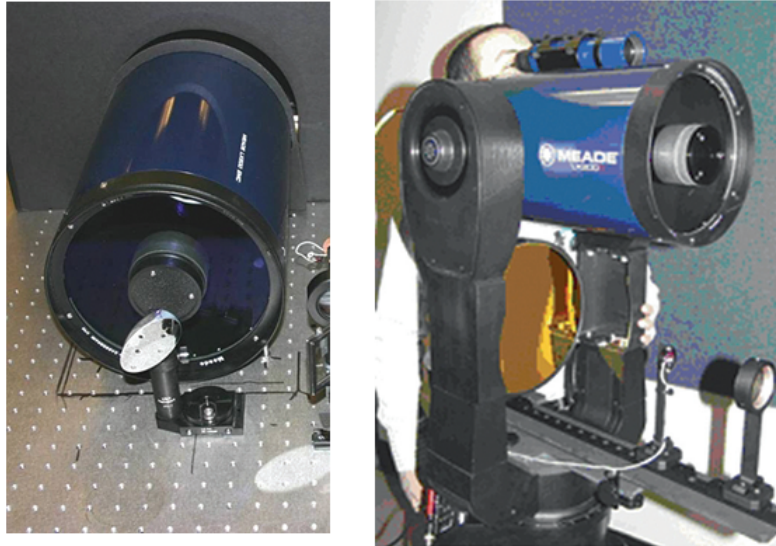


Fig. 2.10 Examples of long range iris acquisition devices [60], with kind permission from Springer Science and Business Media.

Even though the long range iris acquisition system such as iris on the move seem to be unconstrained, the users are constrained to walk past a multi-camera acquisition point employing high-end optical systems, where multiple images are acquired under controlled illumination conditions usually in indoor light conditions. In these devices, optical and image sensing subsystems are not size constrained. These systems are also provided with a stable mount, and where the subjects in motion will typically feature multiple cameras. In contrast, acquisition on handheld devices introduces a challenging set of conditions: (i) uncontrolled illumination condition, (ii) limited processing power, (iii) optical constraints introduced by miniature camera modules, (iv) pixel resolution limited by optical and cost considerations, (v) an unstable hand-held platform introducing motion blur artefacts, and (vi) an unconstrained moving object - the human eye.

2.5 Iris Recognition on Smartphones: A Literature Review

Even though, iris recognition is not more than two and half decades older, a very large number of publications on this topic can be found. A detailed review of these topics can be

found at [59, 61, 62]. Staying within the theme of this thesis, a brief survey of literature on iris recognition on smartphones is presented in the following sections.

The first published work on iris recognition on mobile phones was by Cho *et al.* in 2005 [63]. Cho *et al.* proposed a pupil and iris localization technique with a focus on implementing them on low processing power mobile phones. The localization technique is based on detecting dark pupil region and corneal reflection by changing the brightness and contrast value. They excluded the floating point operations to implement it on an ARM 9 CPU of cell phones. Cho *et al.* used a Samsung SPH-S2300 mobile phone in which internal IR cut filter was removed. An additional halogen lamp was used as an illumination source. This device has a camera which can capture images of 3.2 Mega Pixels resolution (2048×1536 pixel) and 3x optical zoom. Such a device is shown in Figure 2.11. Later, the authors [65]



Fig. 2.11 Samsung SPH-S2300 mobile phone. Adapted from [64].

improved the proposed segmentation technique by following Daugman's 'growing wedge' approach [27] to reduce the occlusion of eyelids and eyelashes in the segmentation process.

Jeong *et al.* used Samsung SPH-S2300 (Figure 2.11) with a cold mirror (a filter which absorbs the visible spectrum light) in front of the lens. Instead of the halogen lamb, the authors used the built in Xenon flash for image acquisition [66]. In this work, feature extraction was carried out using 1-D adaptive Gabor filter. The Gabor filter parameters were adapted to four different image acquisition scenarios - (i) indoor, no-blur image capture, (ii) indoor, blurred images, (iii) outdoor, no-blur images and (iv) outdoor, blurred images.

In a follow up work, Park *et al.* [67] added dual IR illuminators to Jeong *et al.*'s modified Samsung SPH-S2300. This modified camera system has an operating range of 35-40 cm (with the help of optical zoom) and captures dual eye regions. The user has to align his eyes with the specific area indicated on the cold mirror in order to accurately estimate the eye

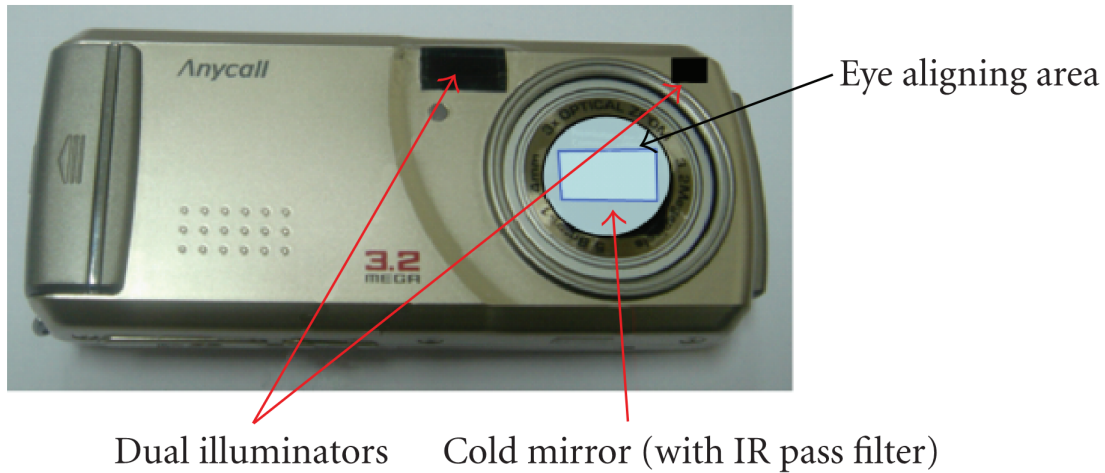


Fig. 2.12 Samsung SPH-S2300 mobile phone used in Park *et al.*'s work [67].

location. Successive ON/OFF of the dual IR illuminators were used to detect the corneal specular reflection. Considering a standard iris of size 11mm, approximately 210 pixels across iris will be present in the images acquired using this setup. A significant portion of this research paper focuses on determining optical and motion blur from the specular reflections in the pupil.

In november, 2006, OKI system announced iris scanners using OKI's original iris recognition algorithm for symbian and windows mobile operating system [68]. OKI claimed that only standard optical cameras that are equipped in mobile terminals are used in their solution. An example of such a solution released by OKI is shown in Figure 2.13.



Fig. 2.13 OKI iris solution. Adapted from [68].

Kurkovsky, Carpenter and McDonald proposed an approach which requires no additional hardware to adapt iris recognition on resource constrained mobile phones [69]. The proposed

approach includes applying Hough transform assuming iris and pupil are concentric circles. Eyelashes or eyelids were not masked and iris normalization was avoided. Even though the authors claim this as a technique for mobile phones without any additional hardware requirements, the experiments were carried out in high quality NIR images captured using CASIA in house camera, which is a fixed mount NIR system.

Kang proposed to use two magnetic rings to hold the lens in mobile phones instead of using close-up lenses [70]. While the authors argue their iris pupil localization technique is for mobile devices by implementing it for the ARM 9 processor of SPH- S2300, image acquisition for the experiments were carried out using a professional, constrained acquisition, iris imaging device- Panasonic BM ET100US Authenticam.

Lu *et al.*, developed a smartphone iris recognition system assuming that all eye images are captured at same illumination with same stand-off distance from the camera [71]. In order to follow this assumption, they provided an ‘eye cup’ with a luminous diode attached to a Sony Ericsson P800 as shown in Figure 2.14. They used histogram analysis for iris and



Fig. 2.14 ‘Eye cup’ with a luminous diode attached to a Sony Ericsson P800 to capture iris images with uniform illumination and stand-off distance [71].

pupil localization and Daugman’s approach for feature extraction.

The common characteristic of all the above mentioned techniques are (i) image acquisition is constrained - close subject-camera distance and/or requirement to align the eyes to

device and (ii) irreversible modification of smartphone camera for iris recognition - normal photography using these devices will not be possible.

Recently, AOptix introduced an iPhone 4 accessory called ‘Stratus’ (Figure 2.15) [72]. This software and wrap-around device combination enables the iPhone for iris, fingerprint,



Fig. 2.15 AOptix Stratus - the iPhone wrap-around device for biometrics. A use case scenario is also shown. Adapted from [72].

face and voice recognition [72]. While AOptix stratus is attached to iPhone, unlike an unsupervised smartphone user authentication, it is aimed at supervised person authentication scenarios such as healthcare, disaster relief, humanitarian aid and border control.

Similarly, organizations such as IriTech claim to have mobile iris recognition technology using the current hardware available in smartphone and extra surface-mount device (SMD) type LEDs [73]. In May, 2015, NTT DoCoMo launched world’s first smartphone with iris unlock feature. This device - ARROWS NX F-04G (shown in Figure 2.16), developed by Fujitsu is powered by Delta ID’s ActiveIRIS® technology [33, 74, 75]. This device contains an infrared LED and an infrared camera with IR filter adjacent to the user facing camera.

2.6 Summary

In this chapter, the background information required for the rest of the work presented in this thesis is provided. A brief discussion about the unique structure of the iris is given, followed by the various milestones in iris recognition and a quick review of a baseline iris recognition system. Further discussions presented iris recognition as an ideal candidate for smartphone



Fig. 2.16 NTT DoCoMo - Fujitsu ARROW NX F-04G: World's first smartphone with iris recognition. An additional infrared LED and infrared camera is used for iris recognition. Eye bands are provided for eye alignment. Adapted from [33, 74].

user authentication. Various challenges in realising smartphone user authentication based on iris recognition are discussed. A brief literature review of iris recognition on smartphones is presented.

It is worth mentioning that, when the work presented in this thesis started in the late 2013, smartphone user authentication using iris recognition was quite speculative. But over the last two years, there has been strong emerging demand from industry for such a practical working solution. This drove both the academia and the industry to research on providing a reliable iris recognition solution for smartphones. Nevertheless, 2015 witnessed the appearance of various such solutions, including the work presented in this thesis.

Chapter 3

Current Smartphones and Iris Recognition

Commerically-deployed iris acquisition devices operate in the near infra-red (NIR) region of the electro-magnetic spectrum . This is mainly to obtain the rich iris texture, even in a heavily pigmented iris. Also, NIR is resilient to the changes in the ambient illuminations and reflections that may present in the iris region, if acquired in the visible spectrum. The advantages of NIR for iris are discussed in Section 2.2.1. On the other hand, smartphone cameras typically operate in the visible spectrum. Hence, colour iris images acquired using these cameras may not be suitable for classical iris processing algorithms. This leads to an interesting question: how close are we to obtaining good-quality iris recognition performance using current state-of-the-art smartphones?

A portion of this chapter (Section 3.1) was originally published in IEEE Transactions on Consumer Electronics, vol.61, no.2, pp.245-253, May 2015 as “Iris authentication in handheld devices - considerations for constraint-free acquisition”.

3.1 Smartphone Case Study

As a case study on the use of existing smartphone cameras for iris image acquisition, one of the state of the art, smartphone rear-facing cameras - HTC One M8 UltraPixel camera - is analyzed. The specification of this camera is shown in Table 3.1.

For smartphones, a typical use case is the user authentication while holding the device at a comfortable arm's length (approximately 15-30cm from face) as in Figure 3.1.

Table 3.1 Camera specifications.

Parameter	Value
Sensor Size	1/3 inch
Aspect Ratio	16: 9
Sensor Resolution ($w \times l$)	2688×1520
Pixel size	$2\mu\text{m} \times 2\mu\text{m}$
Focal length (f)	3.82mm
F number (F)	2



Fig. 3.1 A typical smartphone user authentication scenario. The distance between camera and eye is approximately 250mm.

3.1.1 Optical Analysis

Considering a typical iris acquisition scenario using smartphones with a stand-off distance $d = 250\text{mm}$ and assuming a circle of confusion $c = 2\mu\text{m}$ (one pixel), the far point (S) and near point (R) (Figure 3.2) in which the image is in focus are given by [76],

$$[R, S] = \frac{df^2}{f^2 \pm Fcd}, \quad (3.1)$$

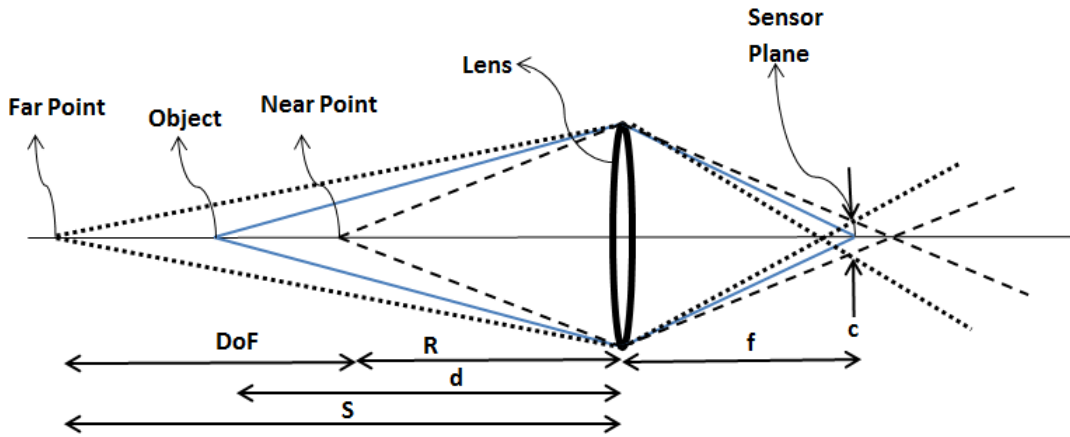


Fig. 3.2 Optical analysis parameters: DoF - Depth of Field, S -the far point and R - near point in object plane in which the image is in focus, d - object stand-off distance and c - circle of confusion.

which gives

$$S = 268.4\text{mm}, R = 234.0\text{mm}. \quad (3.2)$$

Hence, the Depth of Field (DoF) is,

$$DoF = S - R = 34.4\text{mm}. \quad (3.3)$$

At a stand-off distance of $d = 250\text{mm}$, this camera will have a magnification factor M ,

$$M = \frac{f}{d - f}, \quad (3.4)$$

$$= \frac{3.82}{250 - 3.82}, \quad (3.5)$$

$$= 0.0155. \quad (3.6)$$

That is, this camera will magnify the iris by 0.0155 on to its sensor. The horizontal field of view (FoV_h) can be calculated as below [76],

$$FoV_h = 2 \arctan \left(\frac{l}{2f} \right) \quad (3.7)$$

$$= 2 \arctan \left(\frac{2688 \times 2\mu\text{m}}{2 \times 3.82\text{mm}} \right) \approx 70^\circ. \quad (3.8)$$

Similarly, a vertical field of view of 43° can be obtained.

3.1.2 Equivalent Pixel Dimensions and Optical Resolution

Hence, at 250mm stand-off distance, this camera will enable us to capture a horizontal distance,

$$d_h = 2 \tan\left(\frac{FoV_h}{2}\right) \times d \approx 350\text{mm}. \quad (3.9)$$

Similarly, a vertical distance (d_v) of $\approx 200\text{mm}$ can be obtained. That is, at 250mm, this camera can provide a capture box of $350\text{mm} \times 200\text{mm}$ and a depth of field of 34.40mm. Considering a maximum inter-pupillary distance of 78mm [77], this capture box will be sufficient to obtain both eyes simultaneously. Further, assuming an iris of size 11mm [17], a magnification of 0.0155 (as shown in Equation 5.4) will result in an iris image of $170\mu\text{m}$ diameter on the sensor. The sensor has a pixel spacing of $2\mu\text{m}$, so assuming a fill factor of 100%, the iris will have 85 pixels diameter on the sensor. Within the depth of field, the iris will have pixel range of 79 to 91 pixels on sensor. This is less than the marginal quality (100 pixels) of an iris image as outlined in ISO/IEC 19794-6 and NIST Mobile ID best practice [56, 45], but may be acceptable as per the studies shown in [78, 55]. Note that the effect of Bayer filter on the detector has been ignored, and of course, this commercial camera has only RGB pixels and no NIR channel.

The modulation transfer function (MTF) at 250mm standoff distance of this camera was measured in white light using the Imatest tool [79]. The MTF plot is shown in Figure 3.3. From Figure 3.3, one can note that, at 60% modulation, the optical resolution is 1.7 line pair/millimeter on the object plane. This optical resolution is below the marginal image quality (2 line pairs/millimeter) as suggested by ISO/IEC 19794-6. One reason may be that the lens is designed to be cost effective rather than perfect.

3.1.3 Diffraction Limit Calculation

An optical system is diffraction limited, if it is only limited by diffraction and not by other system degradations. That is, such a system will be of high quality and free from optical aberrations [76]. The Airy disk of a diffraction limited optical system is the image of a point formed by the system, which represents the distribution of light at the focus point f . The

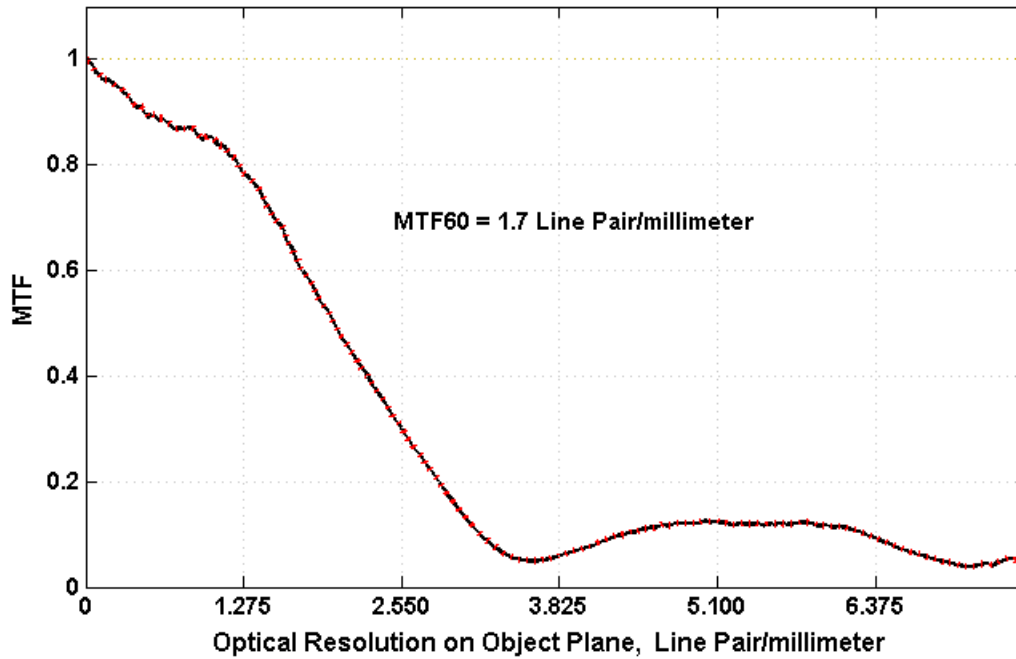


Fig. 3.3 Smartphone case study: Modulation transfer function at 250mm stand off distance.

radius of the Airy disk can be calculated for visible wavelength ($\lambda = 550 \text{ nm}$) as,

$$r = 1.22F\lambda, \quad (3.10)$$

$$= 1.34\mu\text{m}. \quad (3.11)$$

According to Rayleigh criterion, two separate point images can be resolved if the radius of the airy disk is less than the pixel size. That means, this is the smallest theoretical pixel of detail [76, 80]. At the longer NIR wavelength of 850nm, this radius would be approximately 2.07 μm . However it is clear from the MTF that the lens is far from diffraction-limited.

3.1.4 Considerations for Infrared Imaging

Here it can be concluded that the example smartphone is marginally capable of iris image acquisition with acceptable optical quality for visible iris image if we ignore the consequences of RGB Bayer pattern, with the camera-to-iris distance of 250mm. It can be observed from Equation 5.16 that at NIR wavelengths the effects of the diffraction limit become noticeable, potentially restricting iris quality even if improved lenses are incorporated. Also, at NIR wavelengths, there may be a shift in focus, compared to the visible focus, due to longitudinal chromatic aberration, producing a blurring effect.

3.2 Smartphone Visible Iris Recognition

The performance of an iris recognition system can vary significantly depending on the wavelengths used to acquire the images. Most of the studies in this context observed that NIR iris recognition outperforms its visible counterpart [34, 81]. But, there has been research on iris recognition on images acquired under the visible spectrum [82–84]. These efforts on visible spectrum iris recognition have motivated researchers to pursue iris recognition using the images captured by existing smartphone cameras [32, 85–88].

3.2.1 MICHE Database

The MICHE dataset- created by BIP Lab of University of Salerno- contains iris acquired using three different mobile devices – iPhone 5S, Samsung Galaxy S4 and a Samsung Galaxy Tab II. The images in the database are captured by the subjects holding the capturing device by herself/himself [32]. The subjects were asked to capture their own iris images using both front and rear camera of these devices in two different scenarios –indoor and outdoor. There is a minimum of 40 images per subjects. The average capture distances for smartphones were 10cm for the front camera and about 13cm for the rear camera (Note that this is smaller than the stand-off distance we considered in 3.1). For the Tab, this stand-off distance is about 5cm. Examples of images in MICHE database are given in Figure 3.4.



Fig. 3.4 Examples of images from the MICHE database: First row contains images captured using rear-facing camera and second row contains images captured using front-face camera.

3.2.2 Evaluation of Existing Smartphone Iris Recognition Techniques

MICHE dataset can be considered as an ideal representative of the iris images that can be captured using existing smartphones. The types of noise present in the smartphone

acquisition scenarios include (a) reflexes: artificial light sources, natural light sources, people or objects in the scene during the acquisition; (b) defocus blur; (c) motion blur: either due to an involuntary movement of the hand holding the device, or due to an involuntary movement of the head or of the eye during acquisition; (d) occlusions: eyelids, eyeglasses, eyelashes, hair, shadows; (e) device: artifacts due to the low resolution and/or to the specific noise of the device; (f) off-axis gaze; (g) variable illumination; and (h) different color dominants are present in this dataset. Hence evaluating this dataset with existing literature on smartphone iris recognition [87] and traditional commercial iris implementation will give the sense of how close are we to attaining high-performing iris recognition on smartphones.

We have partially followed the experiments speculated by Raja *et al.* [87]. The Galaxy Tab II is not considered in any of our analyses as the device has a low spatial resolution camera and images were captured at very close standoff distance (5cm). Such a solution is not expected to be widely accepted in the consumer market. A summary of this subset is given in Table 3.2.

Table 3.2 Summary of various acquisition parameters of the MICHE subset.

Parameter	iPhone Rear	iPhone Front	S4 Rear	S4 Front
Camera Resolution (Mega Pixels)	8	1.2	13	2
Stand-off Distance	13cm	10cm	13cm	10cm
Average Pupil Radius (Pixels)	36	21	66	24
Average Iris Radius (Pixels)	180	105	280	110

The experiments are divided into two main categories- (i) experiments on images captured in outdoor illumination condition and (ii) experiments on images captured in indoor illumination conditions. Each of these sets are further divided into four groups based on the camera used to acquire the images. The comparison results are tabulated in Table 3.3. Table 3.3 presents equal error rates (EER, refer Section A.2) in percentage for the 8 subsets of MICHE. The results obtained by six academic iris recognition implementation [89], one method which uses visible iris and peri-ocular information [90], one technique optimized for smartphone images such as the ones in MICHE [87] and one commercial iris recognition algorithm (MIRLIN, which is based on [91]) are compared. It has to be noted that except for Raghavendra *et al.* [90] and Raja *et al.* [87], all other algorithms are developed for NIR iris images. All these algorithms differ mainly in their feature extraction technique and/or iris segmentation.

From Table 3.3, one can note that, even though MIRLIN is used ‘as is’ (without any modification for visible images), it turned out to be the single algorithm which has the largest number of best performing results. Also, it has to be considered that the MIRLIN outperforms the algorithms which use periocular information along with iris; and the algorithm which is optimized for databases like MICHE.

One another important observation can be made is, in majority of the cases subsets under the indoor illumination conditions perform better than their outdoor illumination counterpart. This could be due to the comparatively controlled nature of indoor acquisition, which reduces large uncontrolled reflections on iris region. Also, MIRLIN noted that, in all these experiments, the rear camera images outperform the front ones. As expected, this could be because the images captured using the rear camera are of better quality than the ones captured using the front facing cameras.

A closer look at the results of MIRLIN shows that, there is a significant number of segmentation failure cases, where MIRLIN either failed to find an iris or wrongly segmented the iris. This could be due to the fact that MIRLIN is designed for NIR images and does not expect to encounter reflections on iris regions during segmentation. MIRLIN segmentation accuracy is compared with Raja *et al.* [87] in Table 3.4. In the segmentation case also, one can note that indoor illumination cases are better segmented as compared to the outdoor ones. Also the rear camera image produce better segmentation results due to the higher quality of images as compared to the frontal camera images.

These observations highlight that, iris recognition with the images acquired using the current smartphones faces several significant challenges, especially when the recognition is done outdoors.

Table 3.3 Equal error rate (%) for various iris recognition schemes on MICHE subset.

Schemes	OUTDOOR ILLUMINATION				INDOOR ILLUMINATION			
	iPhone Rear	iPhone Front	S4 Rear	S4 Front	iPhone Rear	iPhone Front	S4 Rear	S4 Front
Daugman [17]	10.41	6.78	10.52	12.45	8.35	3.74	6.16	8.399
Masek [92]	24.01	21.86	20.83	21.22	13.90	17.01	17.26	18.83
Ma <i>et al.</i> [93]	29.98	22.01	20.63	20.60	12.84	17.01	18.68	17.10
Ko <i>et al.</i> [94]	21.78	18.11	18.05	17.70	11.29	14.58	14.68	14.06
Rathgeb and Uhl, 2010 [95]	28.12	27.43	24.39	27.30	20.83	21.05	25.68	21.13
Rathgeb and Uhl, 2011 [96]	30.39	26.76	26.04	31.09	26.31	26.84	33.17	30.43
Raghavendra <i>et al.</i> [90]	8.57	7.82	6.29	8.11	0.48	2.07	4.18	4.23
Raja <i>et al.</i> [87]	6.25	4.18	2.06	6.27	6.25	0.02	3.96	2.50
MIRLIN	1.12	3.33	3.32	5.98	2.84	2.73	3.16	3.33

Table 3.4 Comparison of segmentation accuracy (in %) in MICHE subset.

Algorithm	OUTDOOR ILLUMINATION				INDOOR ILLUMINATION			
	iPhone Rear	iPhone Front	S4 Rear	S4 Front	iPhone Rear	iPhone Front	S4 Rear	S4 Front
Raja <i>et al.</i> [87]	81	64	74.5	62	64.5	76.5	65	77
MIRLIN	49.77	35.14	58.06	36.46	78.65	52.38	79	56.25

3.3 Discussion and Conclusions

From the analyses in the previous sections, it could be observed that using the existing smartphones ‘as is’ for iris recognition will not be an ideal solution, both in terms of user convenience and recognition performance. While, the state of the art commercial iris recognition algorithms result in stellar recognition performance in large-scale databases captured in NIR [29, 97], the recognition performance of smartphone images is not even close, even when the state-of-the-art algorithms are used. Also, the experiments noted that these images suffer severely from the ambient noise.

Moreover, using visible spectrum iris recognition does not allow the smartphones to harness the improvements made in the iris recognition research in last 25 years. Also, visible images will be a barrier for interoperability of iris recognition. That is existing iris databases, let it be the border control, or corporate or governmental ones, will not be able to cross compare with the smartphone iris images. This will restrict the additional capabilities current smartphones can have when a standard iris recognition is implemented on them such as ‘Bring Your Own Device -BYOD’ concept [98]. Hence, it will be ideal for the smartphones to have NIR iris recognition capabilities that are compliant with international standards and interoperable with the existing systems and databases.

Chapter 4

Iris Authentication in Smartphones: Considerations for Constraint Free Acquisition

From the previous chapter, it is observed that acquiring iris images using current smartphones and using them with the state of the art iris recognition algorithms will not result in a highly reliable smartphone user authentication. This chapter envisages a high performing, unconstrained smartphone iris recognition system. That is, when a user picks up his phone, it automatically tracks their eyes until a ‘good’ iris region can be acquired. This ‘good’ iris is passed to a workflow that unlocks the device and its resources and services once the device user is authenticated. The goals of this chapter are to (i) define what is meant by a ‘good’ iris region; (ii) define various challenges that directly affect the design of such an iris recognition system - especially the acquisition device. and (iii) outline the acquisition framework, associated workflows and key challenges in successfully implementing iris authentication in the unconstrained use case for a handheld imaging device.

The material in this chapter was originally published in the IEEE Transactions on Consumer Electronics, vol.61, no.2, pp.245-253, May 2015 as “Iris authentication in handheld devices - considerations for constraint-free acquisition”. It has been modified to suit the presentation of ideas in this thesis. Additional materials have been included, notably in Sections 4.2.4 and 4.3

4.1 Iris Image Quality Requirements

The standard ISO/IEC 19794-6 outlined iris image quality parameters for an iris recognition system [56, 57]. Similarly, the NIST Mobile ID Device-Best Practice Recommendation (MID-BPR) [45] also provides guidelines for capture and use of iris images as a biometric modality in mobile devices. A detailed quality analysis of iris based systems is available from NIST [55]. Based on these studies, the most important iris image parameters to be considered in the design of an iris authentication system for smartphones are discussed in the following subsections.

4.1.1 Iris Image Size and Quality

The number of pixels across iris diameter can be considered as one of the main criteria affecting iris image quality. This number depends on the iris acquisition device and the standoff distance. ISO/IEC 19794-6 suggests a minimum of 100-149 pixels across iris (8.3 pixels/millimeter considering the average iris size of 11-13 mm), 60% modulation at 2 line pair/ millimeter in the iris plane as marginal and recommends above 200 pixels across iris (16.7 pixels/ millimeter, 60% modulation at 4 line pair/millimeter) [56, 57]. Daugman notes that 80-130 pixels across iris is more typical in the field trials [17]. Also, NIST MID-BPR [65] states 140, true non up-sampled pixels across iris diameter as the minimum acceptable. This is broadly in agreement with the NIST study [55] and provides the basis for standard commercial iris recognition system.

However it may be feasible to use lower iris resolution for consumer applications. Some preliminary studies suggest that usable iris patterns with practical discrimination ability can be obtained from iris images of lower pixel resolution [78]. A detailed analysis is given in Section 4.2.3.

4.1.2 Other Relevant Image Quality Parameters

Other relevant image quality parameters that are likely to affect the smartphone iris recognition performance include:

Usable Iris Area NIST IQCE classifies usable iris area as the quality parameter which has the greatest effect on recognition performance [55]. Usable iris area is the percentage of iris available for matching after masking off the occlusions and specular reflections present in the iris area. Pupil dilation also affects the usable iris area. The occlusions in iris area affect

iris segmentation which leads to reduction in performance. ISO/IEC 19794-6 suggests at least 70% of usable iris area to be present in an iris image used for biometric authentication.

Iris Pupil and Iris Sclera Contrast Iris-pupil and iris-sclera contrast plays an important role in proper iris segmentation and hence in the recognition performance. Illumination wavelength, capture device characteristics, eye diseases, shadows etc. can cause poor contrast between iris-pupil and iris-sclera. A capture device which can resolve sufficient contrast between these three regions can positively impact iris segmentation and enhance recognition performance. The ISO/IEC 19794-6 standard requires a minimum of 50 gray level separations between iris and pupil and 70 gray level separations between iris and sclera.

Image Sharpness Images with low sharpness inflate false rejection rate (FRR) and false acceptance rate (FAR) (For details about the biometric error rates used here, refer Section A.2) [55]. Defocus, compression and motion of camera or eye/head can reduce the image sharpness. By ensuring in-focus acquisition of iris images, recognition performance can be significantly improved. Focus performance can be improved using auto-focus algorithms optimized for the eye region, and through optical designs that increase depth of field [99]. Different focus assessment techniques presented in the literature can be used to select a well-focused image from a set of acquired images or to recommend re-acquisition of image.

Gaze Angle Off-axis images present a significant challenge to iris recognition technology. According to the NIST IQCE evaluation, gaze angle significantly affects the FRR. Realtime gaze compensation techniques can be used for this purpose [100, 101]. Schuckers *et al.* [101] noted considerable improvement on iris recognition performance when gaze angle was compensated for in images which are up to 15° offaxis. Also, current gaze estimation techniques can estimate gaze angle with an average 3.5° error over a 50° range [102].

4.2 Proof-of-Concept Tests

Having outlined the various image quality parameters that may affect smartphone iris recognition performance, the next consideration is on quantifying the minimum quality requirements which play an important role in the acquisition system design. In this section, experiments to confirm the lower thresholds of iris size that provide acceptable results are summarized. A study on the effect of defocus blur and motion blur that can creep in to the images while acquisition is also evaluated.

The iris size partially depends on the spatial resolution of the camera, while the defocus blur and motion blur will play a part in choosing the shutter mechanisms and focussing elements. The experiments are carried out in two large publicly available databases- CASIA v4 interval and MMU 1 databases. This specific choice of database is based on the observation that these databases contain high quality images as compared to its successors, hence the effect of other noises will not be interfering in the experiments (Figure 4.1).

4.2.1 Test Databases

CASIA and MMU databases consist of NIR iris images. CASIA v4 interval database consists of high quality NIR images collected using a close up iris camera [16]. This database comprises 249 subjects and an overall 2639 images, each image of resolution 320×280 and has approximately 200 pixels across iris [16]. MMU1 iris database consists of 450 iris images from 46 subjects. Iris images are of size 320×240 , with an average 110 pixels across iris diameter. These images were captured at a range of 7-25 cm from the subject [103].

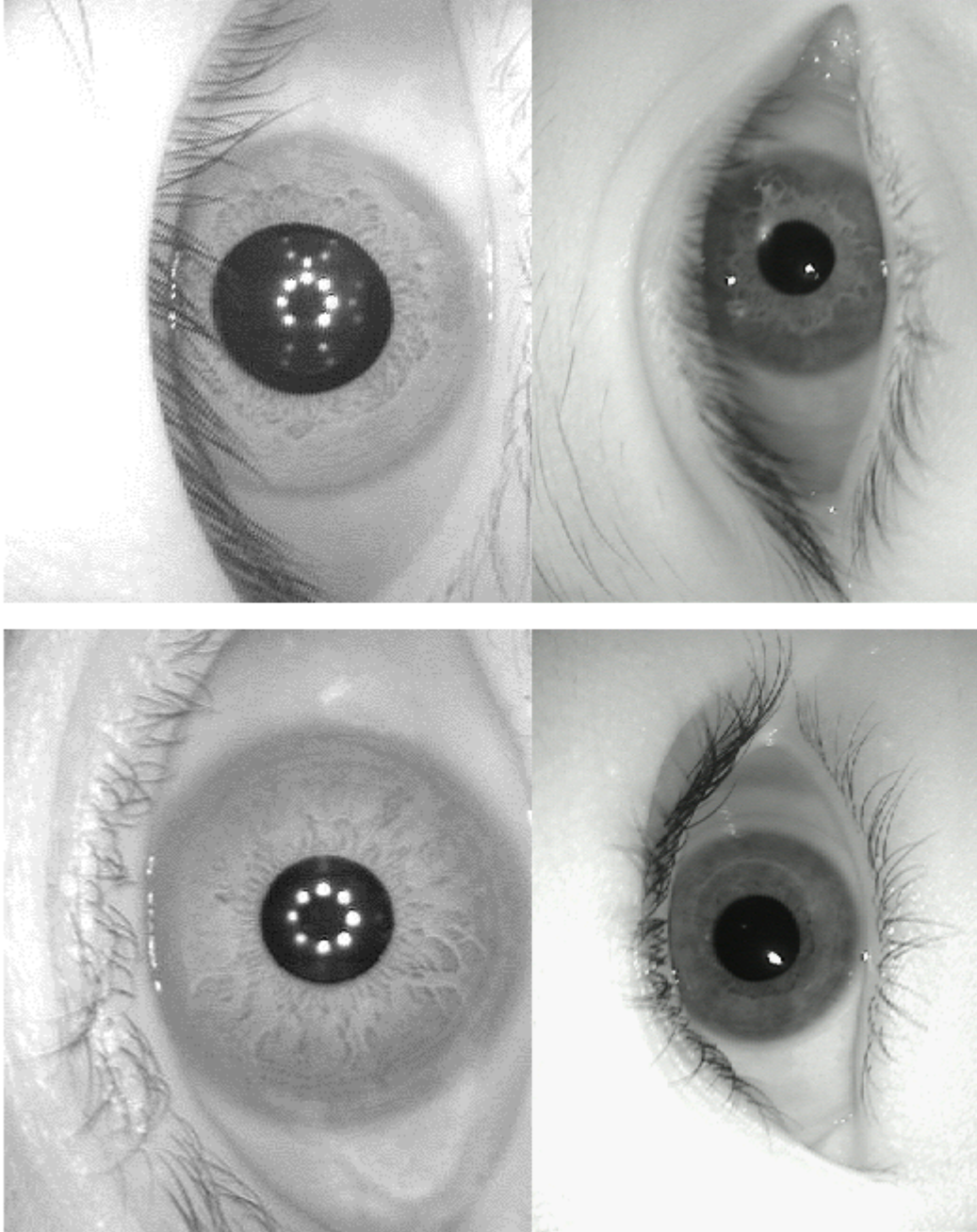


Fig. 4.1 Examples of images from CASIA v4 Distance and MMU1 databases. First row is from CASIA database and second row from MMU. Images are of Original size. Extreme high quality clear iris pattern is visible in these images.

4.2.2 Test Algorithm

An open source, high-performing iris recognition algorithm -OSIRIS 4.1- is used in the experiments in this chapter [104]. The choice of this algorithm is based on its three properties - (i) this reference system is open source, which facilitates reproducible research, (ii) the system is high performing [104] and (iii) its impact in the research community [104]. A brief description is given in Figure 4.2.

OSIRIS 4.1 generally follows Daugman's approach, with variation in iris segmentation and normalization. Iris image is segmented based on a optimal contour detection based on Viterbi algorithm. A non-circular iris normalization is carried out based on the non-regular sampling of the contours [104]. Feature extraction follows Daugman's approach of 2-D Gabor filters at various scales and resolution. The extracted iris codes are matched based on the dissimilarity score obtained by hamming distance comparison. A detailed description of this algorithm can be found in [104].

4.2.3 Impact of Spatial Resolution

The impact of spatial resolution on iris recognition performance was analysed by carrying out the experiments according to the NIST IQCE Study Methodology [55]. To simulate the impairments caused by a low-resolution camera, experiments are carried out by down-sampled iris images using block averaging of different scales. These images are then up-sampled by bi-cubic interpolation to restore the original image size (640×480) since commercial iris comparators cannot process images below the size of 640×480 . The original images have approximately 220 pixels across the iris diameter. Note that, following the analysis by Daugman [17], left and right irises of the same person are considered as different classes in these experiments.

Results and Observations

Receiver operating characteristic (ROC) curves (Section A.2) for each database are shown in Figure 4.3. From Figure 4.3, it can be observed that, the performance curves of images above 50 pixels across the iris diameter (approximately) in all the three databases represent similar performance while the performance curve of images below 50 pixels across the iris diameter shows significant decrease as compared to the rest. This suggests that 50-100 pixels across the iris diameter contain sufficient information for iris recognition, which can be approximated as 5 pixels per millimeter spatial resolution at the iris. These results can be summarized in terms of the verification performance as shown in Figure 4.4.

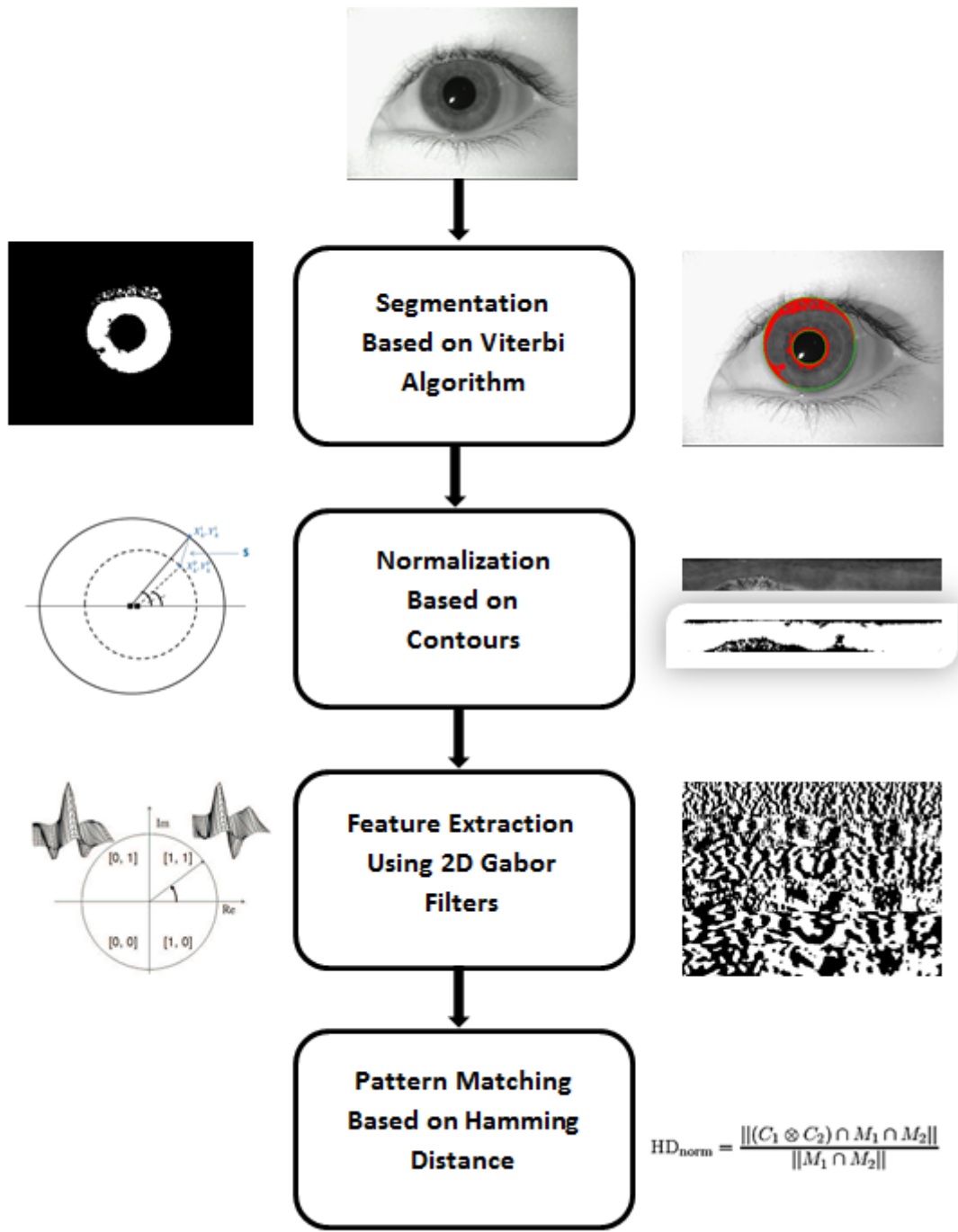


Fig. 4.2 Outline of OSIRIS reference system.

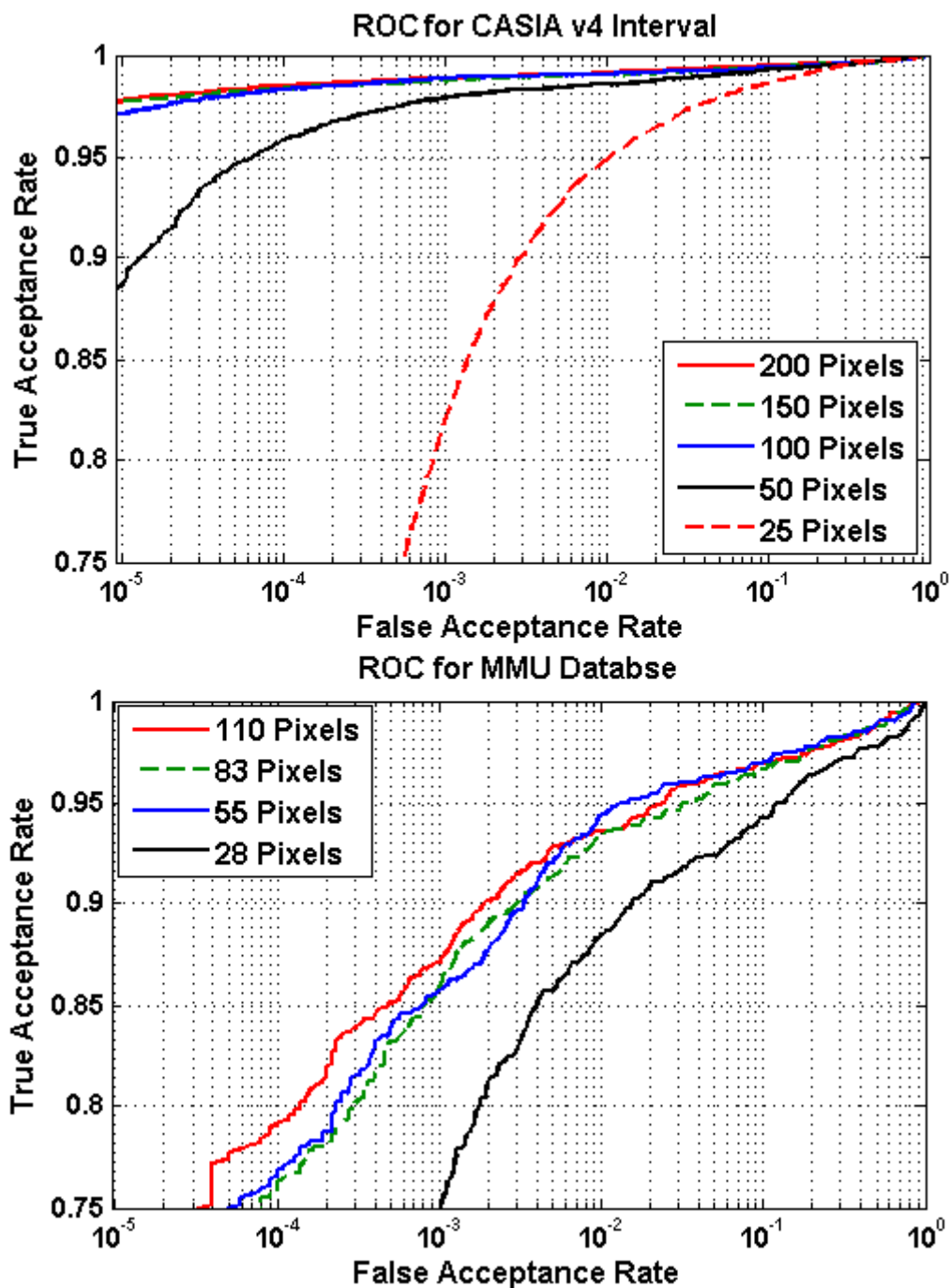


Fig. 4.3 ROC Curves for CASIA v4 interval and MMU1 databases for different number of pixels across iris diameter.

From Figure 4.4, it can be observed that there is no significant performance improvement when the effective number of pixels across the iris diameter is increased above 50 pixels. Further, increasing the number of pixels above 100 across iris diameter does not improve

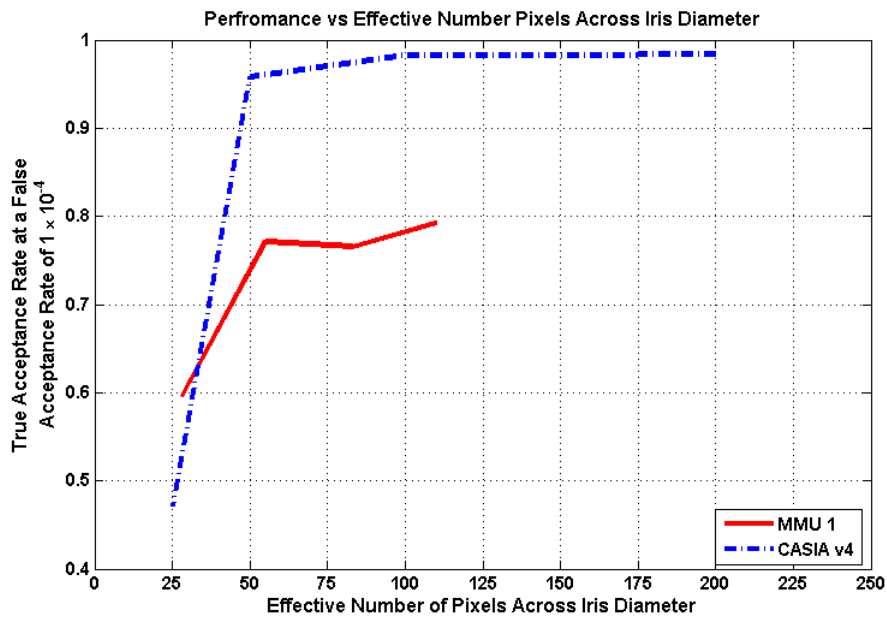


Fig. 4.4 Iris recognition performance for different databases as a function of effective number of pixels across iris diameter.

recognition performance at all. In a typical smartphone use case this suggests 5 pixels per millimeter spatial resolution, assuming good image quality. Note that, spatial resolution is also related to optics and sampling along with the pixel count [78]. These results are essentially in agreement with the NIST evaluation [5]. Further, after examining in detail the false rejection cases in the results, it was observed that the main cause for false rejection is the failure to correctly segment the iris. A secondary cause is the relatively small usable iris area in some images. In particular occlusions due to eyelids and eyelashes contribute to incorrect segmentation and reduction in the usable iris area.

Thus it can be concluded that iris images between 50 and 100 pixels in diameter along with commercial grade iris recognition algorithm may provide sufficient discriminating capability. It is also clear that the accurate segmentation of the iris region is critical to achieve a high degree of recognition. Given the unconstrained nature of handheld devices and the variety of environments in which they are used, one key challenge will be to adapt existing acquisition and segmentation techniques to operate in a range of typical use cases for iris biometrics.

4.2.4 Impact of Blur Induced by the Acquisition Device

The acquisition device can introduce mainly two types of blur in the acquired image - defocus blur and motion blur. The defocus blur is induced when the subject is out of the depth of field of the device, while motion blur is due to the movement of object and/or the device. The device design such as aperture size, focal length, depth of field, exposure time, shutter speed can affect the amount of blur induced in the images. Hence, it is important to understand the impact of these two blur types in the performance of an iris recognition system.

Experiments are carried out with the CASIA v4 interval and MMU1 database. The effect of defocus blur is induced by filtering the image with a Gaussian filter of standard deviation σ pixels and a window size of $z \times z$, where $z = 2 \times (\lceil 2 \times \sigma \rceil) + 1$. The $\lceil x \rceil$ function computes the smallest integer not less than x in order to avoid fractional window size. The standard deviation σ is varied to attain different levels of defocus blur. Examples of images for different levels of defocus blur are shown in Figure 4.6. Iris recognition performance is also given in Figure 4.5.

From the performance curves in Figure 4.5, it can be noted that, a small amount of defocus blur ($\sigma = 3$) does not have any effect on the system performance while further increase in blur deteriorate performance, especially at a low false acceptance rates. For example, at a false acceptance rate of 1×10^{-4} , a defocus blur of $\sigma = 5$ and $\sigma = 10$ is negligible in CASIA database. A similar trend can be observed in MMU database also. This may seem surprising initially, but in turn we have to note that only a very small amount of information, in the form of a compact binary code, is used to represent an iris image (2048 bit in Daugman's original approach [17]). The rest of the information is neglected while feature encoding. Also, many of the feature encoding schemes (such as a Gabor filter) employ a Gaussian filter in the processing pipeline. Hence a small defocus blur will not have a large impact on iris recognition performance. But, it has to be noted that, increase in defocus blur adversely affects iris segmentation, which in turn affect the recognition performance.

Similarly, the effect of motion blur is induced by convolving the iris images with a filter that approximates the linear motion l of the camera in pixels. Iris recognition performance was carried out for various lengths of camera motion. For the better approximation, all images are assumed to have motion in 45° from the horizontal image axis. Examples of various motion blur values used in testing is shown in Figure 4.7. It has to be noted that a real-world motion blur is more complex than the linear model presented here. But, the analysis with controlled motion will provide a better approximation of the extent of motion blur an iris recognition system can tolerate. The effect of motion in iris recognition performance is depicted in Figure 4.8.

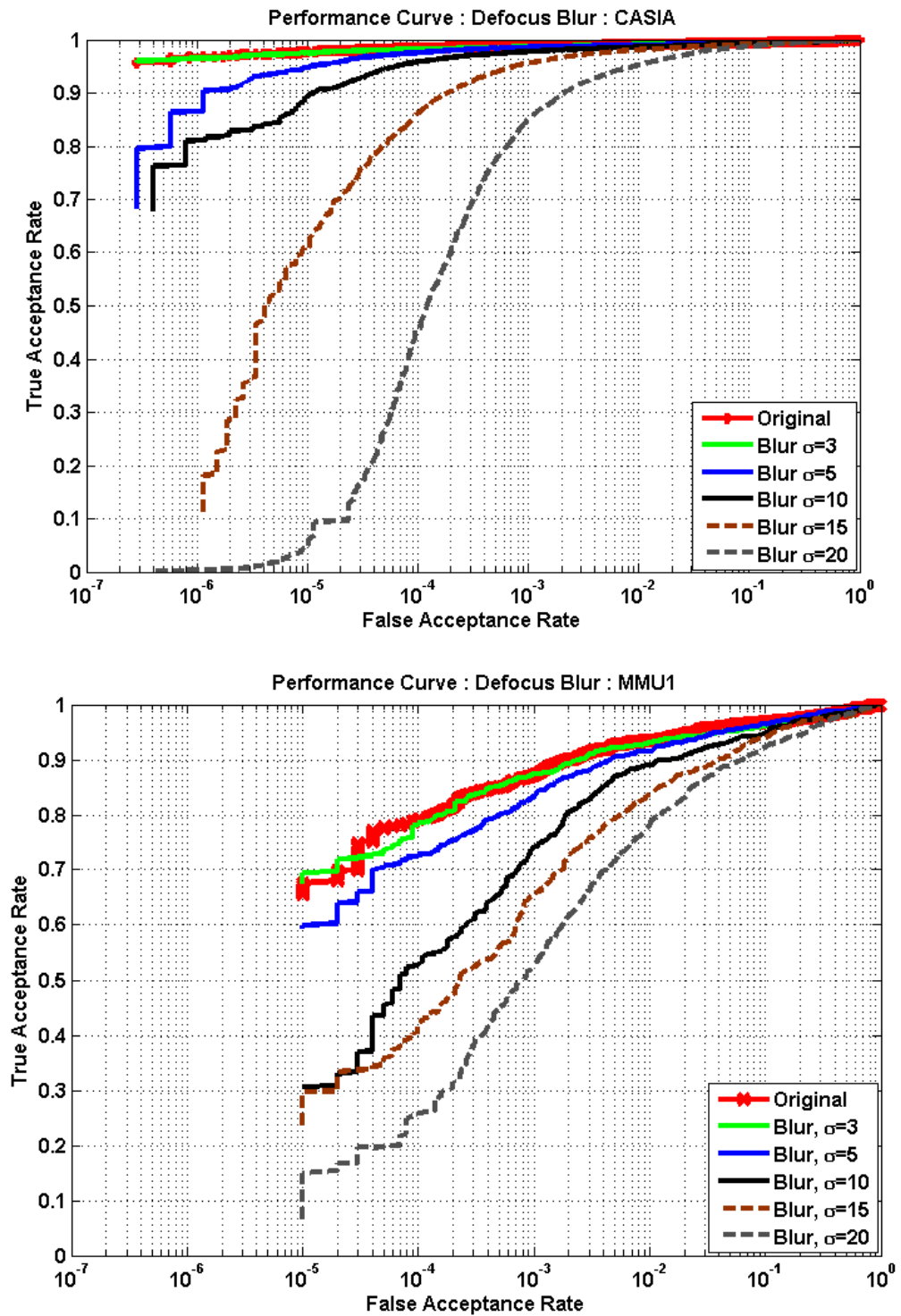


Fig. 4.5 Performance Curves for CASIA v4 interval and MMU1 databases for different defocus blur.

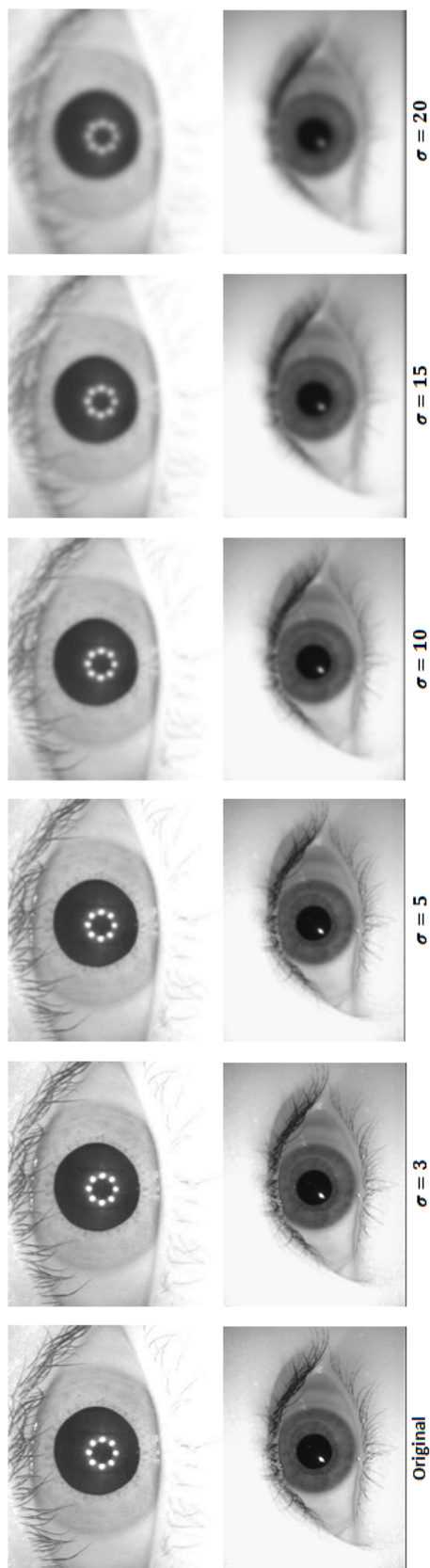


Fig. 4.6 Examples of images with different defocus blur. First row is from CASIA database and second row from MMU.

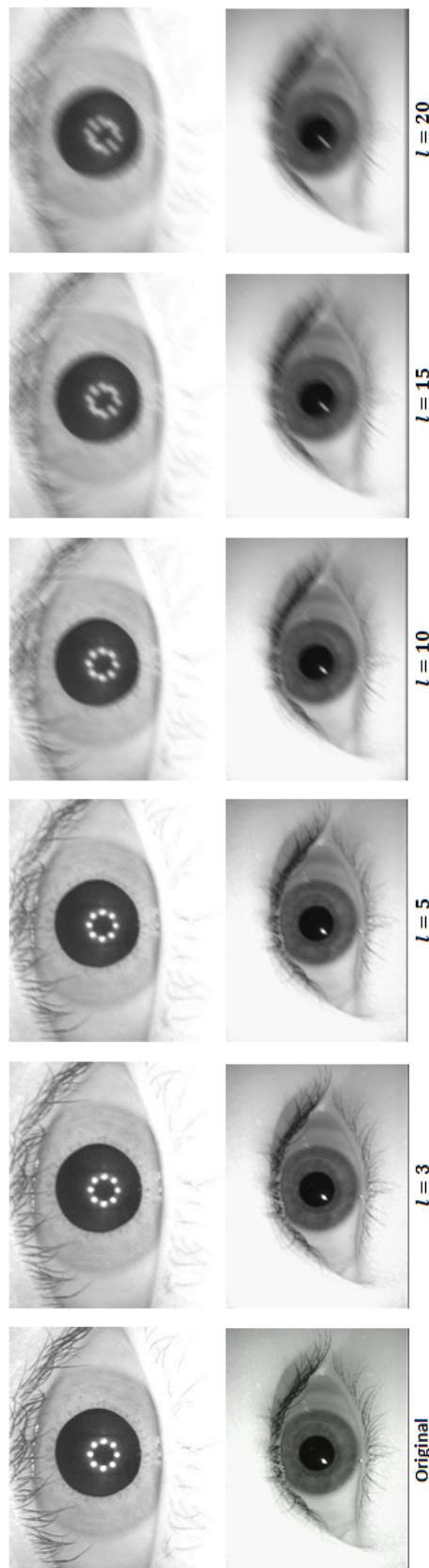


Fig. 4.7 Examples of images with different motion blur. l represent length of motion in number of pixels along anticlock wise from horizontal image axis. First row is from CASIA database and second row from MMU.

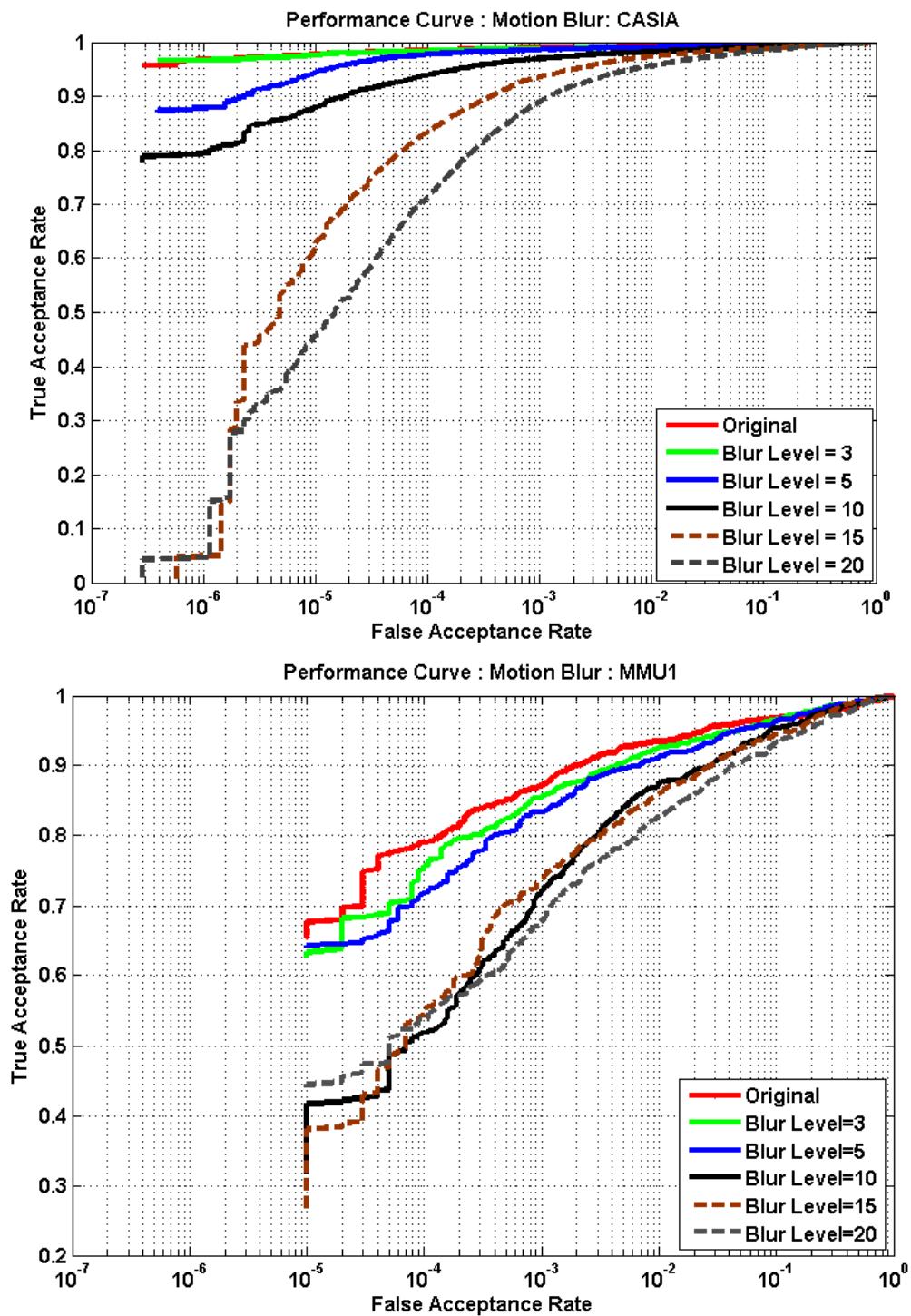


Fig. 4.8 Performance curves for CASIA v4 interval and MMU1 databases for different length of camera motion.

From Figure 4.8, it could be noted that, increase in motion blur deteriorate iris recognition performance significantly as the blur level increases. Also, this deterioration in performance due to motion blur is more severe as compared to similar amount of blur caused by defocus. This may be due to the fact that unlike defocus, motion could change the shape of iris texture in the captured image. Also, these results appear to indicate that an MTF of 60% at 2 line pairs/mm in the iris plain may be an overly high specification coined by ISO/IEC [56, 57].

One another scenario that may arise in smartphones is that the user has a well-focused sharp image acquired for enrollment. This image is matched with one of the blurred images acquired when user is trying to authenticate himself.

Two sets of experiments are carried out to analyze this scenario - (i) images with a defocus blur of level $\sigma = 5$ are matched against the original images in both CASIA and MMU1 database, (ii) images with a motion blur of level 5 are compared with the original images. The original images in the database are considered to be a sharp enrollment image, while the blurred image is considered as an authentication attempt. Performance of such scenarios is compared in Figure 4.9. From Figure 4.9, it can be noted that, iris recognition system is comparatively tolerant to defocus blur as compared to a similar level of motion blur when the blurred images are tested against the sharp enrolled images. This points that, when an iris acquisition system is designed, it is a higher priority to reduce the motion blur compared to the defocus blur. Hence a lower exposure time and a global shutter will play a crucial role than using extended depth of field (eDoF) elements.

4.3 Acquisition System Requirements

From the discussions in previous sections, a flow diagram of iris recognition systems for smartphones can be anticipated as in Figure 4.10. A complete iris recognition system consists of four principal modules (i) Image acquisition device which consist of an illumination source and a camera, (ii) pre-processing module, which mainly deals with liveness detection and image quality check and quality enhancement, (iii) main processing module, which is responsible for the core iris recognition tasks such as segmentation, normalization and feature extraction and (iv) the matching module contains a comparator and a security module. The matching module is connected to an iris database which may be present locally in the device or accessed remotely in a server. Each module is described in detail in the following sections.

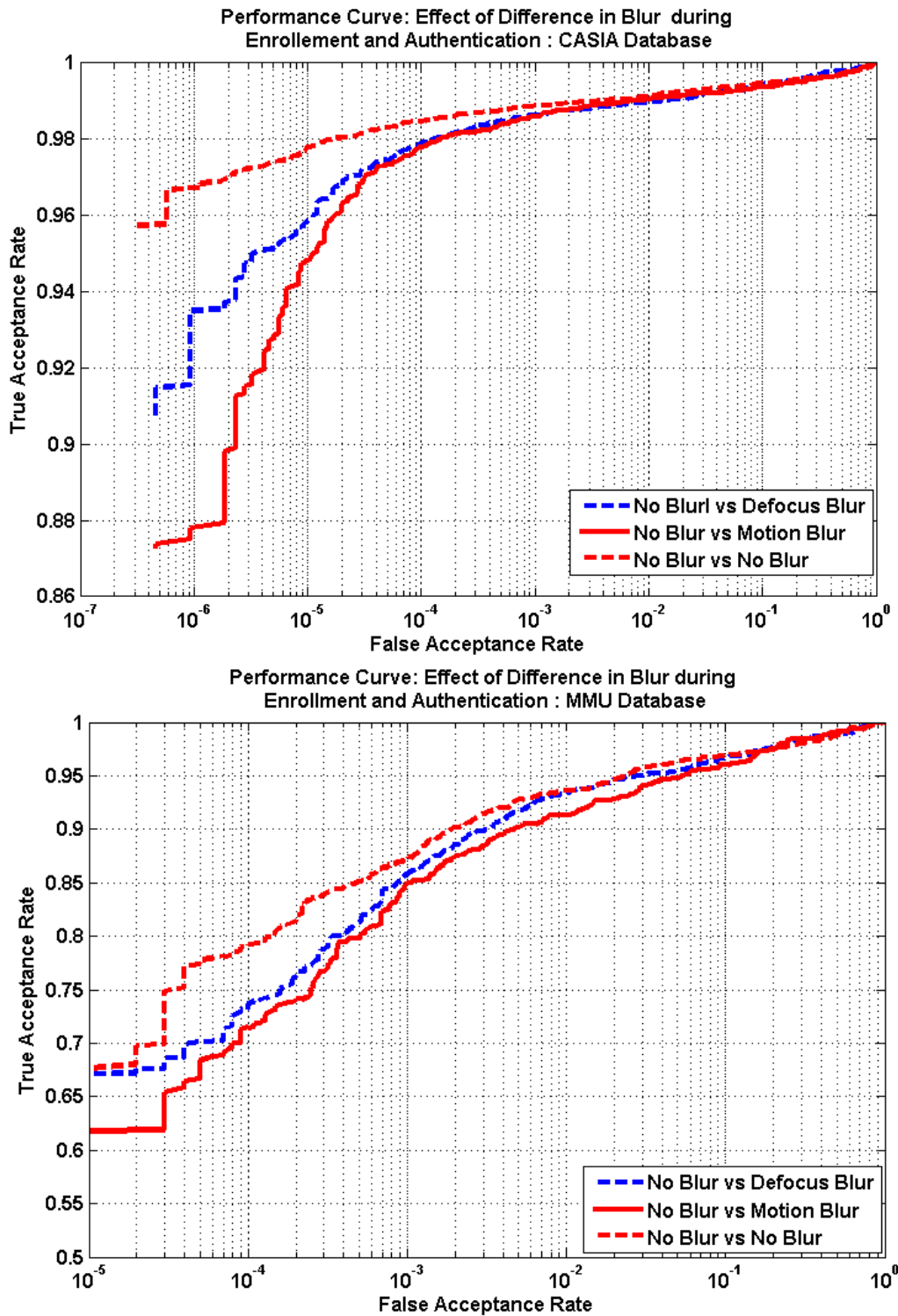


Fig. 4.9 Performance curves for CASIA v4 interval and MMU1 databases for different levels of blur during enrollment and authentication.

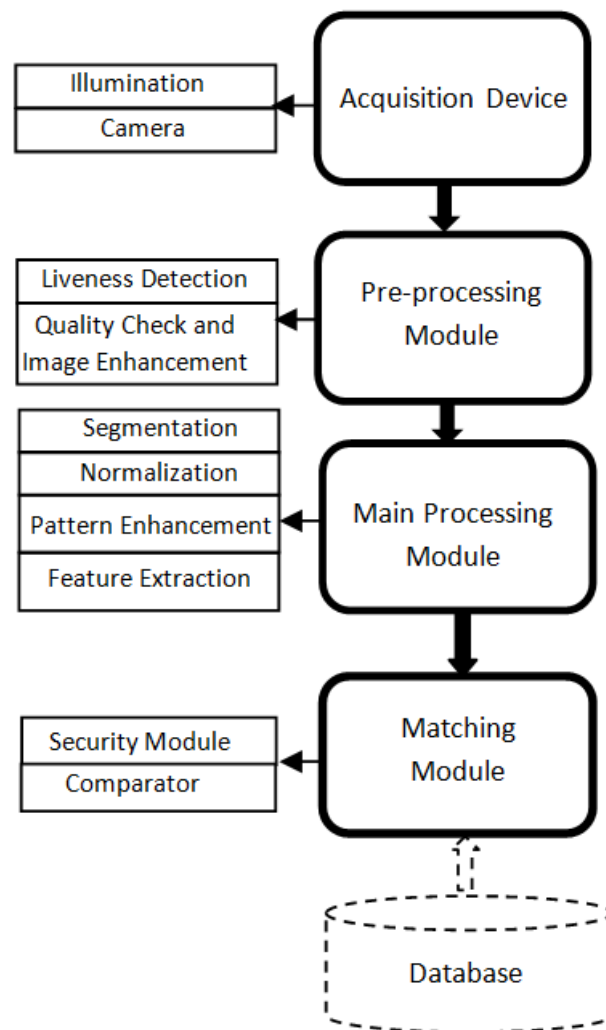


Fig. 4.10 Flow diagram of the proposed smartphone iris recognition system.

4.3.1 Acquisition Process: Wavelength and Illumination

Existing commercial systems use near infra-red (NIR), in the range 700-900 nm for iris image acquisition [59], [17]. This wavelength range has been chosen because NIR illumination is non-intrusive as well as it helps in revealing the detailed underlying iris pattern even for a heavily pigmented iris. Some studies have used visible light to determine and identify iris patterns [82–84]. However only lighter colored iris regions can provide useful patterns in visible light and in fact visible light will degrade the iris patterns in heavily pigmented iris [21]. A detailed discussion of the advantages of NIR over visible light acquisition is discussed in Section 2.2.1.

Studies have been made on the use of different wavelengths for iris image acquisition. Ross, Pasula and Hornak [81] explored the possibility of iris image acquisition beyond 900nm wavelength. Boyce *et al.* [34] discussed the potential of using multispectral information associated with NIR, and visible (RGB) wavelengths of the electromagnetic spectrum to improve segmentation and employ user specific wavelength for iris image acquisition. NIST MID-BPR recommends illumination of the wavelength 700-900nm which is compliant with various standards such as IEC 825-1 and International Standard ISO 60825-1 [45].

Thus, for optimal iris region acquisition it is recommended to use an NIR illumination and a band pass NIR filter on the acquisition system. In the context of a consumer device this requires redesigning the current imaging system and sensor. The availability of low cost NIR LED sources is of interest and these are often used in automotive environments, but have not yet been widely adopted in handheld imaging systems. Such NIR sources could be placed alongside or below the main user-facing camera to prevent shadows caused by eyebrows [56, 57]. ISO/IEC 19794-6 recommends an angle of 5 degree between the line extending from the center of the illumination source to the pupil center and the optical axis of the camera in order to avoid a NIR red-eye effect [56, 57]. An advantage of NIR illumination is that a non-visible light source does not annoy the user. The illumination intensity should be within the safety limits, but should take into account the shutter mechanism and exposure time to ensure that a good-quality, well-illuminated iris image is obtained.

4.3.2 Acquisition Process: Camera

The key element for acquiring high quality iris images is the imaging system. Early iris acquisition devices were user unfriendly and required high levels of user co-operation. These cameras typically provide a chin rest, or head bar to constrain the user during acquisition. A comparatively less constrained iris acquisition device was first presented by Wildes *et al.* [105]. This device uses an array of illuminators, a diffuser, a polarizer, two square edges and a silicon intensified camera as shown in Figure 4.11. This set up was intended to give a uniform illumination to cover a wider region and to reduce specular reflection.

One research direction from the literature has been focused towards designing a compact acquisition device that can provide high quality iris images. An example for such an acquisition device is given by Cambier and Siedlarz [106] as shown in Figure 4.12. This device uses a CCD or CMOS camera of focal length 14.2mm with a 1/3" monochrome sensor and a cold mirror.

Daugman noted that monochrome CCD cameras of resolution 480×640 are typical in commercial iris recognition systems [17]. These devices also assume user cooperation and

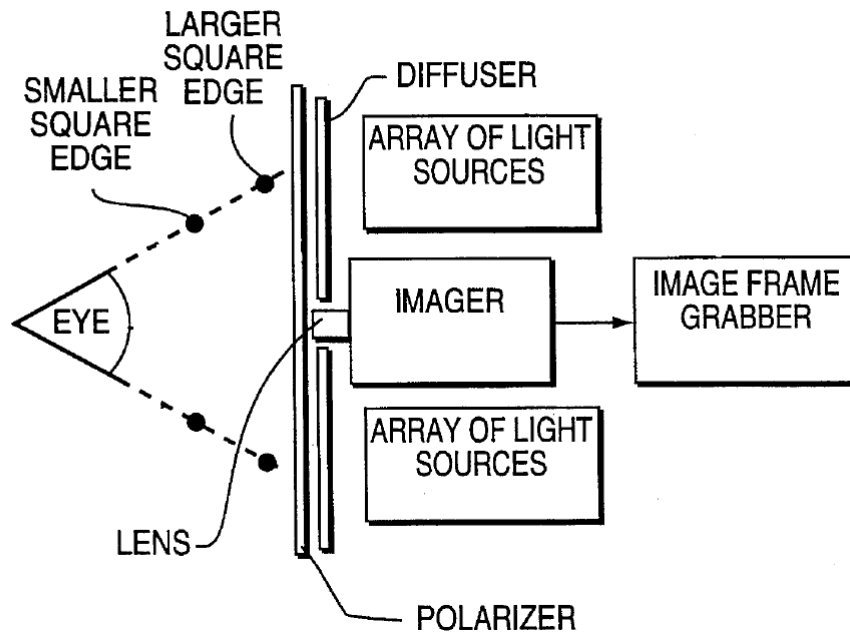


Fig. 4.11 Wilde's iris image acquisition device. Adapted from [105].

the size of optics make it impossible to use in today's thin smartphones. A comprehensive review of iris acquisition devices is given by Rakvik *et al.* [54].

A dedicated iris acquisition system is needed to provide a working solution based on the technology available in today's smartphones. Several key design questions that will shape a working reference design are considered below.

Dual Eye or Single Eye Capture?

One of the primary design considerations is whether the device should be a dual-eye image acquisition one or not. The NIST IREX III evaluation shows that false negative identification rate was reduced by a factor of two when both eyes are used for identification as compared to a single eye case [97]. Further, it is shown that dual iris approach is significantly better, particularly when the number of enrolled images is small as is likely for a personal smartphone [107]. NIST Mobile ID Best Practice recommends capturing both irises simultaneously for higher subject acquisition profiles, which will help to achieve higher accuracy and comparison speed [45].

Using both eyes together can greatly enhance recognition performance. It is noted that the false acceptance rate (FAR) (Section A.2) can decrease up to 1 in 1.2 trillion when both

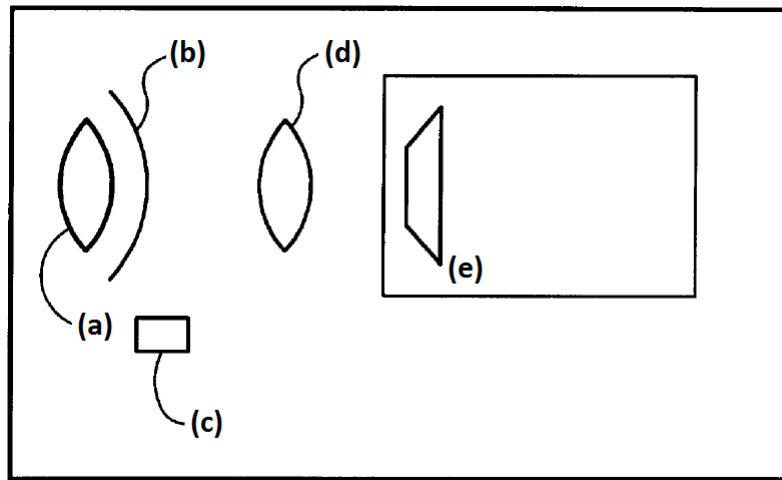


Fig. 4.12 Iris image acquisition device presented by Cambier and Siedlarz- (a) optical diopter correction lens, (b) mirror, (c) illuminator, (d) imaging lens and (e) sensor. Adapted from [106].

eyes are used, where an FMR of 1 in 1.2 million is noted when a single eye is used [28]. This is particularly important as we may find that it is necessary to compromise other aspects of iris image quality. However there are some challenges as such an approach requires a dual illumination system and it is challenging to ensure that both eyes are equally illuminated in an unconstrained environment.

The most practical approach may be a single-eye acquisition system that can obtain a pair of eyes sequentially, while tracking the individual eye regions. Such an approach could be implemented by requiring the user to execute an eye sweep or side-to-side head movement, or alternatively by employing a directed light source that illuminates each iris region in turn. This will certainly take longer and be a greater burden on the user. Also, in large scale deployments, it is noted that the performance of iris recognition when two iris images of an individual are acquired one after the other are less accurate than the case where both eye images are acquired simultaneously [108].

One Camera or Two?

The best use case for iris acquisition on a smartphone is in the ‘video-call’ mode when the user-facing camera is naturally acquiring a stream of images. However today’s user-facing cameras do not have sufficient quality to acquire a useful iris pattern at NIR wavelengths, as they are designed for a wide field-of-view, usually have fewer pixels than the higher quality rear-facing camera and are optimized for visible RGB imaging.

A hybrid single-camera design was investigated but presents some difficult design challenges: (i) a movable NIR optical filter might be needed to support iris acquisition mode, or alternatively a dedicated second NIR detector must be provided; (ii) optical design at visible and NIR wavelengths has to be optimized for two different sets of requirements, but using the same CMOS sensor. Such systems can be depicted as in Figure.4.13(b).

Another solution presented by Kim *et al.* [109] uses two sensors - one designed for visible light and another designed for NIR radiation is used. A reflection/ penetration filter is used to allow the light in the visible area to pass through and reach the specific visible light sensor and reflects the NIR waves to the iris sensor. The feasibility of this camera for today's ultra-thin smart phones has yet to be examined in detail, but on initial evaluation it too appears infeasible.

The alternative is a dual-imaging system (Figure.4.13(a)). This increases costs, but has several advantages: (a) the field of view (FoV) of the infrared imaging system can be reduced, increasing pixel resolution and image quality in the iris region; (b) visible and infrared optical designs are independent, so that both can be optimized independently and (c) no movable IR filter is needed. Despite the added costs of a second imaging system the two-camera approach has some compelling advantages.

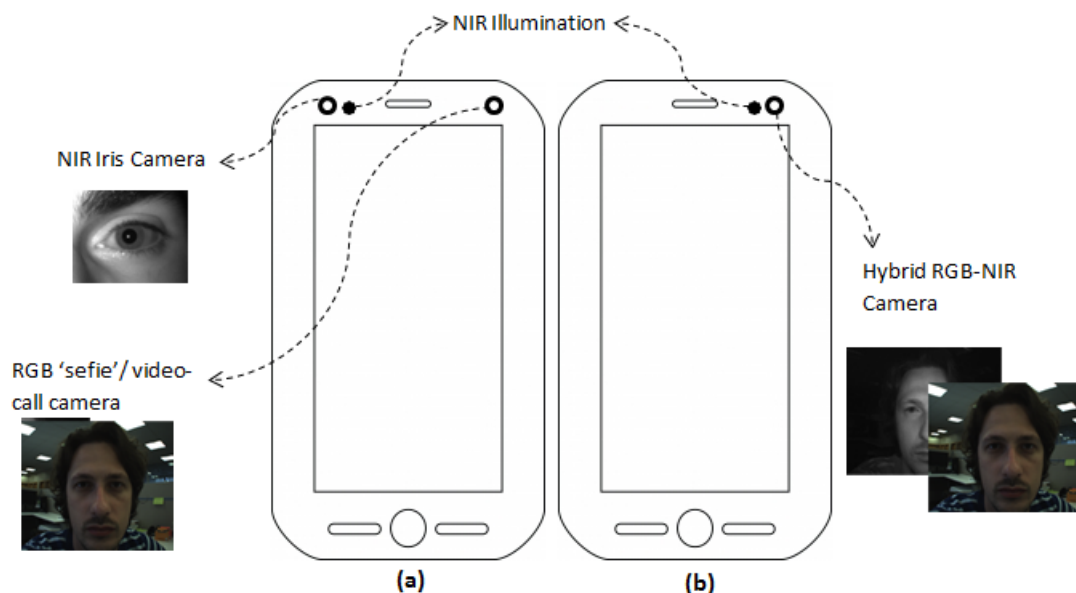


Fig. 4.13 Iris acquisition on smartphones. (a) Dual camera system - one camera for general purpose use such as video call and one dedicated iris camera for iris acquisition, (b) hybrid front facing camera - This camera will acquire both RGB and NIR images simultaneously.

Irrespective of the choice between a single hybrid imaging system or a dual-imaging system, there are further design considerations such as scanning type, SNR and maximum exposure time [56, 57, 45]. Also, as per the studies carried out in Section 4.2.2, the acquisition system should be able to capture an iris with 50-100 pixels across iris diameter. This will define the spatial resolution of the sensor and field of view(FoV) of the lens for a given subject stand off distance from camera. In the near future, progressive scanning and global shutter are expected to be used to reduce the effect of motion blur in the iris images.

4.3.3 Face and Eye Tracking, Focus and Exposure

Modern cameras implement hardware face detectors [110] to track faces and eye-gaze [111, 112]. Tracking data can be used in turn to perform a continuous focus on the face region [113]. Also, face detection can be used to optimize image exposure on handheld devices [114]. The proximity sensor of the phone or the measure of interpupillary distance can be used to precisely calculate the distance of the person from the phone. This enables acquiring images when the eyes are in the depth of field of the camera. Given the extent of established technologies embedded in today's camera modules, acquiring well-focused eye regions in an image should not prove unduly challenging.

4.3.4 Iris Analysis and Authentication: Preprocessing

As an initial step, the iris recognition system has to make sure that a legitimate live user is accessing the system, instead of presenting the adversary copies of the biometric sample (in our case, iris image) such as a recorded video, printed contact lens or a high quality iris image kept in front of original eye. Reference [53] discusses various liveness detection techniques for iris biometrics in detail. Though, human supervision can be the most effective way for this and used widely in many applications including UAE border control program, it is not possible in case of smartphones. Hence, effective automatic liveness detection is necessary. It has to be noted that, even though liveness detection is an essential part of iris recognition system as a countermeasure against spoofing, it comes with the cost of an increase processing time, increase in hardware or software and negative effect on recognition performance [53].

As we have seen in the previous sections, a good quality iris image affects the recognition performance positively. The majority of the image quality factors depends on the acquisition system, the acquisition scenario or the capture practice. Typically a sequence of images is captured and an image quality evaluation is carried out on these images. One or two best quality images among the lot are selected for further processing and/or the image quality will be enhanced using state of the art iris image enhancement techniques [115].

4.3.5 Iris Analysis and Authentication: Main Processing

Most commercial iris recognition systems use Daugman's original approach to iris recognition [17]. His work showed that it will take only 0.45 seconds for the whole iris recognition process from assessing the focus, iris localization, occlusion detection and masking, feature extraction to comparison of two feature vectors on a 300MHz RISC processor. This algorithm can be used 'as is' in today's smartphones and the computation power of such devices guarantees fast iris recognition. Recent improvements on segmentation, pattern enhancement, feature extraction, and other techniques will improve system performance and reliability. In the proof of concept tests summarized in Section 4.2, it is shown that segmentation plays a crucial role in recognition performance. State of the art techniques can be used to improve segmentation [116], [117]. Feature extraction can be further improved by using techniques like fragile bit masking, dividing iris region into different groups and encoding by giving each region different weights [118, 119] or using computationally efficient techniques presented by Savvides *et al.* [120].

4.3.6 Iris Analysis and Authentication: Security

The security module is one important part of an iris recognition system. This module is responsible for the template security and can be considered as a template protection system. The two major requirements of this module are the irreversibility and unlinkability of the protected biometric template [121]. This can be achieved in two ways, either by using a biometric cryptosystem or using cancellable biometrics. A detailed review is given by Rathgeb and Uhl [121]. Fuzzy vault scheme proposed for fingerprint template protection on mobile device can be easily extended to iris data and can be considered as a potential candidate [122]. However, the biometric data is vulnerable to attack and theft if it is stored in the device or a central database. Instead, using the biometric data to generate an enrolment key, which is stored and used for comparison, can be used to overcome this situation [46]. In this way, by restricting the biometrics analysis to the device and not storing any biometric data, we can counter the concerns related to biometric theft. This supposes a two-stage authentication where both person and device are required to complete the authentication procedure.

4.4 Discussions and Conclusions

In this chapter, the feasibility of iris authentication in smartphones using a constraint-free acquisition workflow is explored. Various image quality parameters that may affect the iris

recognition performance on such devices are identified. Initial experiments and analyses were carried out to determine the minimum spatial resolution, effect of defocus blur and motion blur in order to define key design criterias. Based on these analyses, various potential system design strategies were presented. A summary of primary design considerations for smartphone iris acquisition is shown in Figure 4.14. The analyses and discussions presented

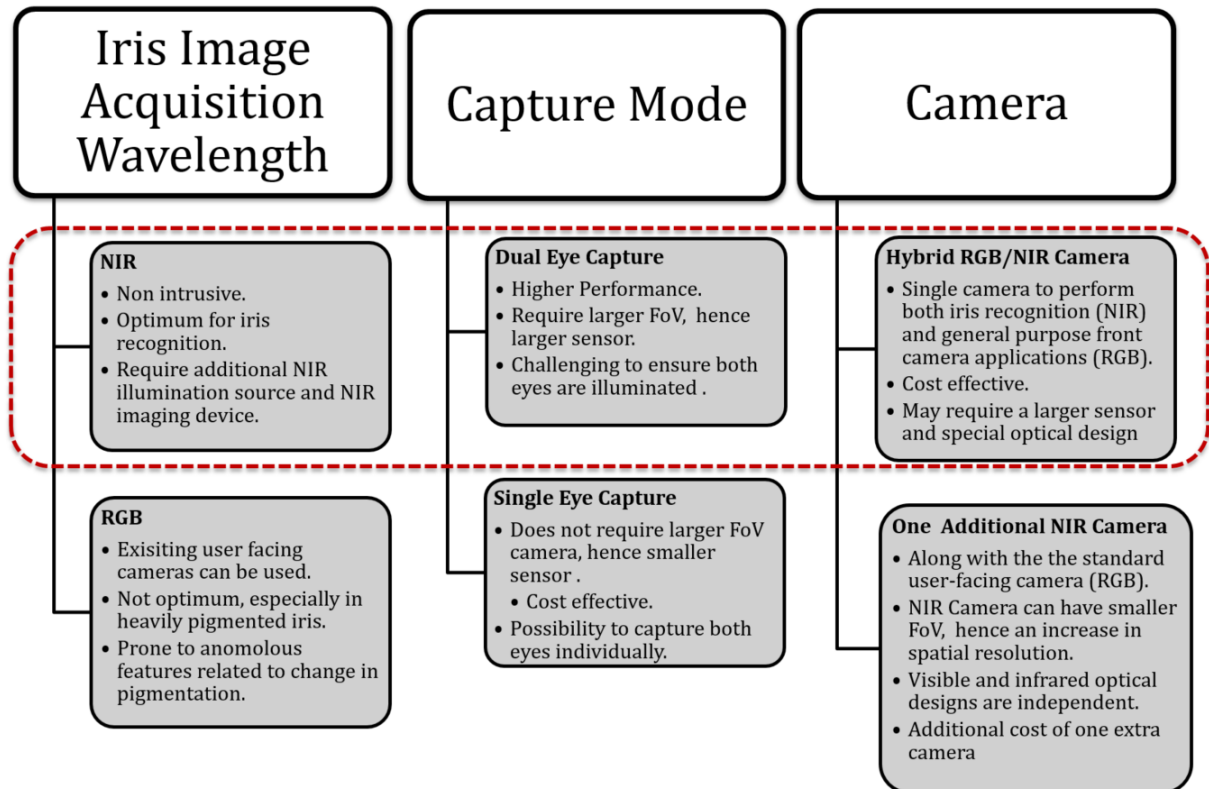


Fig. 4.14 Summary of primary design considerations for smartphone iris acquisition device. Our recommended choice based on the performance and cost-effectiveness is shown in the highlighted selection.

in this chapter lay a foundation for the design of more reliable, unconstrained iris recognition systems for next-generation smartphones.

Chapter 5

Proof-of-Concept and Evaluation of a Dual Function Visible/NIR Camera for Iris Authentication on Smartphones

A detailed analysis and various design considerations for an iris acquisition system for smartphones were presented in the previous Chapter. While the visible wavelength camera systems on today's devices can aid iris detection and segmentation, the final acquisition is best performed at NIR wavelengths. One potential working solution described in Chapter 4 is a dual camera visible and NIR imaging system. However this solution has associated increased costs and the additional complexity of integrating a dual imaging system into the device.

The work presented in this Chapter takes advantage of the recent availability of dual visible/NIR CMOS sensors [123, 124] to provide an alternative design that combines both visible and NIR imaging into a single optical and sensor system. Although these sensors have not yet seen significant adoption, they can provide benefits in low-lighting conditions where NIR illumination enhancement does not impact on the human visual system. NIR image data can also serve to enhance the quality of visible images, thus justifying the additional costs associated with such hybrid sensors.

A prototype device based on such hybrid sensors is presented in this chapter and evaluated for its feasibility to implement iris recognition on smartphone. This chapter is a consolidated version of the following publications– (i) Shejin Thavalengal, Petronel Bigioi and Peter Corcoran, “Evaluation of Combined Visible/NIR Camera for Iris Authentication on Smartphones”, in proceedings of the 2015 Computer Vision and Pattern Recognition (CVPR 2015) Biometric Workshop, Jun.2015, Boston, USA; and (ii) Shejin Thavalengal, Istvan Andorko, Alexandru Drimborean, Petronel Bigioi and Peter Corcoran, “Proof-of-concept

and evaluation of a dual function visible/NIR camera for iris authentication in smartphones”, IEEE Transactions on Consumer Electronics, vol.61, no.2, pp.137-143, May 2015. Note that printed circuit board (PCB) design and system implementation are due to engineers from the industry partner that sponsored this thesis research. The author’s contributions are the testing and evaluation of the system as documented in this chapter.

5.1 Dual Function RGB NIR Camera for Smartphones

For smartphones, a typical use case could be user authentication while holding the device at a comfortable arm’s length. A single user-facing camera to capture both visible (such as video call, selfie imaging) and NIR (iris) image data is considered to be ideal in terms of cost and usability. Such an RGB-NIR dual function prototype camera is presented here along with a feasibility study of iris recognition through the use of such a device. Various important components of the prototype device can be described as:

5.1.1 Sensor

Single sensor digital cameras use colour filter array (CFA) to sample different spectral components. In this kind of arrangement, only one colour is sampled at each pixel location. The most commonly used CFA is a Bayer pattern, which is shown in Figure 5.1(a) [125]. US 8446470 B2 presented a combined RGB and IR imaging sensor. This sensor replaces half of the green pixels with IR pixels in the normal CFA [123]. The CFA of such a sensor is shown in Figure 5.1 (b).

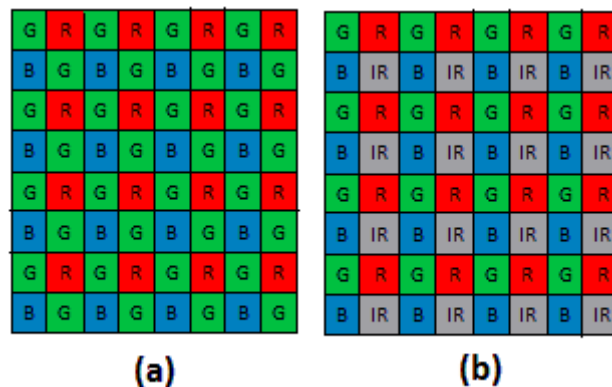


Fig. 5.1 Example for CFAs: (a) Bayer CFA, (b) CFA presented in US 8446470 B2 [123]. R, G an B represents Red, Green and Blue colour sampling filters respectively. IR represents NIR sampling filter.

This sensor was primarily aimed for use in an imaging system for vehicles to obtain a more accurate true colour representation of the pixels and to limit infra-red colour wash out [123]. Such a sensor could be used in developing a hybrid front facing dual purpose camera for smart phones.

OmniVision's OV4682 is such an RGB-IR single sensor, which is aimed to be used in cellular phones and other digital still cameras [124]. This sensor has a maximum lens chief ray angle of 21° , which restricts the focal length of the optical system to be approximately 4 mm. This sensor is used in the development of our prototype device.

5.1.2 Filters

In every single sensor digital camera with silicon sensors, the spectral sensitivities of red, green, and blue pixels will have a peak in NIR wavelength region [126]. Current commercial cameras, including the smartphone ones, employ an IR-absorbing filter to prevent these NIR waves reaching the sensor. Such a hot mirror could not be used in a prototype device for iris recognition as this device aims to acquire NIR iris images. Two of the possible solutions in this case are- (i) the complete removal of the IR filter or (ii) the use of a dual-band pass filter which is tuned for both the RGB and a narrow region of NIR wavelengths.

The first option, with no IR filter, would be the optimal solution for iris recognition, as the IR sensor elements would capture information from a wide range of IR wavelengths. The issue in this case is that the proposed sensor should also be capable to reproduce good quality RGB images if it is to be used as a user-facing camera. With the rise of the self-portrait, or 'selfie', these cameras have become a key feature of modern smartphones, requiring an ability to acquire high-quality personal portrait image. Thus if IR light is not prevented from entering the R, G and B sensing elements of the sensor, the quality of the image would be significantly altered. For this reason, the second option was chosen for our proof-of-concept implementation.

The dual band-pass filter used in the proposed system design follows the filter response characteristics illustrated in Figure 5.2. This filter will not only pass all the RGB information as in any other standard camera, but also passes a narrow range of wavelengths around 850nm. This second passband is provided to facilitate iris recognition.

The red, green and blue pixels will typically have similar NIR response as the IR-only pixels. Hence, even with such a filter, there is a possibility of NIR inference in the RGB image, particularly if there are high levels of ambient NIR e.g. in bright sunlight. This effect is expected to be minimum as a very narrow band of NIR is passed with the current filter. This effect can be corrected by using an appropriate colour correction algorithm such as a

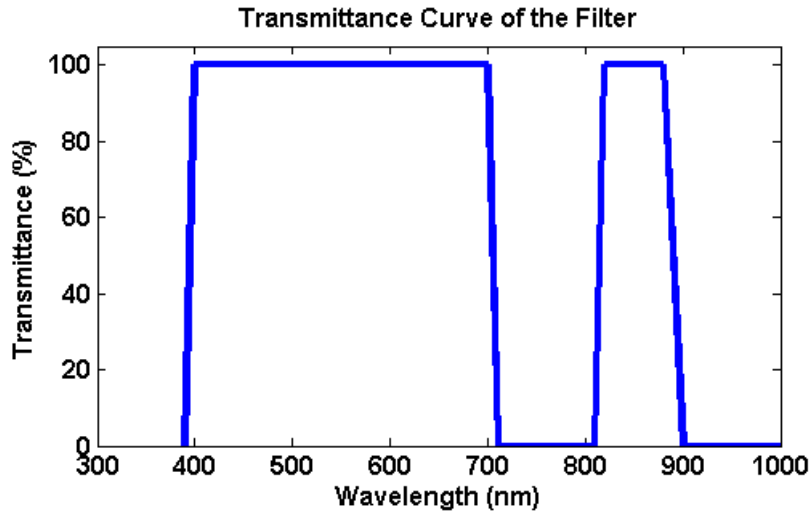


Fig. 5.2 Transmittance curve of the filter used in the proof-of-concept device.

weighted subtraction of IR pixel intensity from red, green and blue pixels in a 2×2 sub pixel array [123].

5.1.3 Illumination

Two near infra-red LEDs of wavelength 850 nm and half intensity angle 60° are used on each side of the camera as the active illuminator in the proposed system. The choice of these specific illuminators is mainly based on the transmittance characteristics of the filter used on the sensor as well as the general practice in iris recognition. The LEDs are placed in such a way that it illuminates both eyes of the user and the specular reflections are confined inside the pupil area for our typical operating range of 15-25 cm from the camera.

The overall specification of this prototype device is shown in Table 5.1. A typical NIR

Parameter	Value
Sensor Size	1/3"
Aspect Ratio	16:9
Sensor resolution ($w \times l$)	2688×1520
Pixel size	$2\mu m \times 2\mu m$
Focal length (f)	4mm
F number (F)	2
Scan Mode	Progressive
Active Illumination (λ)	850nm

Table 5.1 System parameters.

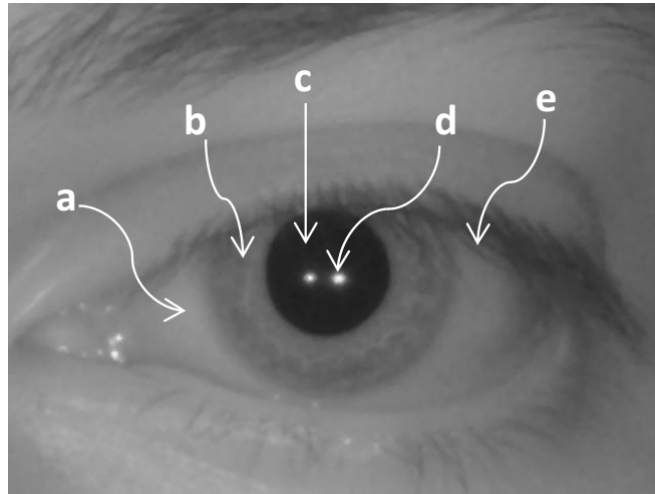


Fig. 5.3 A typical eye image captured using the prototype device. (a) sclera, (b) iris, (c) pupil, (d) specular reflection and (e) eyelashes.

eye image captured using this prototype device is shown in Figure 5.3. Also, the prototype device is shown in Figure 5.4.

5.2 System Dataflow

The captured data goes through several processing stages before it is sent to the iris recognition module and the RGB image signal processor (ISP). These processing stages are shown in Figure 5.5

The images obtained by the frame grabber are sent to the image resampling module. This module separates RGB and NIR channels and send to their respective processing modules as requested by the application. These processing stages are described briefly in the following subsections.

5.2.1 Frame Grabber

The first stage of the data flow is the frame grabber. This stage is responsible for tracking face and eye regions and acquiring the image when triggered by an application. A realtime face tracking technique is used for this purpose [127]. The frame grabber will capture the mosaic pattern (as the one shown in Fig. 1(b) at a resolution of 2688×1520). This mosaic pattern is then transferred to the image resampling module.

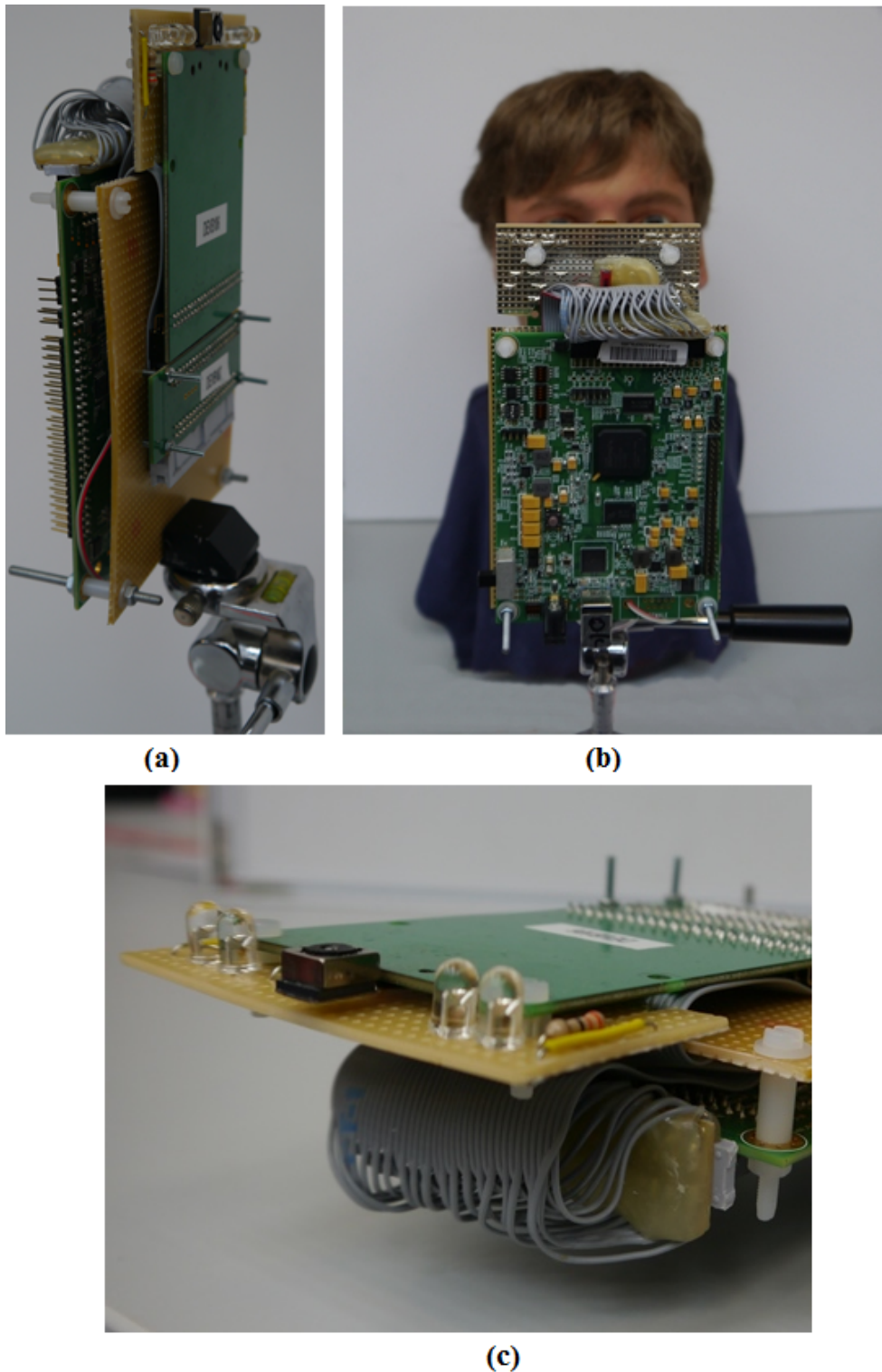


Fig. 5.4 The prototype device: (a) side view - Smartphone form factor optics can be observed, (b) rear side -This image represents a typical iris image capture scenario, (c) close up view of the optics.

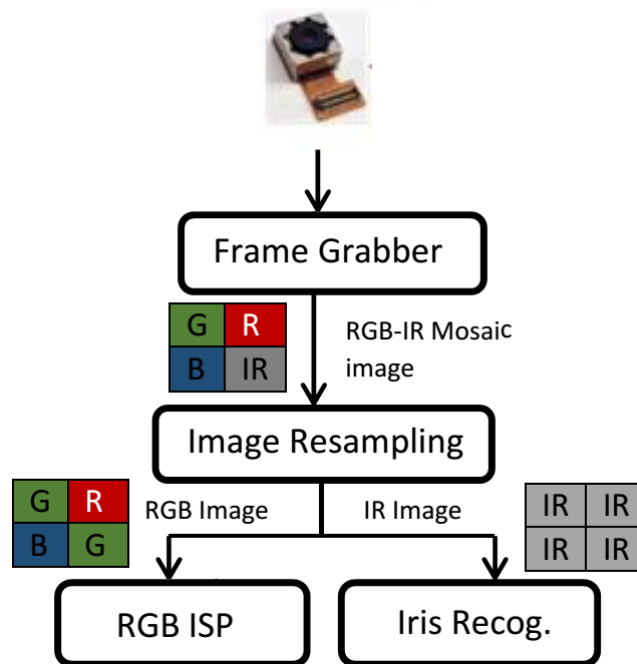


Fig. 5.5 System overview of the proof-of-concept device.

5.2.2 Image Resampling Module

During this stage, RGB and IR data is separated. The missing G pixel values are restored by analyzing the 2x2 neighborhood to obtain the standard Bayer pattern (as the one shown in Fig. 1(a)). This Bayer pattern is transferred to the RGB ISP for further processing.

In the case of IR information processing, such as iris recognition, eye region is cropped from the mosaic pattern. IR pixels in these cropped regions are enhanced and super resolved using a proprietary algorithm. This algorithm uses RGB information for guided IR image super resolution. Also, red and green channel information is used for reducing the noise in the IR image and hence enhancing the image quality. This enhanced iris image is then passed to the iris recognition module.

5.2.3 RGB ISP

RGB ISP is responsible for demosaicing, noise removal, lens shading, white balance and tone reproduction of the RGB Bayer pattern. A detailed discussion on RGB ISP can be found at [128].

5.2.4 Iris Recognition Module

Iris recognition module processes the input eye image and authenticates the user by analyzing his iris pattern. Iris and pupil are detected from the input IR eye image. The iris is segmented and the segmented iris image is encoded based on a specific encoding scheme. This encoded feature vector is then matched to the feature vectors stored in the database to authenticate the user.

5.3 Optical Analysis of the Prototype Device

This section analyses the suitability of the prototype device for iris recognition. The important camera parameters are shown in Table 5.1. Considering a typical iris acquisition scenario using smartphones with a stand-off distance $d = 200\text{mm}$ and assuming a circle of confusion $c = 2\mu\text{m}$ (one pixel), the far point (S) and near point (R) in which the image is in focus are given by [76],

$$[R, S] = \frac{df^2}{f^2 \pm Fcd}, \quad (5.1)$$

which gives

$$S = 210.53\text{mm}, R = 190.48\text{mm}. \quad (5.2)$$

Hence, the Depth of Field (DoF) is,

$$DoF = S - R = 20.05\text{mm}. \quad (5.3)$$

At a stand-off distance of $d = 200\text{mm}$, this camera will have a magnification factor M ,

$$M = \frac{f}{d-f} = 0.02041. \quad (5.4)$$

That is, this camera will magnify the iris by 0.02041 on to its sensor. Also, vertical field of view (FoV_v) and horizontal field of view (FoV_h) can be calculated as below [76],

$$FoV_v = 2 \arctan \left(\frac{l}{2f} \right) \quad (5.5)$$

$$= 2 \arctan \left(\frac{1520 \times 2\mu\text{m}}{2 \times 4\text{mm}} \right) \approx 42^\circ \quad (5.6)$$

$$FoV_h = 2 \arctan \left(\frac{w}{2f} \right) \quad (5.7)$$

$$= 2 \arctan \left(\frac{2688 \times 2\mu\text{m}}{2 \times 4\text{mm}} \right) \approx 67^\circ. \quad (5.8)$$

5.3.1 Equivalent Pixel Dimensions and Optical Resolution

Hence, at 200mm stand-off distance, this camera will enable us to capture a horizontal distance,

$$d_h = 2 \tan \left(\frac{FoV_h}{2} \right) \times d \approx 265\text{mm}. \quad (5.9)$$

Similarly, a vertical distance (d_v) of $\approx 154\text{mm}$ can be obtained. That is, at 200mm, this camera can provide a capture box of $265\text{mm} \times 154\text{mm}$ and a depth of field of 20.05mm. Considering a maximum inter-pupillary distance of 78mm [77], this capture box will be sufficient to obtain both eyes simultaneously. Further, assuming an iris of size 11mm [17], a magnification of 0.02041 (as shown in 5.4) will result in an iris image of $224\mu\text{m}$ diameter on the sensor. The sensor has a pixel size of $2\mu\text{m}$, so assuming a fill factor of 100% the iris will have 112 pixels diameter on the sensor. But, due to the nature of the particular CFA used here, IR values are sampled at alternate locations on the sensor. Hence, the number of true IR pixels across iris will be reduced by a factor of two in both horizontal and vertical directions. That is, in this set up, iris will have 56 true, non-up sampled pixels across the diameter.

Within the depth of field, the iris will have pixel range of 53 to 59 pixels on sensor. This is less than the marginal quality of iris image as outlined in ISO/IEC 19794-6 and NIST Mobile ID best practice [56, 45], but could be acceptable as per the studies shown in [78, 55, 129].

However, some valid NIR information would also be available from the RGB pixels (as the colour filters do not block light at 850nm and the global cut off IR filter will have to have a pass band around 850nm to allow the IR pixels to function). This information could be used to obtain complimentary estimates of NIR intensity for R, G and B pixels which could help in iris recognition.

5.3.2 Modulation Transfer Function of Diffraction Limited System

For a perfect optical system, with uniformly illuminated and uniformly transmitting aperture, the modulation transfer function (MTF) can be calculated as [79]

$$MTF_{optics}(v) = \frac{2}{\pi} (\phi - \cos \phi \sin \phi) \quad (5.10)$$

where v is the spacial frequency in *cycles/mm* and ϕ can be obtained as,

$$\phi = \arccos(F\lambda v). \quad (5.11)$$

where F is the F number and λ is active illumination. The limiting resolution for the aberration free system can be calculated as,

$$v_0 = \frac{1}{F\lambda} = 588.2 \text{ cycles/mm}. \quad (5.12)$$

That is, the optical system presented here cannot transmit information at a higher spatial frequency than $v_0 = 588.2 \text{ cycles/mm}$.

Sensor MTF can be calculated assuming square pixels and 100% fill factor as,

$$MTF_{sensor}(v) = \text{sinc}(v\delta_x) \text{sinc}(v\delta_f) \quad (5.13)$$

where v is the spacial frequency, δ_x is the pixel pitch, δ_f is the detector footprint and

$$\text{sinc}(x) = \frac{\sin(\pi x)}{\pi x}. \quad (5.14)$$

The system MTF can be calculated as,

$$MTF_{system} = MTF_{optics} \times MTF_{sensor}. \quad (5.15)$$

The ideal system MTF for the acquisition device presented here is shown in Figure 5.6. From Figure 5.6, it can be observed that, at 60% system modulation, this set up provides an optical resolution of 1.89 line pairs/mm (lp/mm) on the object plane. This is less than the ‘marginal’ quality of 2 line pairs/mm defined by ISO/IEC 19794-6 standards [56].

Similar analyses can be done on two other stand-off distances - 150mm and 250mm from the device. The results are summarized in the Table 5.2.

From Table 5.2, it can be observed that images captured at 200mm and 250mm stand-off distances will be of unacceptable quality as per the ISO standards [56], both in terms of true number of pixels across iris and optical resolution. But, images captured at stand-off distances 200mm and 150mm will have more than 50 true, non-up sampled pixels across iris

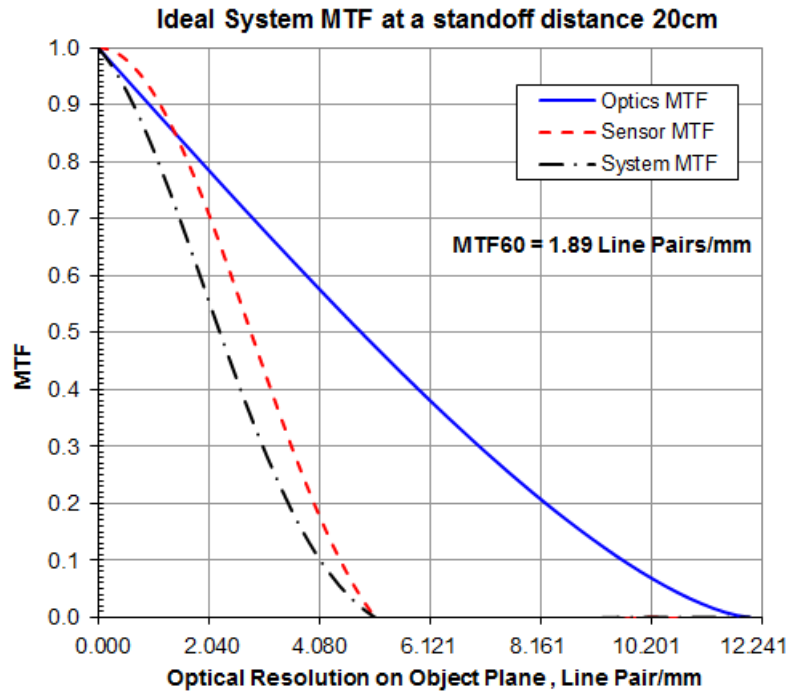


Fig. 5.6 Ideal System MTF plot for 200mm stand-off distance.

diameter, which may contain sufficient information for iris recognition [78, 129]. Images acquired at a stand-off distance 150mm are of better quality as compared to the other two image sets both in terms of number of pixels across iris and optical resolution. The ideal optical resolution at this distance is ‘marginal’ as per ISO standard [56]. Note that, as the stand-off distance decreases, the depth of field also decreases. Hence a use case where images will be acquired at a distance less than 150mm from the smartphone will be overly constrained and user-unfriendly. Also, these properties are calculated assuming ideal optics, 100% fill factor and 100% sensing area for each pixel. The practical system will deviate far from these ideal conditions and hence, can result in reduced image quality. A key goal of this study is to quantify how far the system deviates from acceptable levels of performance.

The practical system modulation transfer function (MTF) at 200mm stand-off distance of this device was measured using the Imatest tool [130]. For MTF calculation, NIR images captured with an illumination of 850nm were used. The MTF plot is shown in Figure 5.7.

From Figure 5.7, it can be observed that, at 60% system modulation, this set up provides an optical resolution of 1.14 lp/mm on the object plane. Similarly, for 150mm stand-off distance, this will be 1.18 lp/mm. These values are less than the ideal values shown in Table 5.2 as well as the ‘marginal’ quality of 2 lp/mm defined by ISO/IEC 19794-6 standards [56].

Parameter	$d=150\text{mm}$	$d=200\text{mm}$	$d=250\text{mm}$
Number of Pixels across iris diameter	72-78	53-59	42-48
Depth of Field	11.21mm	20.05mm	31.37mm
Dual Eye Capture	Yes	Yes	Yes
Optical Resolution at 60% modulation	2.54 lp/mm	1.89 lp/mm	1.51 lp/mm

Table 5.2 Summary of optical analysis for different stand-off distances.

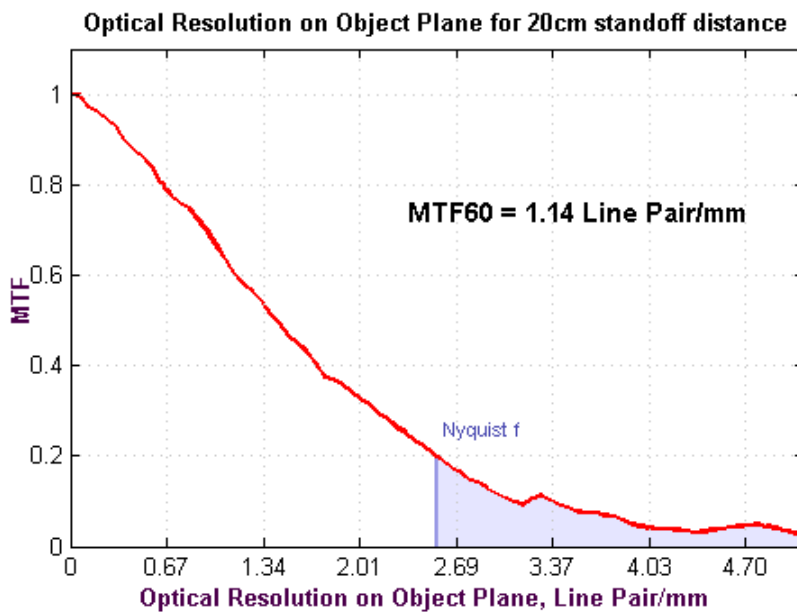


Fig. 5.7 MTF plot for 200mm stand-off distance.

5.3.3 Diffraction Limit Calculation

A brief discussion on diffraction limit is given in Section 3.1.3. The radius of the Airy disk, which is a result of the lens diffraction limit, can be calculated for our prototype system ($\lambda = 850\text{nm}$, $F = 2$) as,

$$r = 1.22F\lambda, \quad (5.16)$$

$$= 2.07\mu\text{m}. \quad (5.17)$$

According to Rayleigh criterion, two separate point images can be resolved if the radius of the Airy disk is less than the pixel size. That means, this is the smallest theoretical pixel of

detail [76, 80]. In the optical system presented here, the radius of the Airy disk is close to the pixel size. However, it is clear from the MTF that the lens is far from diffraction-limited.

5.4 Data Acquisition and Iris Recognition Experiments

The analyses in the previous section (Section 5.3) show that iris images obtained using our device may not be adequate for iris recognition. In order to experimentally evaluate feasibility of iris recognition on these images, we have gathered a database internally¹. The database consists of images from 25 subjects acquired at two different distances- 15cm and 20cm from the device. Active illumination of 850 nm was used for image capture. Ambient illumination was not constrained while images were acquired. The dataset consists of subject with eye colours varying from blue to dark brown. Iris images are cropped automatically by the face and eye detection algorithms developed internally. The images are then fed to an open source iris recognition algorithm - OSIRIS v4.1 [131]. A total of 244 images were captured at 15cm stand-off distance and 311 images for 20cm stand-off distance. Examples for images are shown in Figure 5.8.

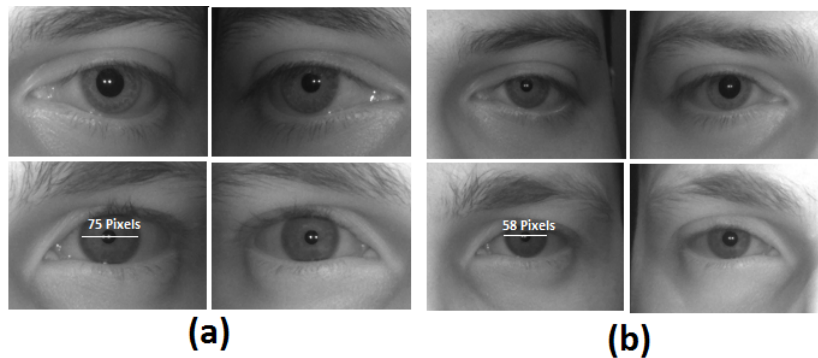


Fig. 5.8 Examples of iris images captured using the prototype device at (a) 15cm standoff distance and (b) 20cm standoff distance. The number of pixels across iris is also marked.

5.4.1 Analyses and Observations

Receiver Operating Characteristic (ROC) curves of these experiments are shown in Figure 5.9. From Figure 5.9, it can be observed that, images captured at a stand-off distance 15cm outperform the images captured at 20cm. This may be due to the fact that the former set of images has a better optical resolution and more number of pixels across iris diameter, and

¹The database will be made available for research once we have obtained the approval of the research ethics committee of NUIG and consent of the industry partner. Relevant processes have been initiated.

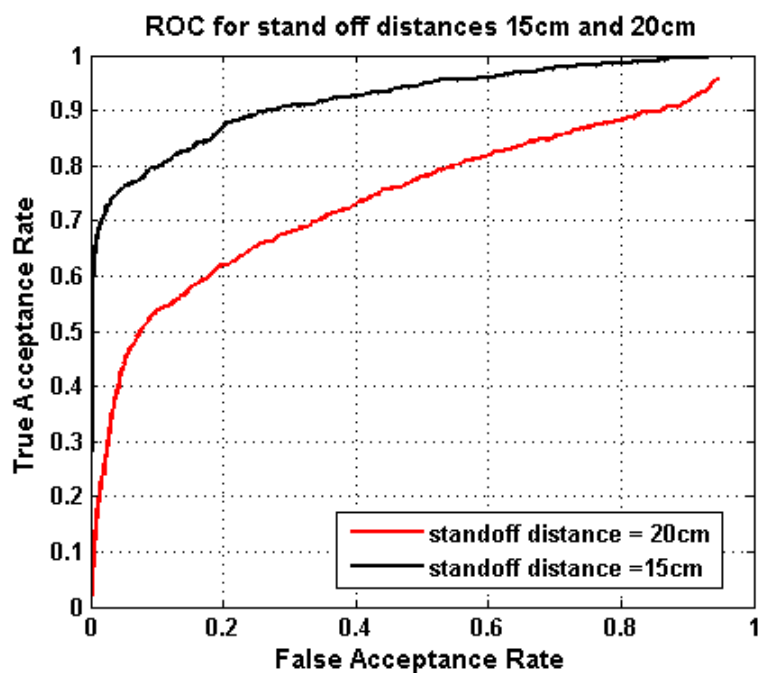


Fig. 5.9 ROC curves for 15cm and 20cm stand-off distances.

hence more information on the iris region. Further, the score distribution of these two sets of experiments are shown in Figure 5.10. From Figure 5.10, it can be noted that, inter-class

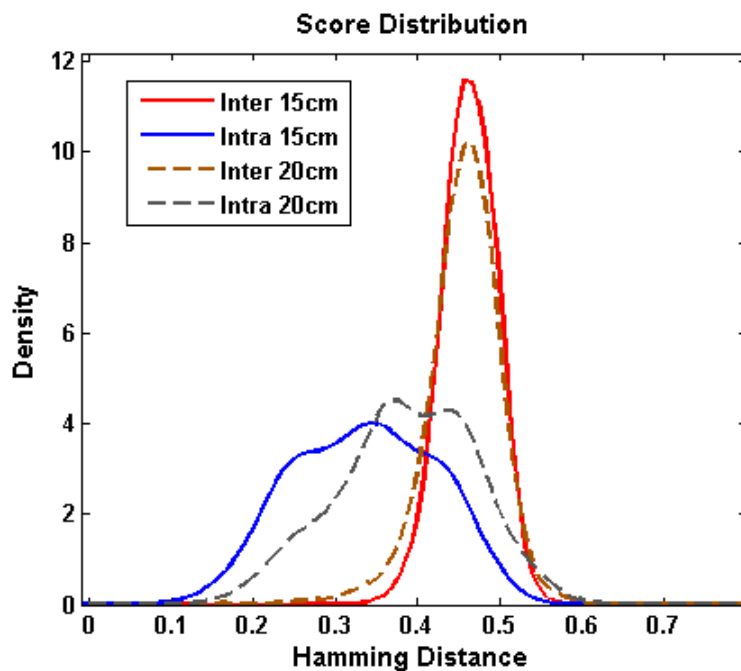


Fig. 5.10 Score distribution for 15cm and 20cm stand-off distances.

comparisons in both cases form a narrow range normal distribution with mean around 0.45 hamming distance. But intra-class comparisons shows a wide distribution with considerable overlap with the inter-class comparisons.

A careful analysis revealed that segmentation algorithm failed to detect the iris and pupil accurately on 10.66% and 27.49% images, on 15cm stand-off distance and 20cm stand-off distance cases respectively. This is most likely the main reason for large hamming distances on intra-class comparison. A second set of experiments was carried out after removing the images in which segmentation algorithm failed to detect an iris or pupil. Images with small segmentation errors were tolerated. The comparison of ROC curves is shown in Figure 5.11.

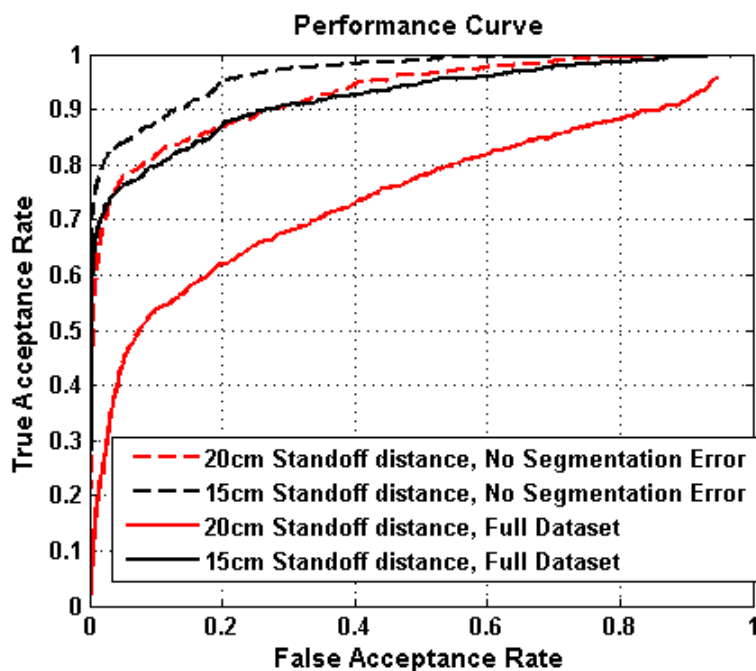


Fig. 5.11 Performance comparison between full image set and image set with improved iris segmentation for 15cm and 20cm stand-off distance.

From Figure 5.11, it is evident that improving iris segmentation can improve the performance significantly. Score distributions of these experiments were compared with the score distribution of the iris recognition experiments carried out on the full database in Figure 5.12 and Figure 5.13.

From Figure 5.12 and Figure 5.13, it can be observed that by removing those comparisons in which the iris and pupil weren't detected accurately, intra class score distribution improved slightly. The remaining large hamming distance cases in the intra class comparisons could be due to the lack of information on the iris region or poor quality images in terms of image sharpness and contrast. One other important observation to be made is that intra class and

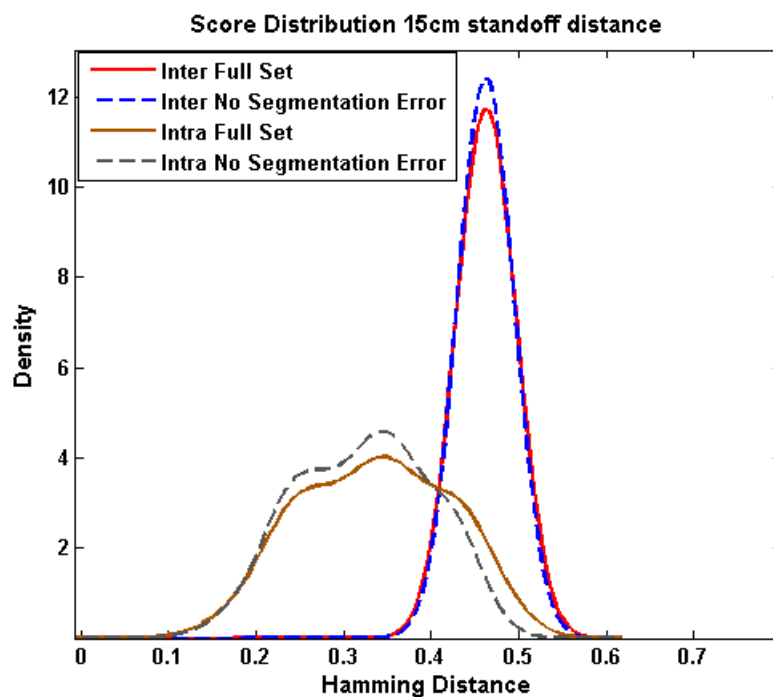


Fig. 5.12 Score distribution comparison for 15cm stand-off distance.

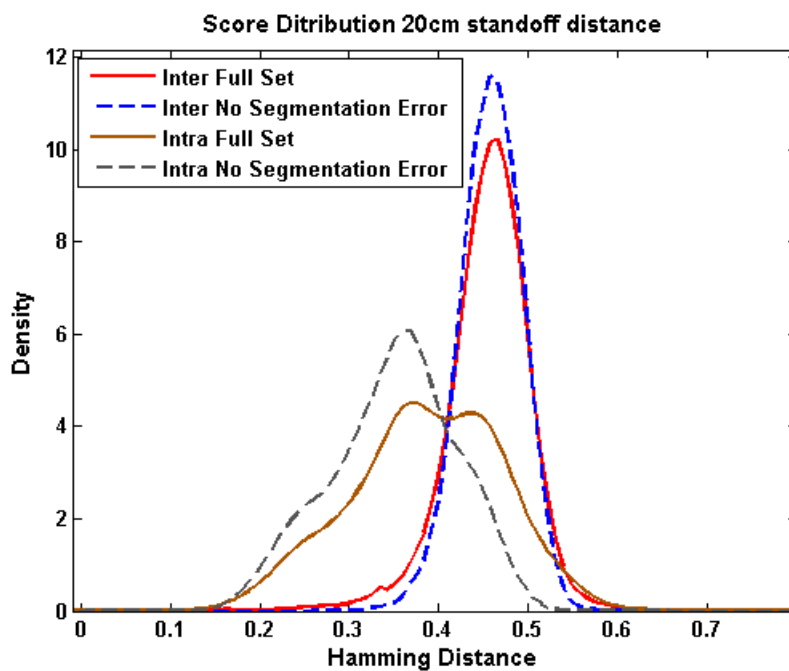


Fig. 5.13 Score distribution comparison for 20cm stand-off distance.

inter class score distribution of 15cm dataset is less overlapped as compared to that of the 20cm case. This is because of the comparatively better segmentation results on these images and the availability of more iris information due to the better image quality.

This can be analysed by measuring different image quality parameters of the iris images captured using our device and comparing with the images of the existing iris databases. Neurotechnology's VeriEye SDK is used for the image quality analysis [132]. This SDK assign scores for different image parameters such as iris-sclera contrast, iris-pupil contrast, sharpness, usable iris area, pupil to iris ratio, iris pupil concentricity, grayscale utilization, pupil boundary circularity, interlace and margin adequacy. An overall image quality score is also assigned to each image. The larger the score, the better the quality of the image [132]. We have measured average iris-pupil contrast, iris-sclera contrast, image sharpness and overall image quality from a representative sample image set on 8 different iris databases. The quality scores are tabulated in Table 5.3.

Database	Iris to Pupil Contrast Score	Iris to Sclera Contrast Score	Sharpness Score	Overall Image Quality
CASIA V4 Interval [16]	68	11	100	62
CASIA V4 Thousand [16]	95	16	94	40
MMU2 [133]	75	28	100	30
MMU1 [133]	81	22	99	47
IIT Delhi [134]	99	23	100	64
CASIA V4 Distance [16]	58	22	96	34
Our Database (20cm stand-off distance)	38	18	80	28
Our Database (15cm stand-off distance)	43	20	80	30

Table 5.3 Comparison of iris image quality scores on different databases. Larger the score, better the quality of the image.

From Table 5.3, it can be observed that, iris images captured using our device have low image quality scores as compared to the other publicly available research databases. The images in these research databases were acquired using a high quality dedicated iris cameras in constrained acquisition scenarios. Also, it can be noted that iris images captured at 15cm have slightly better image quality score as compared to those images captured at 20cm stand-off distance. This is in agreement with the analysis in Section 5.3.

Significant improvements in image quality could be achieved through custom optical design combined with improved NIR illumination sources and using SoA eye tracking data to eliminate low quality acquisitions. However such a system design challenge is an engineering

project for a multi-disciplinary team of electronics and optical experts and lies beyond the scope of this work.

5.5 Summary and Conclusions

In this chapter, the use of a dual-purpose RGB-NIR front facing camera for smartphones is examined. This camera combines the functionality of a conventional front-camera, such as selfie imaging and video call, with the potential for iris authentication. However there are significant challenges in implementing such a system. Even for a close stand-off distance of 15cm, the optical properties of the system are marginal and pixel resolution for iris recognition is below the minimum threshold defined by the current international standards. Also, due to the novelty of the colour filter array in this visible/NIR sensor, the RGB image quality is likely to suffer when compared to a standard front facing camera with conventional Bayer pattern CFA.

In practice, a high quality image must be acquired in order to successfully segment the iris region. This is particularly important for the challenging hand-held use case presented here. In our experiments more than 27% of acquisitions lead to unsuccessful iris and pupil detection/segmentation at a distance of 20 cm from the camera. This figure is improved to just over 10% at 15 cm. Also the recognition performance is noted to be lower than the current state of the art, primarily due to the reduced quality of the acquired iris images. Removing such non-segmenting images demonstrates a much more acceptable level of performance. These illustrate the challenge of implementing iris authentication in this unconstrained use case and suggests that the detection of non-segmenting iris regions could help with improving overall performance significantly.

However the best improvement would be achieved through improved acquisition techniques. These would allow more reliable capture of the iris region when the eye is fully open, minimizing specular reflections and keeping the eye region in sharp focus and high contrast. Enhanced face and eye tracking can help, in particular with the focus requirements. Note that, at 15 cm the focus depth is quite shallow and the iris region can easily lose focus to higher contrast regions of the face. An advanced eye-tracking solution could overcome this particular problem by retaining focus on the eye regions.

Nevertheless this study has shown that iris acquisition is practical in such a system and refined system design could greatly improve the reliability of the acquisition process leading to more acceptable levels of iris recognition performance. In conclusion, it is clear that the preliminary experiments presented here have been limited by the current optical design which is not optimized for optical differences between visible and IR wavelengths. An improved

design would allow more number or a greater density of NIR pixels, thus improving the quality of the acquired images. Design strategies such as sampling colour at a very sparse set of locations and then propagating throughout the image with guidance from an unaliased monochrome NIR channel [135] could possibly be adapted for this purpose. Such a design should accommodate the required optical resolution at both NIR and visible wavelengths and achieve a large iris pixel density, with 100+ pixels across iris diameter. Realizing these design goals may require a 6 or even 8 Megapixel sensor coupled with an advanced optical design, but the front cameras on today's smartphones are already in this size ballpark.

The minimum iris size requirement for good results places a limitation on the distance to subject. Ideally it would also be possible to increase the acquisition distance from 15-20 cm to a more comfortable 25-40 cm. However this suggests an additional doubling of the sensor size to 13-16 Megapixels, which comes with increased cost. The possibility to design, realize and test such a hybrid solution is currently being investigated.

Our conclusion is that iris biometrics can be implemented on mobile hand-held devices using hybrid visible/NIR camera modules similar to the one presented in this article. However significant challenges remain if the industry is to achieve practical working solutions that are sufficiently reliable and robust to meet the demands of today's consumers.

It has to be noted that, this study laid the foundation of the next stage of smartphone iris recognition system which is presented by the industry partner in the Consumer Electronics Show (CES) 2016 in Las Vegas, USA.

Chapter 6

Iris Liveness Detection for Next Generation Smartphone Biometrics

This chapter presents a novel liveness detection method that exploits the acquisition workflow of the hybrid RGB/NIR device presented in Chapter 5 for iris biometrics. As it is shown, these devices are able to capture both RGB and NIR images of the eye and iris region in synchronisation. This multi-spectral information is mapped in to a discrete feature space. An intermediate classifier which uses a distance metric close to Jensen-Shannon divergence [136] is employed to classify the incoming image. Further, a fast, multi-frame pupil localization technique using one dimensional processing of the eye region is proposed and evaluated. This is used to analyze the pupil characteristics. It is shown that such an analysis could detect presentation attacks, even with a 3-D face model made of materials which has similar properties of human skin and ocular region (such as the attack scenarios shown in Fig. 6.2).

This chapter is adapted from the following publications: (i) Shejin Thavalengal and Peter Corcoran, “Iris Liveness Detection for Smartphones”, under review; and (ii) Shejin Thavalengal and Petronel Bigioi and Peter Corcoran, “Efficient Segmentation for Multi-frame Iris Acquisition on Smartphones”, in Proceedings of the 2016 IEEE International Conference on Consumer Electronics (ICCE), Jan.2016, Las Vegas, USA.

6.1 Iris Liveness Detection: A Brief Overview

Smartphone user authentication using iris biometrics is a remote and unsupervised form of authentication. In other words, only the person performing the authentication need to be present during the process workflow. As a consequence it is more susceptible to spoofing of the biometric input than traditional authentication techniques such as PIN entry at a point-of-

sale terminal where the sales clerk is present. A spoofing attack on biometric system is an artificial mimic of a real biometric to gain access to the device and its services. This becomes worrisome as the iris biometric sample can be easily recorded without user cooperation. Hence it is essential to build in protection against such attacks on a system. Various types of spoofing include presenting a picture, a recorded video or a high quality iris image kept in front of original eye while trying to use iris authentication. These attacks are collectively called ‘presentation attacks’ [137].

Liveness detection is an anti-spoofing technique to determine if the biometric being captured is an actual measurement from a live person who is present at the time of capture [53]. Arguably, human supervision can be the most effective way for detecting such presentation attacks and widely used in many applications including UAE border control program. But, it is impractical in the case of smartphones and other CE devices. Hence, effective automatic liveness detection is necessary. Czajka [137] categorizes the automatic liveness detection techniques into three categories: (a) extraction of intrinsic properties of a living body, (b) analysis of involuntary signals and (c) challenge-response method. The extraction of intrinsic properties includes analyzing spectrographic properties of the human eye, analyzing red-eye effect or analyzing 3-D curvature of iris surface. Examples for analyzing involuntary body signals include eyelid movements and hippus. The third category mainly considers user’s response when prompted to carry out some tasks like blinking, or looking at a different direction. A detailed literature review of iris liveness detection can be found in [137].

Even though liveness detection is an essential part of iris recognition system as a counter-measure against spoofing, it comes with the cost of an increase in processing time, increase in hardware or software and negative effect on recognition performance [53].

6.2 Liveness Detection on Smartphones

Iris spoof detection is getting popular these days [53, 137–139]. All of the existing work in the literature can be further classified into two classes – techniques which require special hardware or user interaction [137, 138] and algorithms designed to work on static images/videos (such as high quality printed iris image, iris images presented on a screen, or a video stream) [138]. Techniques which need special hardwares or user cooperation may not be an ideal solution on smartphones as these will increase the cost and decrease the usability. Also, if the techniques demand considerable amount of user effort to make a decision whether it is an attack or not, they will not be adopted for everyday use by the consumers. Note that this is still an emerging technology and even if iris authentication is

feasible there are still ease-of-use issues to overcome in order to achieve a broad adoption of the technology in consumer market.

Hence, a simple, cost-effective yet powerful liveness detection should be incorporated on smartphones. Such a technique ideally should not require any additional hardware or user interaction and should be computationally light enough to be embedded in the smartphone camera pipeline or dedicated iris recognition digital signal processors.

Current research on iris liveness techniques are limited to either NIR iris recognition systems or the visible spectrum ones. But, the smartphone prototype presented in the previous chapter is capable of capturing both visible (for selfies and video calls) and NIR images (for iris recognition) by a single hybrid camera. Hence, harnessing the existence of these two modalities for iris liveness detection may provide efficient liveness detection capabilities to such devices without the need of any additional hardware. The feasibility of this approach is examined in this chapter.

6.3 Proposed Liveness Detection Process

A two stage iris liveness detection technique is proposed in this section. The proposed technique, depicted in Figure 6.1, is motivated by the novel RGB/NIR hybrid sensor and associated workflow presented in Section 5.1. The various steps of the proposed technique are described in the following subsections.

6.3.1 RGB-NIR image acquisition

Once the user has pressed the ‘wake up’ or ‘unlock’ key of the smartphone, the device will start acquiring eye images for further processing. State of the art face detection, eye detection and eye tracking techniques on the image stream in the visible wavelength are employed to obtain a sequence of good quality in-focus eye regions [140]. Once a good quality eye region is detected, both RGB and NIR images of the eye region are acquired. The RGB and NIR image formation can be explained as [141],

$$\mathbf{I}_v = \int_{\lambda_v} \int_p E(p, \lambda_v) R(p) Q(\lambda_v) dp d\lambda_v, \quad (6.1)$$

$$\mathbf{I}_i = \int_{\lambda_i} \int_p E(p, \lambda_i) R(p) Q(\lambda_i) dp d\lambda_i, \quad (6.2)$$

where $\mathbf{I}_v \in \mathbb{R}^{m \times n \times 3}$ is the RGB image, $\mathbf{I}_i \in \mathbb{R}^{k \times l}$ is the NIR image, $\lambda_v \in [350nm, 700nm]$, $\lambda_i \in [750nm, 900nm]$ are the wavelength range of RGB and NIR image respectively. p is the

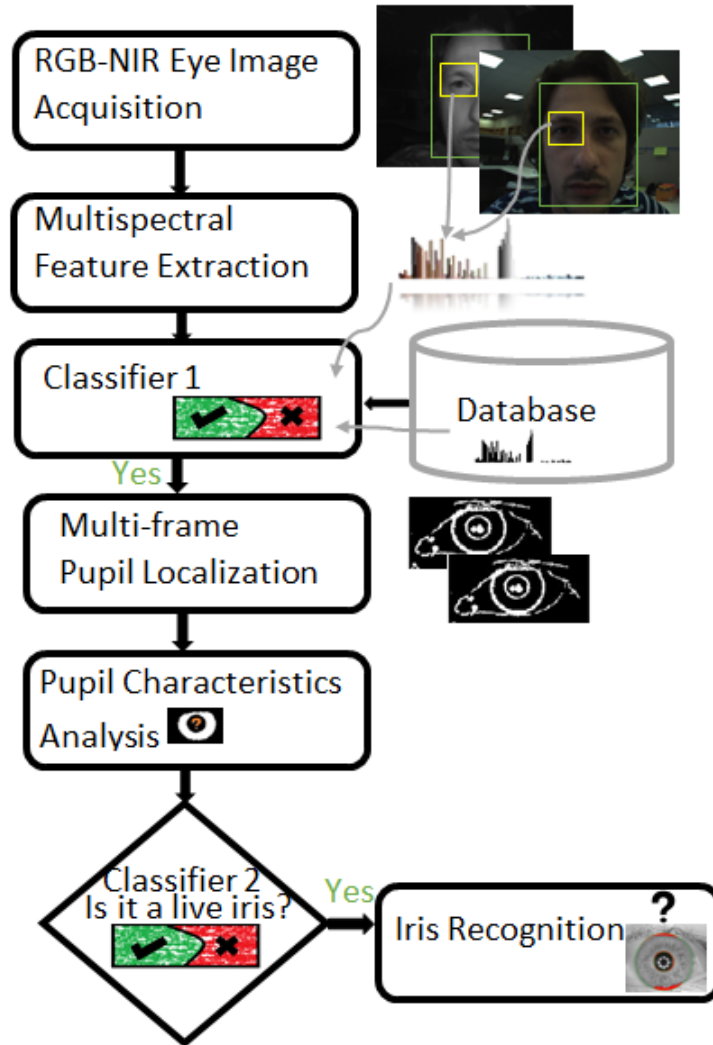


Fig. 6.1 Workflow of the proposed liveness detection technique.

spatial domain of the sensor, R is the spatial response of the sensor, E is the irradiance and Q is the quantum efficiency of the device. $\mathbf{I}_i \in \mathbb{R}^{k \times l}$ is demosaiced/interpolated to obtain $m = k, n = l$.

These two images, \mathbf{I}_v and \mathbf{I}_i are fused to make a hyperspectral image \mathbf{I}_h

$$\mathbf{I}_h = \Gamma(\mathbf{I}_v, \mathbf{I}_i), \quad (6.3)$$

where $\mathbf{I}_h \in \mathbb{R}^{m \times n \times 4}$ and Γ is the fusing operator. Broadly speaking, \mathbf{I}_h represents the ambient light and surface reflectance on the eye at four different wave bands (Blue, Green, Red and NIR). This image is further processed to minimise the effect of ambient light by the metadata

obtained from the camera, which is used for white balancing and auto exposure of the RGB camera image stream [142].

6.3.2 Multispectral Feature Extraction

It can be observed from the previous discussion that the hyperspectral image \mathbf{I}_h is made of four image planes ($\mathbf{I}_{c1}, \mathbf{I}_{c2}, \mathbf{I}_{c3}, \mathbf{I}_{c4}$) of size $m \times n$ representing four different wavebands (Blue, Green, Red and NIR). The pixels in each channel are clustered separately to α predefined clusters as,

$$\mathbf{I}_{cj}^u = \Omega(\mathbf{I}_{cj}), \quad (6.4)$$

where $\mathbf{I}_{cj}^u \in [1, \alpha]^{m \times n}$ represents the label of the cluster which corresponds to the pixels in \mathbf{I}_{cj} , $j \in [1, 4]$ denotes the image channel and Ω is the clustering operator. We have used Ω as nearest neighbourhood clustering operation which groups the pixels in each plane in to one of the α cluster based on the intensity value. Considering the dimensionality and computational complexity, $\alpha = 8$ is chosen. The label maps are further concatenated as

$$\mathbf{I}_h^u = \Gamma'(\mathbf{I}_{c1}^u, \mathbf{I}_{c2}^u, \mathbf{I}_{c3}^u, \mathbf{I}_{c4}^u), \quad (6.5)$$

where Γ' is the concatenation operator. Due to different combinations of clustering made by the concatenation of channels, each element in \mathbf{I}_h^u can have one of the $s = \alpha^4$ unique combinations. The normalized frequency distribution of each combination is calculated using the transform operator H

$$H : \mathbf{I}_h^u \longrightarrow F, \quad (6.6)$$

where $F = (f_1, f_2, \dots, f_s)$ is the number of times each unique cluster combination appeared in \mathbf{I}_h^u . This mapping is used as the feature vector for further processing.

6.3.3 Intermediate Decision Making

The training feature vectors for the live user are calculated during the iris enrolling stage. Sample attack feature vectors are loaded from the pre-computed models adapted to the user's characteristics such as eye colour, peri-ocular skin colour, etc. The current testing follows the 'winner takes all' model. That is, identifying whether the incoming images most likely belong to a live person or a presentation attack.

The distance d between the feature vectors of the query image (F^q) and the representative feature vectors in the database (F^{db}) are computed from a Bayesian point of view. That is,

the distance is measured as the square root of the entropy approximation to the logarithm of evidence ratio when testing whether the query image can be represented as the same underlying distribution of the live images [136]. This can be mathematically represented as,

$$\begin{aligned}
 d^{q,db} &= \sqrt{D\left(F^q \parallel \frac{1}{2}(F^q + F^{db})\right) + D\left(F^{db} \parallel \frac{1}{2}(F^q + F^{db})\right)} \\
 &= \sqrt{\sum_{z=1}^s \left(f_z^q \log \frac{2f_z^q}{f_z^q + f_z^{db}} + f_z^{db} \log \frac{2f_z^{db}}{f_z^q + f_z^{db}} \right)},
 \end{aligned} \tag{6.7}$$

where $D(F^q \parallel F^{db})$ is the Kullback–Leibler divergence of F^{db} from F^q , which is a measure of information lost when the database feature vector F^{db} is approximated from the query feature vector F^q . The above presented choice of distance metric $d^{q,db}$ is based on the observations that it is a close relative to Jensen - Shannon divergence and an asymptotic approximation of χ^2 distance. Also $d^{q,db}$ is symmetric and fulfills the triangle inequality [136].

Intermediate Decision Making - Discussions

It can be noted that the intermediate decision making depends on the surface reflection and refraction of the material present in front of the device. Human skin and the ocular region have distinct reflection and refraction properties. This property should be ideally enough to differentiate a presentation attack from the original live faces. One of the most common presentation attacks is presenting a high quality printed photograph or a video stream on a screen in front of the smartphone [138]. As the photographic material (reflective paper or matte paper) and the displays of devices are significantly different from the human skin, the proposed method is expected to detect such attacks. This can be observed from Fig. 6.2, which represents a number of attack scenarios- (i) high quality RGB colour prints (in matte paper, and glossy paper), (ii) high quality NIR colour prints, (iii) high quality RGB images presented in a screen and (iv) high quality NIR images presented in a screen and (v) the use of a realistic 3-D face model. This mannequin has engineered artificial eyes to duplicate the optical behaviour of human eyes such as generating red-eye effect. Also, it has similar material properties of human skin, hair and eye iris region.

The performance of this stage is assessed by ISO/IEC guidelines for different presentation attacks mentioned [143]. Since there are no publicly available database with RGB-NIR iris image pairs and the different presentation attack scenarios, we gathered a database internally for the proof-of-concept study. This initial database consists of 25 subjects captured using the device presented in Chapter 5. The RGB and NIR image pairs are captured at normal office situation with active illumination of 850nm. Examples for the image pairs captured at

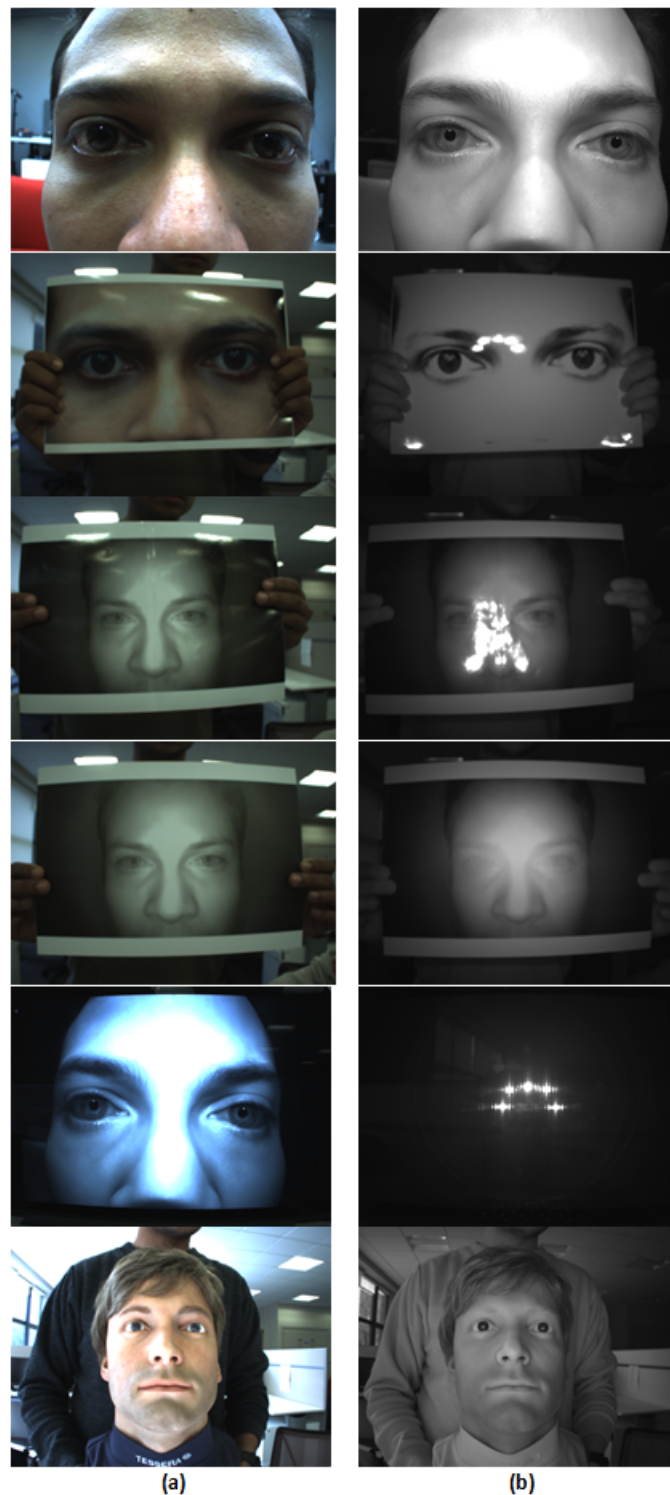


Fig. 6.2 Different test scenarios on the proposed system: (a) Visible Image, I_v , obtained by the system (b) NIR Image captured, I_i . First row is a live person. Second row is attack with a high quality visible printed image. Third row and fourth row is attack with high quality NIR printed image (on two different photographic paper - glossy and matte). Fifth row is attack with NIR image shown in a laptop screen with high resolution retina display. Sixth row represents a mannequin which has similar material properties of human skin, hair and eye iris region.

different stand-off distance are shown in Fig 6.3. One third of the images in the database are

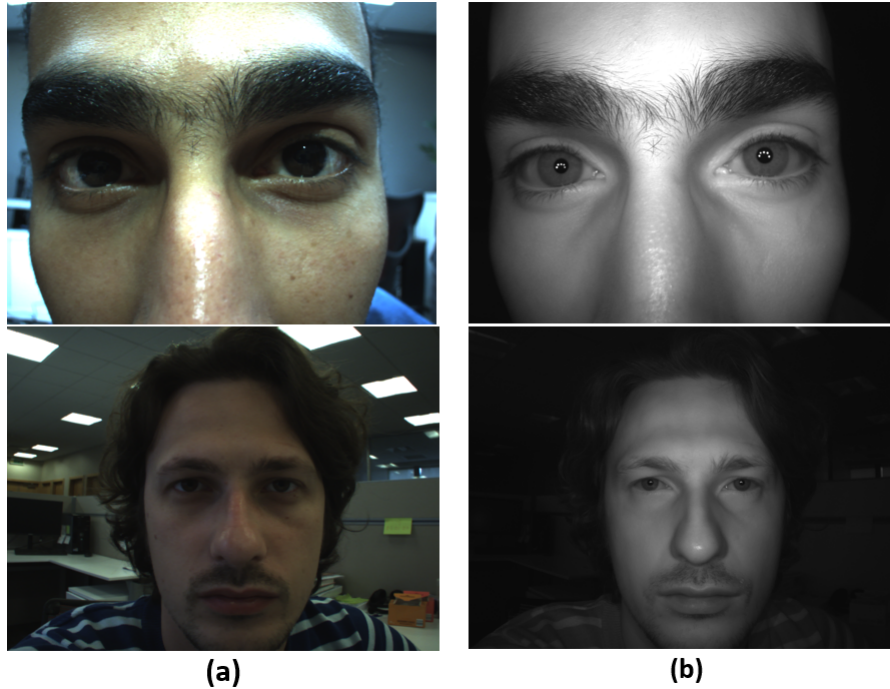


Fig. 6.3 RGB-NIR image pairs in the database: (a) RGB image (b) NIR image.

used as training set. The rest of the database is used for testing.

The tests with presentation attacks using printed photos and images presented on a screen generated a performance of 0% attack presentation classification error rate (APCER) and 0% normal presentation classification error rate (NPCER). The APCER is the percentage of presentation attacks incorrectly classified as a live user and NPCER is the percentage of live users incorrectly classified as presentation attack. But, when we introduced the attack scenario with the mannequin, the APCER is increased to 5.24% while NPCER remained the same. This is due to the fact that this mannequin possesses material properties of human skin and eyes. Also, it has to be noted that, even though this mannequin was wrongly classified as a live user, it is failed to get authenticated to the system in the iris recognition step.

One has to note that the spoofing techniques are evolving swiftly and we cannot guarantee a spoofing attack using only the known materials. The mannequin presented here can potentially keep a printed contact lens with pattern of the genuine user to get access to the system. Hence, analysing the spectral response alone will not be sufficient in such sophisticated attack scenarios. As a consequence, pupil characteristics analysis is recommended as an added security. The pupil analysis is recommended based on its effectiveness for iris liveness detection presented in the state of the art study by Czajka [137]. Mimicking both the pupil

dynamics and material properties of the human skin and ocular region is not feasible with current technologies.

6.3.4 Multi-Frame Pupil Localization

Current smartphones have capabilities to acquire 60-120 frames per second, but likely to double with next-generation technology. Hence, it will be practical to capture as many as 8-10 images within the same time window used today to acquire two images. If we consider 10 frames on average, this will practically give us around 20 images in this time frame (10 RGB and 10 NIR images captured in synchronisation). Hence a fast and sufficiently accurate pupil localization is required in this scenario for pupil characteristics analysis.

One Dimensional Image Processing for Pupil Localization

The iris region of the eye images coming in to the multi-frame pupil localization module may be affected by illumination variations and shadows created by eyelashes. This issue can be addressed using a representation that is less sensitive to illumination variations. One dimensional image processing can be used for this purpose [144]. As compared to other edge based techniques, this technique does not require any thresholding and reduces the smearing of the edges. Further, the choice of this process is motivated by author's previous experience of its success in various applications including face recognition and image super resolution [145, 146].

In the one dimensional processing of a given image, a smoothing operator is applied along one direction, and a derivative operator is applied along the orthogonal direction [144]. Let $\mathbf{I} \in \mathbb{R}^{m \times n}$ be the cropped eye image (The processing is carried out on \mathbf{I}_i). Additionally, \mathbf{I}_v is used to have a more accurate localization). The smoothed eye image can be obtained by

$$\mathbf{I}_\theta^s = \mathbf{I} \left(x, \frac{r + x \sin(\theta)}{\cos(\theta)} \right) \otimes S_\theta(x), \quad (6.8)$$

where $\mathbf{I}_\theta^s \in \mathbb{R}^{m \times n}$ is the smoothed iris image, $S_\theta(x) \in \mathbb{R}^{m \times 1}$ is the one dimensional smoothing function along a line which has a perpendicular distance of $r \in \mathbb{N}$ from the origin and makes an angle $\theta \in \mathbb{N}$ with the x-axis, \otimes is the one dimensional convolution operator. This convolution operation is carried out for each value of r to obtain the smoothed image \mathbf{I}_θ^s . The smoothing function used here is defined by

$$S_\theta(x) = \frac{1}{\sqrt{2\pi\sigma_s^2}} e^{-\frac{x^2 \sec^2 \theta}{2\sigma_s^2}} \quad (6.9)$$

where $\sigma_s \in \mathbb{R}$ is the standard deviation of the Gaussian function used in the smoothing process. A one dimensional derivative operator along the orthogonal direction $(\theta + 90)$ is applied to the smoothed image for different values of r to obtain an intermediate edge gradient image

$$\mathbf{I}_\theta^g = \mathbf{I}_\theta^s \left(x, \frac{r + x \sin(\theta + 90)}{\cos(\theta + 90)} \right) \otimes G_{\theta+90}(x), \quad (6.10)$$

where,

$$G_\theta(x) = \frac{-x \sec^2 \theta}{\sqrt{2\pi\sigma_g^6}} e^{-\frac{x^2 \sec^2 \theta}{2\sigma_g^2}} \quad (6.11)$$

where $\sigma_g \in \mathbb{R}$ is the standard deviation of the derivative operator. The magnitude representation of edge gradient can be obtained by

$$\mathbf{I}_\theta^M = \sqrt{(\mathbf{I}_\theta^g)^2 + (\mathbf{I}_{\theta+90}^g)^2}. \quad (6.12)$$

A transformation operator \mathbf{T} is applied on \mathbf{I}_θ^M ,

$$\mathbf{I}_d = \mathbf{T}_\delta \mathbf{I}_\theta^M, \quad (6.13)$$

where \mathbf{I}_d is the transformed image. The transformation operator \mathbf{T} is chosen in such a way that it binarizes the image \mathbf{I}_θ^M followed by the detection of largest connected region in the image. $\delta \in \mathbb{N}$ is a threshold in such a way that $n_{min}^p \leq \delta \leq n_{max}^p$ where n_{min}^p and n_{max}^p are the minimum and maximum number of pixels which could possibly be in the pupil region in this particular frame. From the face and eye tracking meta data and the camera parameters, an approximate number of pixels in the pupil region can be obtained and the value of δ can be learned for each individual frame [147]. \mathbf{T}_δ stands for the transformation operator \mathbf{T} for a specific threshold δ .

The whole process is depicted in Fig. 6.4. Note that $\theta = 90^\circ$ is used in the experiments. Fig. 6.4(a) represents the original image, Fig. 6.4(b) and Fig. 6.4(c) represent the output of one dimensional image processing for the specific angular direction θ and its orthogonal value. Fig. 6.4(d) is the magnitude image obtained from the result of the one dimensional image processing. The localized pupil is shown in Fig. 6.4(e).

6.3.5 Pupil Analysis

Once the pupil is localized in a sequence of frames, the next step is analyzing the pupil characteristics. We used two simple parameters for this – (i) pupil area and (ii) pixel intensity

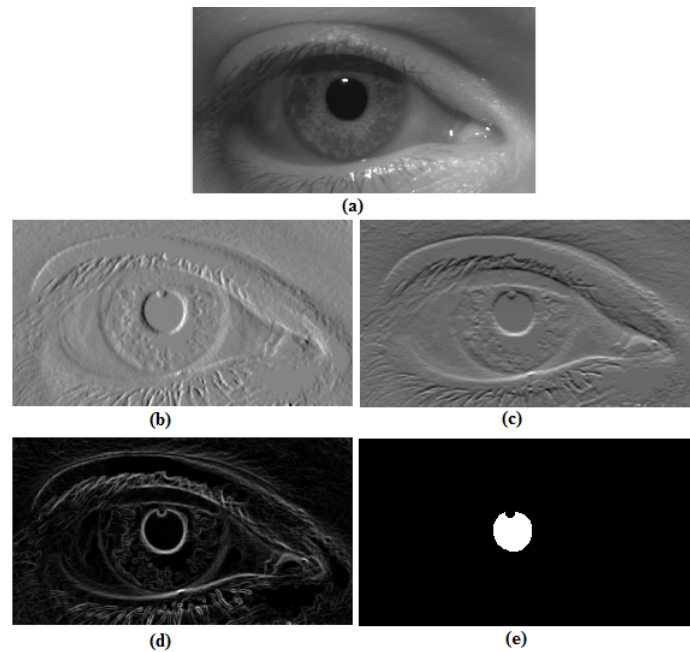


Fig. 6.4 Pupil localization Process: (a) Original NIR image \mathbf{I} (b) \mathbf{I}_{θ}^g (c) $\mathbf{I}_{\theta+90}^g$ (d) \mathbf{I}_{θ}^M and (e) localized pupil \mathbf{I}_d .

in the pupil region. The analysis of pupil area is to note down the eye saccades, hippus and pupil dilation/constriction which may arise naturally as the person moves close to the camera. Also, over a sequence of frames, eye-blinking may happen, which will alter the pupil area. This can be seen from Fig 6.5.

Fig 6.5 represents a sequence of NIR eye images and the pupil localization result of these images. It can be noted from Fig 6.5(b) that the area of pupil varies with time which could be measured with sufficient accuracy using the presented localization technique. The pixel intensity in pupil region will be able to detect the Purkinje image¹ or red-eye like effects [150].

6.3.6 Decision Making

A binary decision tree is used to classify the image as either a live person or a presentation attack. Binary decision tree is a natural choice when different models (in our case intermediate decision making strategy presented in Section 6.3.3 and pupil analyses presented in Section 6.3.5) become responsible for prediction in different regions of input space [151]. The binary decision tree used one root node and one intermediate node as shown in Fig 6.6.

¹The virtual images formed by the light reflected from the four optical surfaces of the human eye are called as Purkinje images. Purkinje images are used for various applications including iris liveness detection and eye tracking [148, 149].

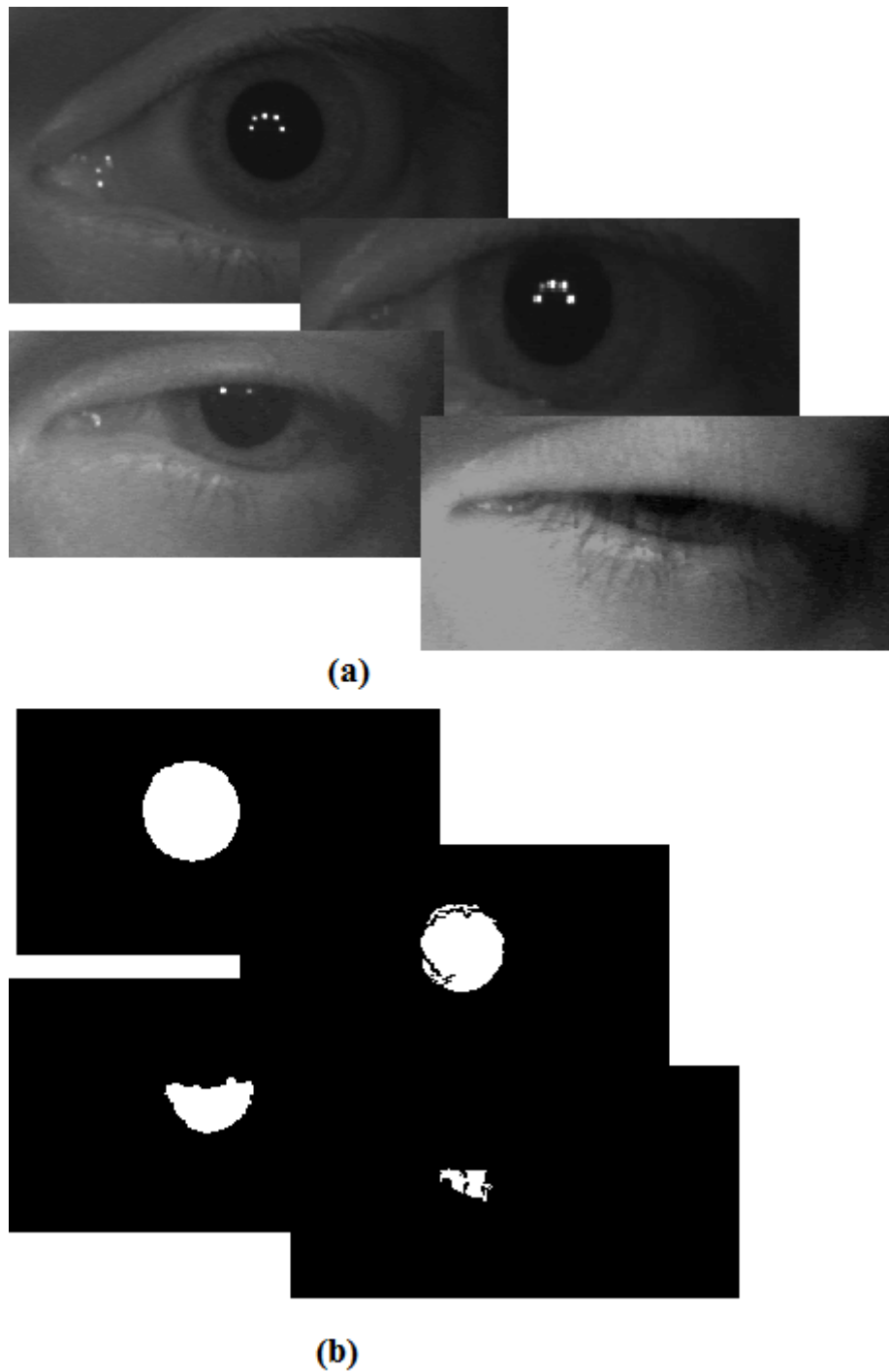


Fig. 6.5 Pupil analysis: (a) NIR iris image frames and (b) localized pupil.

If the resultant image is classified as a ‘live’ image, the image is proceeded for iris recognition. The pupil localization result in Section 6.3.4 is fed to the Iris Recognition unit along with the input images for recognition.

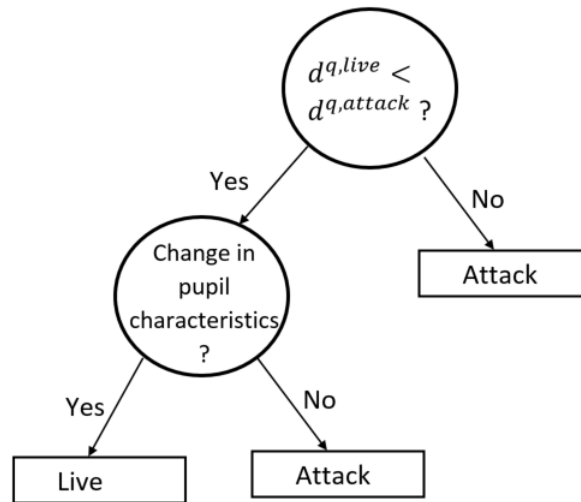


Fig. 6.6 Binary decision tree used for classifying the input image: the root node measures whether the incoming image is close to a live iris or a presentation attack. The intermediate node uses the pupil analysis information to further classify the output of the first node.

When the second stage of pupil analysis is added, the final performance of this system for all the attack types presented in Fig.3 is noted as APCER= 0% and NPCER= 0%. Even though the results are promising, it has to be noted that the experiments are carried out in a relatively small database of 25 subjects. Further experiments over an enlarged user dataset and introducing additional attack scenarios will be needed to fully assess the effectiveness of the presented techniques.

6.4 Conclusions

This chapter presented a novel liveness detection technique to be used with iris recognition on smartphones. This technique relies on the capability of next generation iris biometrics enabled smartphones to acquiring RGB and NIR image pairs simultaneously. We have shown here that harnessing the capabilities of the hybrid RGB/NIR acquisition workflow can provide a robust liveness detection without requiring any additional hardware or significant change in the acquisition workflow. A detailed system description and suitable workflow are presented. Initial proof-of-concept experiments have shown that the proposed technique is effective for detecting a range of presentation attacks including a sophisticated attack based on a realistic mannequin that duplicates the characteristics of a human face and eyes. Future work will involve developing an improved database to verify this technique over an enlarged user dataset and introducing additional attack scenarios.

Chapter 7

Iris Pattern Obfuscation in Digital Images

As the imaging systems in handheld devices continue to improve, both in terms of optical quality and the use of advanced computational imaging techniques, we are close to a point where high quality iris images can be obtained from personal images, which in turn can be used for spoofing attacks on iris recognition system. Thus an emerging challenge for next-generation personal imaging devices is to provide a means to obfuscate iris pattern in digital photographs and videos, but without destroying the photo-realistic qualities of the eye regions in a photograph or video. Such a solution- ‘iris pattern obfuscation’ is presented in this chapter.

This chapter is partly published in (i) Shejin Thavalengal, Ruxandra Vranceanu, Razvan G. Condorovici and Peter Corcoran, “Iris Pattern Obfuscation in Digital Images”, in Proceedings of the International Joint Conference on Biometrics (IJCB 2014), Sept.2014, Florida, USA; (ii) Shejin Thavalengal and Peter Corcoran, “A Practical Challenge for Iris Authentication on Handheld Imaging Devices”, in Proceedings of the 2015 IEEE International Conference on Consumer Electronics (ICCE), Jan.2015, Las Vegas, USA.

7.1 Introduction

Apart from the challenges in implementing a high performing, easy-to-use iris recognition system on hand-held devices, the wide spread use of such a technology faces some inherent challenges of iris recognition. Among these challenges, one of the most significant challenge is the security of the biometric system. Ratha, Connell and Bolle identified eight points in a biometric system which are vulnerable to attacks [152]

1. Presentation attack on sensor.
2. Resubmission of previously stored iris images to the feature extraction module.
3. Overriding the feature extraction process.
4. Presenting fraudulent features to the matching module.
5. Corrupting the feature matching unit to produce pre-selected match scores.
6. Tampering with the stored template in database.
7. Attacking the channel between database and matcher to insert or modify the database template used for matching.
8. Overriding the final decision.

Iris liveness detection techniques may be used to nullify the spoofing attacks on Point 1. An overview of various iris liveness detection techniques is given by Toth [53]. As discussed in the previous chapter, detecting liveness comes at the cost of reducing user convenience, matching accuracy etc. Also, spoofing techniques are swiftly evolving and the life cycle of these countermeasures is limited [53].

Encrypting the communication channel and all the processing units of the iris recognition system as well as using cryptography to encrypt and store the template may be able to eliminate attacks on the rest of the points. But, these points are still vulnerable if the attack manages to break the encryption. A prospective solution is the use of cancelable iris biometrics, where the iris code is intentionally distorted using a non-invertible transform. In this case, the user's true iris pattern never has to leave the client system [153]. This is similar to the discussions in [46] which envisages the smartphone as a key appliance for obtaining personal biometric data and authenticating its user. If biometric analysis is restricted to the device then many issues with respect to the theft of biometric data are countered as the biometric never leaves the personal device. This supposes a two-stage authentication where both person and device are required to complete the authentication procedure. On the other hand, a successful attack on the client device will nullify the efforts of these protocols and will help the attacker gain the original iris image and use it to spoof potentially any iris recognition system [153].

Venugopalan and Savvides [154] successfully generated spoofed iris from iris code template assuming they have access to the iris encoding mechanism. In similar work [155], reasonably realistic looking iris images are generated from the iris code templates using a probabilistic approach based on genetic algorithm. The latter approach does not require

any prior knowledge of the feature extraction technique used or any other components of the iris recognition system. These approaches could fool even commercial iris recognition systems [155]. All these issues open up the vulnerabilities of the existing iris biometric systems and the privacy concerns related to them. In the near future it may even become possible to obtain a person's iris image from the internet and forge their identity to pass the iris recognition system.

7.1.1 Next Generation Camera in our life

The three major components of any camera in hand-held devices- the lens, the imaging unit and the image processing unit - are continuing to evolve day by day. This enables the end user to capture high quality images using these devices. Devices with extended depth of field (eDoF) lenses that can capture images of 5- 8 mega pixel spatial resolution are already in market [156]. These lenses purposefully distort the image in a known way to help the image processing unit to provide an image which is in focus throughout. Similar techniques such as OptiML zoom with advanced image processing techniques can help to provide sharp, clean and distortion free images [156].

Techniques such as high dynamic range (HDR) [157–160] can combine more than one digital image to provide a combined image with improved image quality [161, 159]. This is a standard feature on most smartphone imaging systems and typically two images are acquired in sequence and combined, post-acquisition, to provide a sharper and higher quality final image. Techniques are well known in the literature to combine more than one image and as acquisition systems achieve higher frame rates (currently 60-120 frames per second for preview but likely to double with next-generation technology) it will be practical to capture as many as 8-10 images within the same time window used today to acquire two images. These techniques when combined with today's imaging techniques, are expected to make it possible to extract significantly more spatial and frequency-specific information from conventional images. Taking advantage of sub-pixel registration techniques will enable the generation of images with significantly higher local image contrast and sharpness at the resolution of today's devices.

In parallel, there is significant industry research to improve the quality of smartphone imaging with the use of dual-aperture and employing IR spectral components to enhance visible images [123, 162, 163]. It is very likely that we will see such dual-aperture imaging systems appear on the market within the next few years.

7.1.2 The Elephant in the Room - Personal Images

It is highly likely that images acquired with the next generation of imaging devices will be broadly of sufficient quality to enable the determination of iris patterns from faces in standard images. *A Life Revealed* by Cathy Newman tells how iris recognition is used to identify the 'Afghan Girl' from two face portrait photographs captured by National Geographic photographer Steve McCurry [164, 165]. The first photo was captured in 1984 and the second photo after 18 years. This shows a practical example of how face portrait images could be used to trace people using the iris information present. Reference [166] describes an invention that can identify a person from the face and iris data within a single 5- megapixel image. Nevertheless we note that the latest hand-held devices can feature imaging subsystems with up to 40 megapixel resolutions [167]. This makes normal personal portraits and small-group photos a potential source for personal iris patterns with a high risk of such biometric data being used for a range of criminal activities ranging from identity theft, forging of personal identity document up to gaining access to facilities protected by biometric security measures.

This observation signals an emerging problem for people who capture images of themselves and their family, friends and acquaintances and share such images in social networks on the Internet. Face images of us are widely available from the social networks and other related websites in internet. But a person's appearance can be easily changed and face is not considered as a reliable biometric, on its own, for authentication purpose. The corresponding problem with iris could be more significant as iris is a reliable biometric and relatively stable over time.

This brings us to an emerging research challenge - if iris data can be obtained from our personal photographs, how can we protect the privacy of our biometric data? People are not going to stop taking photographs and vidoes anytime soon. Better, higher quality pictures are on their way, so we need to consider how this problem can be solved. The answer, in a sense, lies in existing cameras. Today we rarely see a red-eye in digital images, not because they do not occur, but rather because they are detected and eliminated in the camera itself [168–170]. In fact many of the pictures we capture with todays digital cameras are not a true representation of the original scene being imaged [156]. Thus, if it is possible to detect and replace flash-eye defects it should also be possible to detect and replace iris regions. The challenge is to find a way to substitute the existing iris region with a similar region that has the same color and appearance but does not match the original iris pattern. We call this process *iris obfuscation*, and ideally it should be implemented within the camera before detailed iris data is transferred to permanent storage or transported over a network link.

This chapter presents initial studies, outlining a handful of techniques that can be used to create replacement iris regions with different levels of complexity, reliability and robustness. Rest of the chapter is organised as follows: proposed iris obfuscation techniques are explained in Section 7.2. Detailed experimental analysis is carried out in Section 7.3. Section 7.4 outlines various challenges in the practical implementation of iris obfuscation techniques. Section 7.5 gives the conclusion of this chapter and the future direction of research.

7.2 Iris Pattern Obfuscation

Iris pattern obfuscation is the process of detecting and obscuring the iris pattern in digital photographs and videos, but without destroying the photo-realistic qualities of the eye regions. This will effectively reduce the chance of obtaining iris patterns easily, which can be later used for spoofing.

The iris pattern obfuscation should be carried out in such a way that the iris recognition algorithm will fail to match the original images with the processed version as well as matching the processed image with any other iris image of the same person. One important concern is that the resultant iris should look natural and the obfuscation technique should be computationally light enough to be used in resource constrained consumer electronic devices. This should be implemented within the camera before detailed iris data is transferred to permanent storage or transported over a network link to avoid any vulnerabilities of attacks.

A re-implementation of Daugman's original idea is used as a reference iris recognition system here [17, 104]. This specific choice is based on the fact that majority of the commercially deployed iris recognition systems follow the framework proposed by Daugman [17]. The proposed techniques in iris obfuscation can be categorized as (i) vertical flipping, (ii) radial blurring, (iii) sector swapping, (iv) quadrant interchanging and (v) iris replacing. A detailed description of each technique is given in the following subsections.

7.2.1 Vertical Flipping

In this approach, trivial flips of the iris image about the vertical axis is carried out and the images is blended back in to the original image [171]. An example is shown in Figure 7.1. As one can see, the resultant images are natural looking. But, this approach could not get past the iris recognition algorithm A threshold of hamming distance (HD) =0.33 is used in assessing the performance. The obfuscation technique is expected to have an HD value above the threshold for it to be successful). This may be due to the fact that a rotation tolerance of

10 bit shift in the iris recognition algorithm is used to compensate for the small deviation in image orientation due to head tilt etc. This 10 bit tolerance may be compensating up to a large extent for the bit changes caused by vertical flipping. Hence the HD between the two images falls below the cut off threshold.

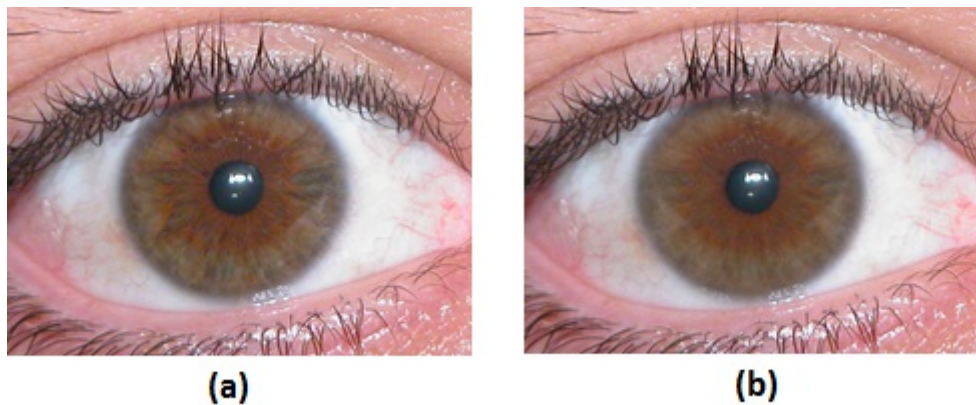


Fig. 7.1 Example for vertical flipping technique: (a) Original image, (b) Output image. Hamming distance between (a) and (b) is 0.241.

7.2.2 Radial Blurring

Another possible way to obscure the pattern is blurring the iris. The iris should be blurred in a controlled way so that it does not affect the surrounding ocular region and also generates sufficiently good looking iris images. For this purpose, a radial blur to the iris about its centre point is applied. It can be seen from the Figure 7.2 that this method generates sufficiently sharp, natural looking eye image.

When iris recognition is carried out on these images, it is observed that this technique less effective as mode of obfuscation. The low values of Hamming distance leading to a good matching between the original image and the blurred image may be due to the robustness of Daugmans homogenous rubber sheet model for iris normalization [17]. This model converts the annular iris image in to a doubly dimensionless pseudopolar coordinate system which has an inherent property to compensate for pupil dilation and constriction. This property may be the reason for the correction of elastic deformation in the iris generated by the radial blurring technique.

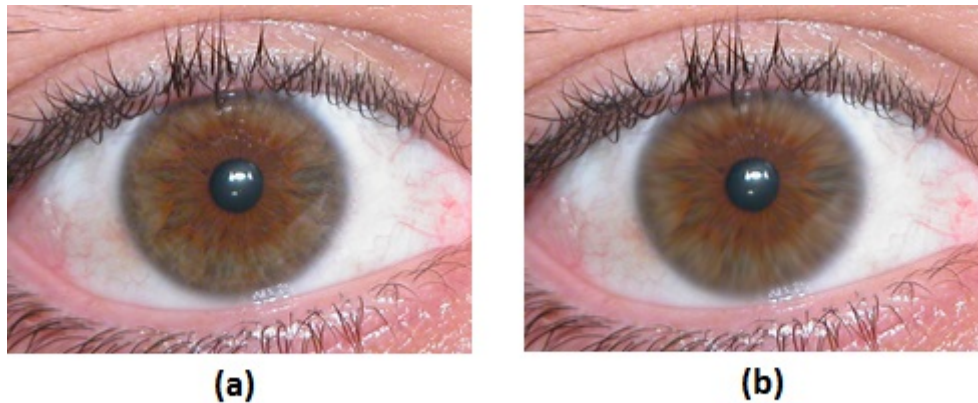


Fig. 7.2 Example of radial blurring: (a) Original iris image; (b) Output image; Hamming distance between (a) and (b) is 0.096.

7.2.3 Sector Swapping

In this method, initially, an iris is divided in to a number of sectors. These sectors are randomly swapped with each other and overlaid on the original image. This overlaid image will not be smooth and natural looking. Hence, alpha blending [171] is used to smooth the transition between the overlaid iris and the original image. The whole approach is iteratively repeated a number of times using various swapping orders. This will generate a smooth and natural looking iris at the same time nullifying any possibility of reversing the iris in to its original pattern. The sector swapping technique is depicted in Figure 7.3.

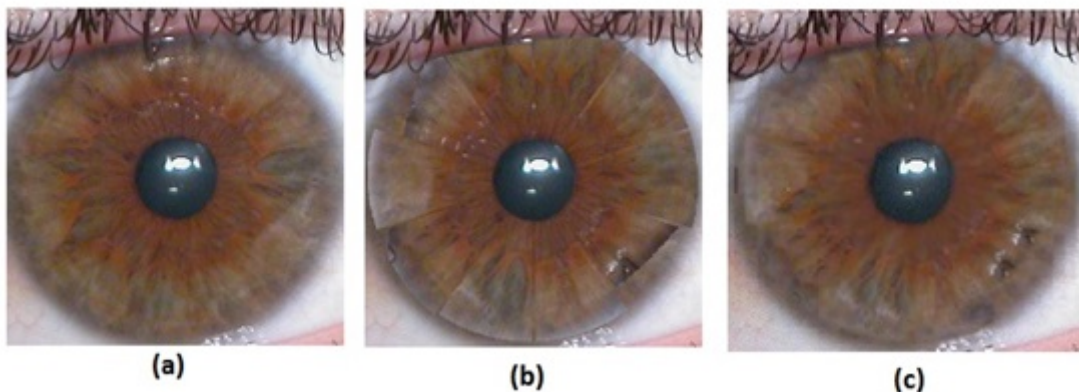


Fig. 7.3 Example for Sector Swapping technique. (a) Original image, (b) Image with sectors swapped and overlaid on original image, (c) Output image.

Figure 3(a) is the original image. Here, the iris is divided in to 10 partitions for swapping. Figure 7.3(b) shows the image in which the swapped iris partitions are overlaid on

Figure 7.3(a). One can note that the transition between each sectors and the sectors with the background image are not smooth. Figure 7.3(c) shows the final iris image after alpha blending. It can also be observed that the output of the process (Figure 7.3(c)) preserves the colour and shape of the original image. The HD between Figure 7.3(a) and Figure 7.3(c) is 0.432. Considering an optimal threshold HD of 0.33 as suggested by the large scale studies of iris recognition [29], this value shows sector swapping could be an effective obfuscation technique.

7.2.4 Quadrant Interchanging

As the name suggests, in this technique, the iris is divided in to four different quadrants and the details of these quadrants are interchanged at different scales with predefined rules.

An iris image $\mathbf{I} \in \mathbb{R}^{m \times m}$ is cropped out of the input eye image in such a way that \mathbf{I} is centered at the pupil. A transformation operator ζ is applied on \mathbf{I} ,

$$\mathbf{I}_d^k = \zeta(\mathbf{I}, k), \quad (7.1)$$

where \mathbf{I}_d^k is the transformed image, $k \in \mathbb{R}^{m \times m}$ is the scale parameter. The transformation operator ζ is chosen in such a way that \mathbf{I}_d^k represents an image which contains iris details only. This is followed by another operator \mathbf{Q} on \mathbf{I}_d^k which will interchange the quadrants of \mathbf{I}_d^k for different scales k in a specified manner.

$$\mathbf{I}_s^k = \mathbf{Q}(\mathbf{I}_d^k, k), \quad (7.2)$$

where \mathbf{I}_s^k is the scrambled image. Further, the details in \mathbf{I}_s^k which doesn't intersect with \mathbf{I}_d^k are omitted. The \mathbf{I}_s^k and \mathbf{I}_d^k are combined with different weights depending on the scale factor k to obtain the final image, $\mathbf{I}_f \in \mathbb{R}^{m \times m}$

$$\mathbf{I}_f = \mathbf{I} - w^k \mathbf{I}_d^k + w_s^k \mathbf{I}_s^k, \quad (7.3)$$

where, $w^k, w_s^k \in \mathbb{R}$ are the weights given to original iris detail image and the scrambled iris detail image for different scales k . An example for this technique is shown in Figure 7.4.

Input eye image is shown in Figure 7.4(a) and Figure 7.4(b) represents the cropped out image \mathbf{I} . Each quadrant in \mathbf{I} named as Q1, Q2, Q3 and Q4 respectively. Here, ζ is chosen as an operator which will apply box filtering on \mathbf{I} using a $k \times k$ kernel and subtract the resulting filtered image from \mathbf{I} to obtain \mathbf{I}_d^k . Five different scales k is used here (in the experiments each scale represents the percentage of crop length of the image m). For each scale, the quadrant interchange operator is applied in such a fashion shown in Table 7.1

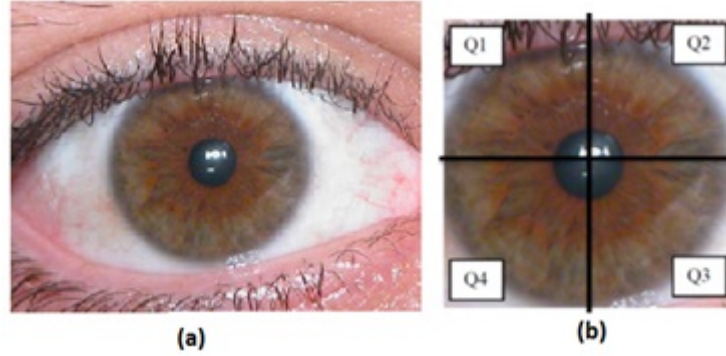


Fig. 7.4 Various stages of quadrant interchanging technique. (a) Original image, (b) Original image cropped keeping pupil as center, the four quadrants are also marked.

Table 7.1 An example for quadrant interchange operator for different scales.

Scale k	Q1	Q2	Q3	Q4
1	Q2	Q1	Q4	Q3
2	Q2	Q1	Q2	Q1
3	Q3	Q4	Q1	Q2
4	Q4	Q3	Q1	Q2
5	Q4	Q3	Q2	Q1

Figure 7.5(a) and Figure 7.5(b) depicts \mathbf{I}_d^k and \mathbf{I}_s^k respectively for a particular scale k and quadrant interchange operator \mathbf{Q} in the fashion shown in Table 7.1. For the computation of final image \mathbf{I}_f , we chose the values of w^k, w_s^k as in Table 7.2,

The final result along with the original image is shown in Figure 7.6. The output image appears natural and free of visual artifacts. The HD between Figure 7.6 (a) and Figure 7.6 (b) is 0.459, which is above the optimal HD threshold of 0.33.

7.2.5 Iris Replacing

The principle behind this approach is to replace the iris details of the original image with the details of a standard iris. This standard iris can be an artificially generated iris using one of the techniques in literature [172–174]. It is highly recommended to have a good quality non occluding iris image as the standard image. The iris details are obtained from the input image and the standard image using the same transform operator ζ explained in Equation 7.1, i.e,

$$\mathbf{I}_{d,o}^k = \zeta(\mathbf{I}_o, k), \quad (7.4)$$

$$\mathbf{I}_{d,g}^k = \zeta(\mathbf{I}_g, k), \quad (7.5)$$

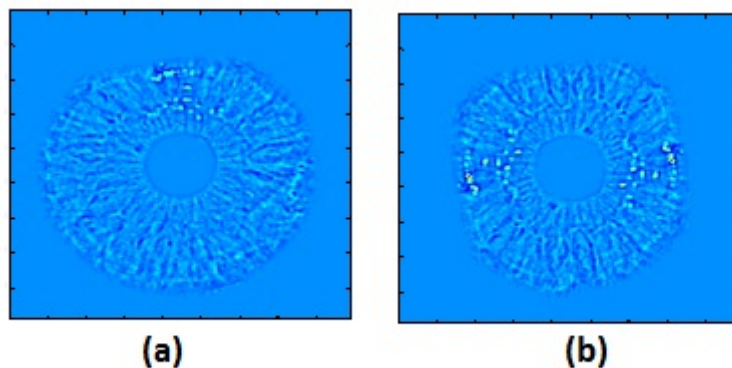


Fig. 7.5 Example for iris detail images for a particular scale.

Table 7.2 An example for w^k, w_s^k selection for different scales.

Scale k	w^k	w_s^k
1	1	0
2	4	1
3	4	1
4	2	1
5	1	1

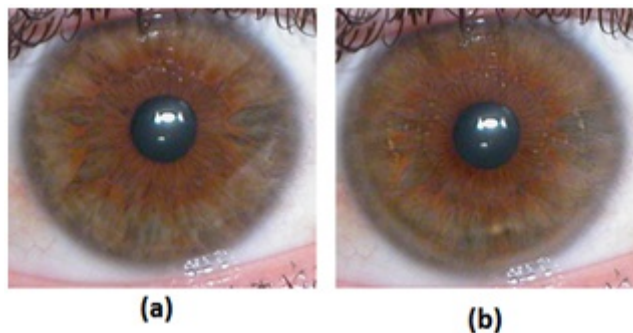


Fig. 7.6 Example for quadrant interchanging technique (a) Original image, (b) Output image.

Where $\mathbf{I}_o \in \mathbb{R}^{m \times n}$ is the original iris image of size $m \times n$, $\mathbf{I}_g \in \mathbb{R}^{m \times n}$ is the standard gallery iris image of size $m \times n$. $\mathbf{I}_{d,o}^k$ and $\mathbf{I}_{d,g}^k$ are the images containing only iris details of \mathbf{I}_o and \mathbf{I}_g respectively for a particular scale k . The details of the original iris \mathbf{I}_o at each scale k is replaced with that of the standard gallery iris. The final image $\mathbf{I}_f \in \mathbb{R}^{m \times n}$ is obtained by ,

$$\mathbf{I}_f = \mathbf{I} - \mathbf{I}_{d,o}^k + \alpha \mathbf{I}_{d,g}^k, \quad (7.6)$$

Where $\alpha \in \mathbb{R}$ determines the prominence of the iris details of the gallery image in the final image.

An example for this technique is shown in figure Figure 7.7. Figure 7.7(a) is a standard

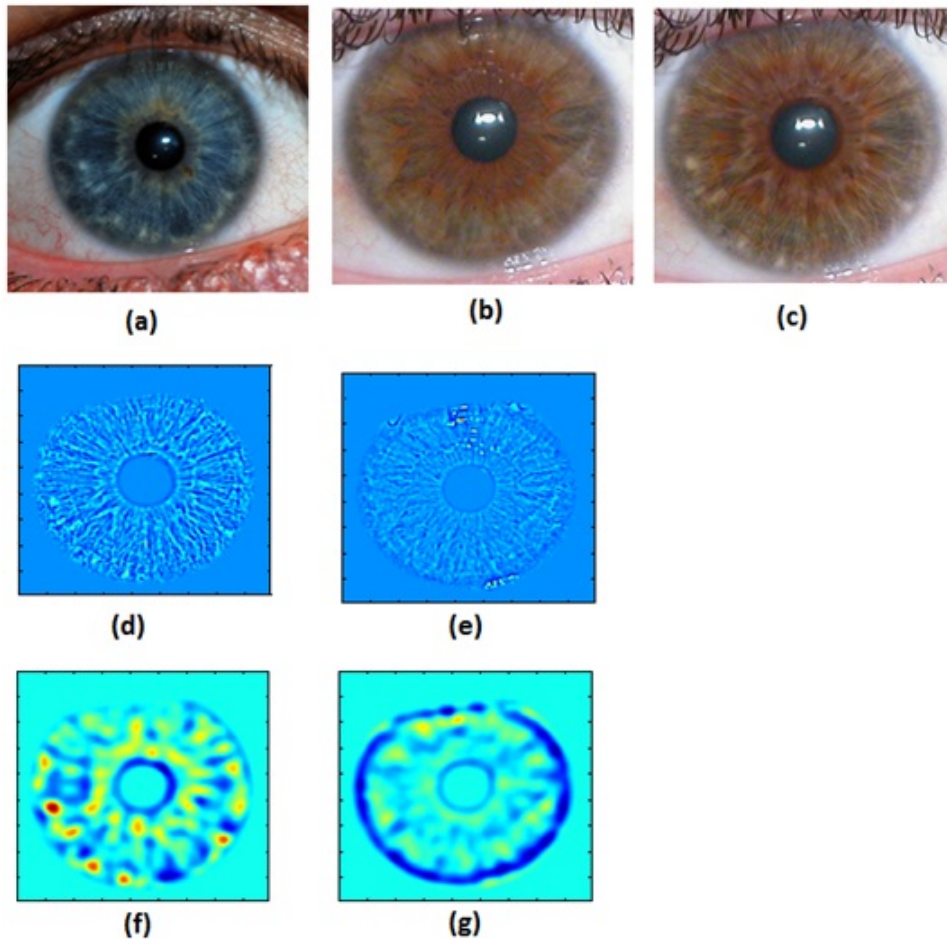


Fig. 7.7 Example for iris replace technique. (a) Standard gallery image, (b) original image, (c) out put image of iris replacing technique. (d) and (f): iris details of gallery image for two different scales.(e) and (g): iris details of original image for two different scales.

gallery image, Figure 7.7(b) is the original input image, and Figure 7.7(c) represents the output image after iris replacing. One immediate observation from Figure 7.7(c) is that, even though the original image and gallery images have different occlusion types and pigmentation, the output image preserves the shape and colour of the input image. Only the iris pattern in the original image is replaced with the gallery image. A prominence factor α as 0.75 is used in this example. Figure 7.7(d) and Figure 7.7(f) represents the iris image details of the standard gallery image obtained with the help of the transform operator ζ for different scale. Similarly Figure 7.7(e) and Figure 7.7(g) are the iris details of original input image. The

output image appears natural and free of visual artifacts as in the quadrant interchanging technique. Also, the hamming distance between the original image I_o and the final output image I_f is 0.446, which is above the threshold of 0.33. This indicates the proposed technique could be a potential solution for iris pattern obfuscation.

7.3 Experiments and Analysis

The experiments and analysis of the proposed iris obfuscation techniques were carried out in two large publicly available databases CASIA v4 Interval and UBIRIS v1.

CASIA v4 Interval dataset consists of 2639 images from 249 subjects which is divided in to a total of 395 classes. These images are obtained using CASIA close-up iris camera and images have extremely clear iris texture [16]. UBIRIS v1 database consists of 1877 images collected from 241 subjects. The images are captured using a Nikon E5700 camera [175]. Images from session 1, where images are classified in to 241 classes with five images per class, were used in the experiments presented here.

The reason behind choosing these two databases is that they contain high quality iris images. The primary target of the experiments is to evaluate the effectiveness of the proposed iris obfuscation techniques. As the UBIRIS v2 or MICHE [176] is collected in a less constrained environment, with subjects at a distance and on the move. This database consists of a large number of poor quality iris images and not apt for the analysis presented here.

The recognition experiments and analysis are conducted assuming that the iris obfuscation was carried out by the imaging system (in our case the consumer electronic camera) and only the resultant eye image is available for the recognition system. All stages of iris recognition such as iris segmentation, normalization, feature extraction and pattern matching were carried out on these resultant images.

Some representative examples for the proposed iris obfuscation technique on images from CASIA v4 interval dataset are shown in Figure 7.8. Figure 7.8(a) is the original image, Figure 7.8(b) is the image obtained by vertical flipping, Figure 7.8(c) by radial blurring, Figure 7.8(d) by sector swapping, Figure 7.8(e) by quadrant interchanging and Figure 7.8(f) by the iris replacing technique. We have used the same standard gallery image shown in Figure 7.7(a) for the iris replacing technique. The comparison results are given in Table 7.3.

As the first two obfuscation techniques presented- vertical flipping and radial blurring - were shown to be ineffective in the initial observation itself, further analysis of these two techniques were not carried out. The rest of the techniques - sector swapping, quadrant interchanging and iris replacing- were analysed in both UBIRIS and CASIA v4 for the three comparison schemes - (i) Original vs Obfuscated: in this analysis, the original images are

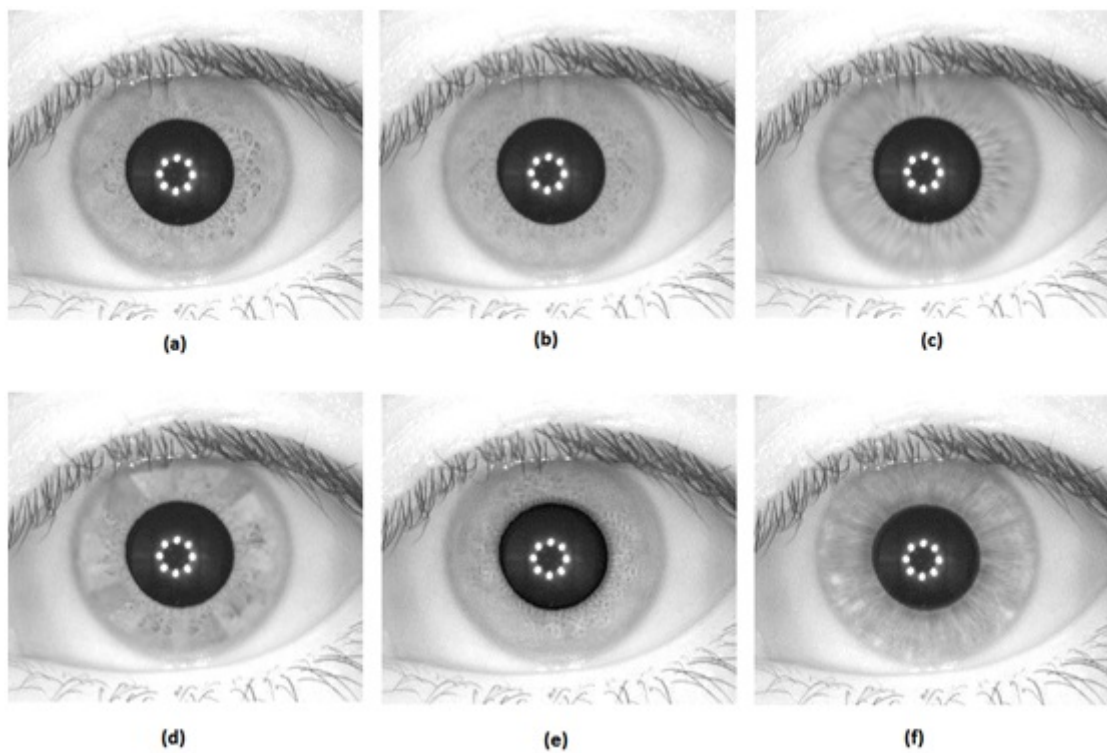


Fig. 7.8 Example for different iris obfuscation techniques on CASIA database. (a) Original image, (b) vertical flipping, (c) radial blurring, (d) sector swapping, (e) quadrant interchanging and (f) iris replacing.

Table 7.3 Comparison results of images shown in Figure 7.8.

Comparison	HD
Figure 7.8(a) vs. Figure 7.8(b)	0.247
Figure 7.8(a) vs. Figure 7.8(c)	0.16
Figure 7.8(a) vs. Figure 7.8(d)	0.385
Figure 7.8(a) vs. Figure 7.8(e)	0.371
Figure 7.8(a) vs. Figure 7.8(f)	0.410

compared with the obfuscated version of it. (ii) Intra-class comparison: the obfuscated iris is compared with the images from the same class of the original image. (iii) Inter-class comparison: the scrambled iris is matched with the rest of the images in the database. The comparison results are shown in Figure 7.9.

In Figure 7.9, horizontal axis represents the hamming distance and the vertical axis represents the probability density of the HD distribution.

An optimal threshold HD of 0.33 was considered as suggested by the large scale studies of iris recognition [29]. Comparing the curves obtained from the three types of comparisons, it can be noted that that iris replacement technique generates the best results as compared to other techniques. While using iris replacement technique, the outcome of the technique failed to match with any of the iris images in the database. When the sector swapping technique is used for obfuscation, a considerable amount of Original vs. Obfuscated and intra-class comparisons fall below the above mentioned threshold. This technique leads to the worst results obtained among the three techniques analysed here.

From these results, we can observe that iris replacing technique is best suited for iris obfuscation in digital images. While using iris replacement technique, the outcome of the technique failed to match with any of the iris images in the database. Moreover as it can be observed from the Figure 7.7(c) that the obfuscated iris image is natural looking and preserves the colour, shape and size of the original image. The quadrant interchanging technique has small amount of HD distribution lying below the threshold value of 0.33. When the sector swapping technique is used for obfuscation, a considerable amount of Original vs. Obfuscated and intra-class comparisons fall below the above mentioned threshold. From these results, we can observe that iris replacing technique is best suited for iris obfuscation in digital images.

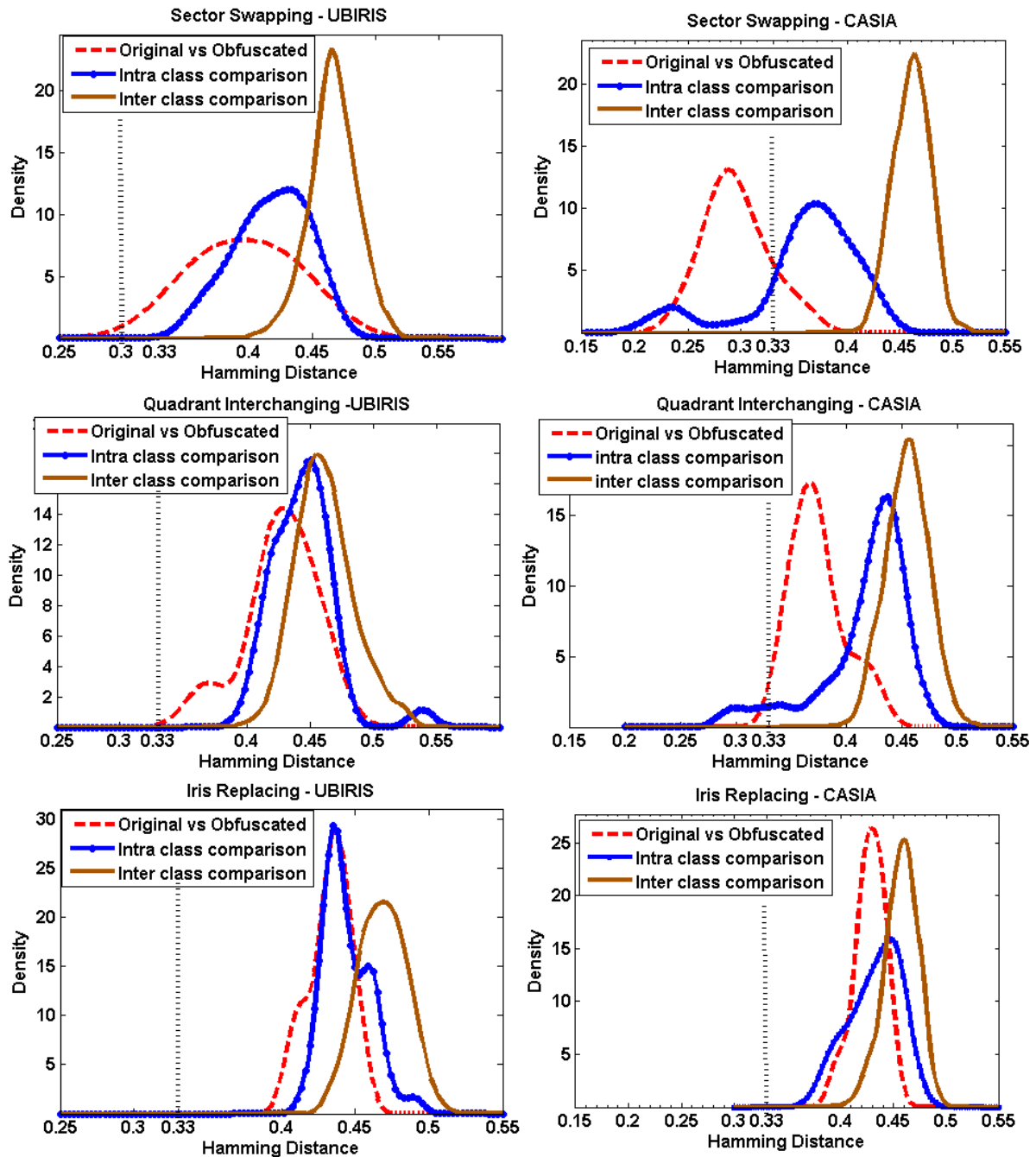


Fig. 7.9 Results: First column represent probability density plots for the three obfuscation techniques (sector swapping, quadrant interchanging and iris replacing) in UBIRIS database. The second column represent density plots for the three obfuscation techniques in CASIA database. The 0.33 cut-off HD is marked with dotted black line.

7.4 Challenges in Implementing Iris Pattern Obfuscation

Having outlined the rationale for iris obfuscation and a detailed analysis of various techniques presented, the next target is to address the challenges facing the real world implementation of this proposed new technology.

7.4.1 Undetectable modification of Eye Regions

It can be noted that iris pattern obfuscation requires precise segmentation for photo-realistic, undetectable modification of the iris region. As a general rule, iris recognition relies on precise segmentation and recent developments in face and eye-tracking techniques and the fact that these technologies are embedded in many of today's imaging devices suggests that hand-held imaging devices will provide computationally efficient tools to automatically and accurately segment iris regions.

While most individuals will not notice changes in their own iris patterns or those of their loved ones as the human perception of the eye region relies mainly on eye-color, there are likely to be outlying examples where changes in the iris pattern prove disconcerting. Some examples of obfuscation results are shown in Figure 7.10.

In Figure 7.10, it can be noted that when the segmentation is accurate (first three rows), the result of obfuscation is undetectable. The fourth and fifth row shows an example where eye segmentation failed, which resulted in a failed attempt of obfuscation. The resultant images have visible artifacts.

7.4.2 Robust detection of 'At-Risk' Eye Regions

This problem parallels that of the detection problem for red-eye (flash-eye) artifacts. As one might expect this is nontrivial as shown by the detailed analysis of related patents provided in [177]. At present, the use of in-camera face detection and eye-gaze [111] technologies facilitates the location and determination of the properties of eye-regions in each image frame. This is sufficient to detect the location and the approximate orientation of each eye region. Frontal facing eye regions are the principle candidates for obfuscation and an additional check on the 'openness' of the eye [140] completes a determination if obfuscation is needed. The significance of this step could be observed in Figure 7.10 fifth row, where the obfuscation technique attempted to detect and obfuscate the iris pattern. The resultant image shows visible artifacts, which could have been avoided if an additional check on the 'openness' of the eye was carried out.

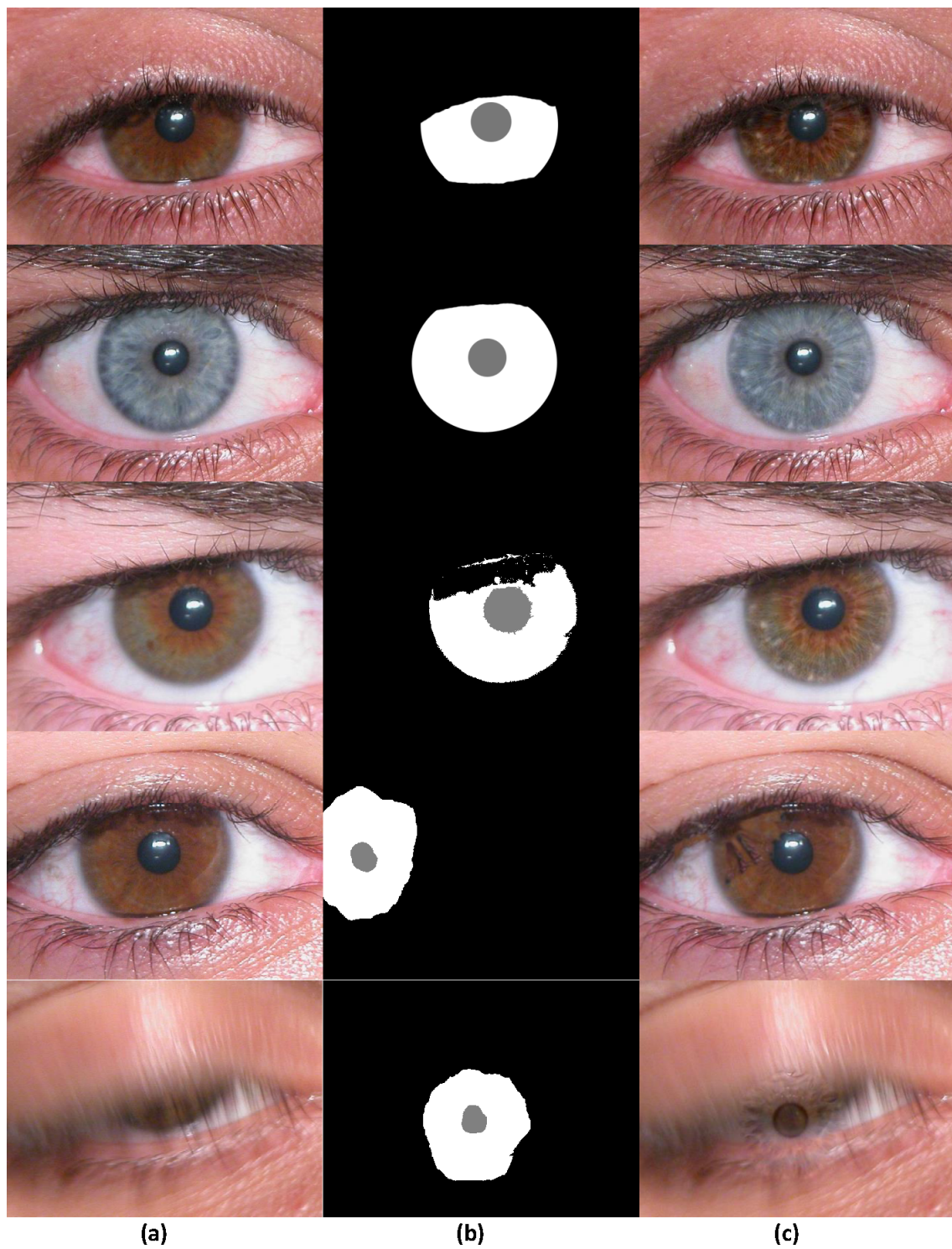


Fig. 7.10 Examples for Obfuscation (a) Original Image, (b) Segmentation mask and (c) Result of Iris Replacing technique.

However, the most challenging cases are those where the eye-gaze is at a non-frontal angle, or the eye is partially open. In these cases obfuscation is not straightforward to implement, but there is a risk that some of the iris pattern may be available, enabling a determined attacker to gather multiple complimentary iris region images and process these to reconstruct the original iris pattern.

7.4.3 Real Time Implementation

Real-time implementation of iris obfuscation is perhaps the key challenge- this techniques must operate at full HD and be capable to scale to 4k video rates. For a practical in camera system, this demands a hardware implementation of key algorithmic primitives.

7.5 Conclusion

In this chapter, an initial study on iris obfuscation in digital images as a potential solution to some of the privacy concerns related to iris recognition technology was carried out. One of the major drawbacks of biometric recognition systems is the fact that a biometric trait can not be replaced once it is stolen. Particularly, if the security of an iris recognition system is broken at any stage and the iris biometric data is obtained this information will be compromised once and for all. The iris obfuscation techniques we suggested here are aimed to obscure the iris pattern of the captured iris images in such a way that the iris recognition algorithm will fail to match the resultant iris image to the original iris images of the person. This way the person's iris biometric information is preserved from misuse such as iris spoofing. At the same time the resultant iris image will look natural and have the similar appearance of that of the original image in the context of color, intensity, iris area etc.

This initial study proposed and analyzed five iris obfuscation techniques – vertical flipping, radial blurring, sector swapping, quadrant interchanging and iris replacing. The first two techniques are found to be ineffective from the initial analysis itself due to the robustness of iris recognition technology. The remaining three techniques show considerable effectiveness in obfuscating the iris pattern. The iris replacing technique, in which the iris pattern of an image is replaced with the pattern of a standard gallery iris image, is found to be highly effective among the lot. Experiments carried out in CASIA v4 interval and UBIRIS v1 show that the iris replacing technique made the original iris scrambled in such a way that the recognition algorithm failed to match the image with any other image in the database in all our comparisons. Hence, iris replacing technique can be considered as a potential iris obfuscation method to be used with the next generation consumer devices. Also, various

practical challenges in implementing such an obfuscation system in next generation devices were discussed.

Chapter 8

Conclusions and Future Work

8.1 Conclusions

In this dissertation, smartphone user authentication using iris recognition was studied. The aim of such a study was to provide a practical, well performing smartphone iris biometrics in consumer market.

Iris image acquisition on handheld devices was noted to introduce a challenging set of conditions: (i) uncontrolled illumination condition, (ii) limited processing power, (iii) optical constraints introduced by miniature camera modules, (iv) pixel resolution limited by optical and cost considerations, (v) an unstable hand-held platform introducing motion blur artefacts, and (vi) an unconstrained moving object - the human eye. Hence, adapting existing iris recognition technology to smartphones is challenging, not only due to the unconstrained nature of image acquisition, but also the usability constraints for the wider adoption of the solution by the end users. As a case study on the use of existing smartphone cameras for iris image acquisition, one of the state of the art, smartphone rear-facing camera was analysed. This analysis has shown that at least one model of contemporary smartphone is potentially capable of implementing visible wavelength iris authentication.

Further, evaluation of iris recognition techniques on a representative iris image database acquired using the existing smartphones were analysed. Images in this database were recorded in the visible wavelengths of the electromagnetic spectrum. Visible wavelength authentication was noted to be limited to a segment of the population with lightly-colored iris. While, imaging in NIR region improves identification in individuals with heavily pigmented irises. Also, NIR imaging makes the system robust to reflections and anomolous features related to change in pigmentation. From these analyses, it was observed that using the existing smartphones 'as is' for iris recognition is not an ideal solution, in terms of user convenience, recognition performance and interoperability with the existing systems.

Moreover, the feasibility of iris authentication in smartphones using a constraint-free acquisition workflow is explored. Various challenges that directly affect the design of such an iris recognition system- especially the acquisition device, were defined. The acquisition framework, associated workflows and key challenges in successfully implementing iris authentication in the unconstrained use case for handheld imaging devices were outlined. Initial experiments and analyses were carried out to determine the minimum spatial resolution, effect of defocus blur and motion blur in order to define key design criteria. Based on these analyses, various potential system design strategies were presented which laid a foundation for the design of a more reliable, unconstrained iris recognition system for next generation smartphones. This work- initially presented in the International Conference on Consumer Electronics - Berlin in September 2014- discussed two main design strategies (i) the use of a dedicated user facing NIR camera for iris recognition and (ii) introduce a hybrid RGB/NIR camera for both iris recognition and general purpose front camera application. The former design strategy has several advantages such as (i) the field of view (FoV) of the infrared iris imaging system can be reduced, increasing pixel resolution and image quality in the iris region; (ii) visible and infrared optical designs are independent, so that both can be optimized independently. The latter option is cost effective and easy to integrate in to the existing smartphone designs. The Mobile world congress (MWC) held in Barcelona on march 2015 witnessed industry adoption of the former design strategy.

Based on the discussions carried out, the use of a dual-purpose hybrid RGB/NIR front facing camera for smartphones is examined in detail. A proof-of-concept, smartphone form factor RGB/NIR hybrid camera system was developed and analyzed with the help of engineers from the industry partner. This hybrid device is of 4 Megapixel spatial resolution and combines the functionality of a conventional front-camera, such as selfie imaging and video call, with the potential for iris authentication. However, significant challenges in implementing such a system were noted such as: even for a close stand-off distance of 15cm, the optical properties of the system are marginal and pixel resolution for iris recognition is noted to be below the minimum threshold defined by the current international standards. Also, due to the novelty of the colour filter array in this visible/NIR sensor, the RGB image quality is likely to suffer when compared to a standard front facing camera with conventional Bayer pattern CFA. It is noted that the preliminary analysis have been limited by the current optical design which is not optimized for optical differences between visible and IR wavelengths. An improved design which accommodate the required optical resolution at both NIR and visible wavelengths and achieve a large iris pixel density across iris diameter is desired. We speculated that realizing these design goals may require a 6 or even 8 Megapixel sensor coupled with an advanced optical design. This study laid the foundation of the next

stage of smartphone iris recognition system which was presented by the industry partner in the Consumer Electronics Show (CES) 2016 in Las Vegas, USA.

Apart from the challenges in implementing a high performing, easy-to-use iris recognition system on smartphones, the wide spread use of such a technology faces some inherent challenges of iris recognition. Among these challenges, one of the most significant challenge is the security of the biometric system. As smartphone iris biometrics is a remote and unsupervised form of authentication, it is highly susceptible to spoofing attacks. Hence it is essential to check the liveness of the presented biometric sample on the sensor. A novel liveness detection that exploits the acquisition workflow for iris biometrics on smartphones using the proposed hybrid RGB/NIR camera was presented. The proposed technique is computationally light and does not require any additional hardware or significant change in the acquisition workflow, while providing a mean error rate of 0% in the tested scenarios.

Also, it is noted that imaging subsystem of smartphones are improving and some devices even use NIR information to enhance the color images. Hence, usable iris data can be extracted from these images, which signals a new problem for people who capture the images of themselves, their friends and family and share it in internet. This iris information could be used not only to identify the person and invade his privacy, but also to use his identity for spoofing attacks against iris recognition systems. We argue that a solution to prevent the misuse of iris information in these images is crucial for wider adoption of iris recognition on consumer devices such as smartphones. Such a solution- Iris pattern obfuscation is presented. Iris pattern obfuscation is the process of detecting and obscuring the iris pattern in digital photographs and videos, but without destroying the photo-realistic qualities of the eye regions. Five different techniques- vertical flipping, radial blurring, sector swapping, quadrant interchanging and iris replacing are presented and analysed. The iris replacing technique, in which the iris pattern of an image is replaced with the pattern of a standard gallery iris image, is found to be highly effective and recommended to be implemented within the camera before detailed iris data is transferred to permanent storage or transported over a network link. Also, various challenges in implementing such a solution are discussed.

8.2 Future Work

One of the most significant future work will be improving the performance of iris recognition system presented in Chapter 5. An improved design is being considered, which would allow more number or a greater density of NIR pixels, thus improving the quality of the acquired images. Design strategies such as sampling colour at a very sparse set of locations and

then propagating throughout the image with guidance from an unaliased monochrome NIR channel could possibly be adapted for this purpose.

Also, developing advanced demosaicing algorithms that minimizes the effects of noise introduced in the visible images due to the novelty of the colour filter array in the hybrid RGB/NIR sensor is a future research direction.

Another important aspect to address is the problems arising from low quality images typical of the less constrained scenarios. An overall quality assessment could be incorporated in the first steps of the iris recognition system. To achieve such it is necessary to adapt quality measures to the new imaging conditions. Motion blur occurrence is noted to be sensitive to recognition performance. Detecting and compensating motion blur in these devices may improve the system performance. Further research on that direction may lead to an improved iris recognition on smartphones.

References

- [1] Cambridge University Press, *Cambridge English Dictionary and Thesaurus*. 2015.
- [2] S. Curtis, “Smartphone at 20: IBM Simon to iPhone 6.” *The Telegraph*, 16 August 2014, <http://www.telegraph.co.uk/technology/mobile-phones/11037661/Smartphone-at-20-IBM-Simon-to-iPhone-6.html>. [Accessed: 29 October 2015].
- [3] H. Orman, “Did you want privacy with that?: Personal data protection in mobile devices,” *IEEE Internet Computing*, vol. 17, pp. 83–86, May 2013.
- [4] D. Siewiorek, “Generation smartphone,” *IEEE Spectrum*, vol. 49, pp. 54–58, Sep. 2012.
- [5] Pew Research Center, “The smartphone difference.” April 2015, <http://www.pewinternet.org/2015/04/01/us-smartphone-use-in-2015/>. [Accessed: 14 July 2015].
- [6] J. D. Sutter, “Smartphones : Our national obsession.” *CNN*, 18 October 2010, <http://edition.cnn.com/2010/TECH/mobile/10/18/smartphone.everywhere/>. [Accessed: 29 November 2015].
- [7] S. Curtis, “Quarter of the world will be using smartphones in 2016.” *The Telegraph*, 11 December 2014, <http://www.telegraph.co.uk/technology/mobile-phones/11287659/Quarter-of-the-world-will-be-using-smartphones-in-2016.html>. [Accessed: 13 March 2015].
- [8] S. Richmond, “Smartphones hardly used for calls.” *The Telegraph*, 29 June 2012, <http://www.telegraph.co.uk/technology/mobile-phones/9365085/Smartphones-hardly-used-for-calls.html>. [Accessed: 29 November 2015].
- [9] D. Goldman, “Your smartphone will run your life.” *CNN Money*, 19 October 2010, <http://money.cnn.com/2010/10/19/technology/smartphones/>. [Accessed: 29 November 2015].
- [10] ENISA, “Top ten smartphone risks.” *European Union Agency for Network and Information Security*, <https://www.enisa.europa.eu/activities/Resilience-and-CIIP/critical-applications/smartphone-security-1/top-ten-risks>. [Accessed: 13 March 2015].
- [11] A. J. Aviv, K. Gibson, E. Mossop, M. Blaze, and J. M. Smith, “Smudge attacks on smartphone touch screens,” in *Proceedings of the 4th USENIX Conference on Offensive Technologies*, 2010.

- [12] S. Griffiths, “Beware, your lock screen passcode probably isn’t very secure: 75% of us start secret patterns from a corner, study reveals.” *MailOnline, The Daily Mail*, 24 August 2015, <http://goo.gl/dM3Vjq>. [Accessed: 29 November 2015].
- [13] D. Gross, “Three of 10 smartphone owners don’t use passwords.” *CNN*, 26 February 2013, <http://edition.cnn.com/2013/02/26/tech/mobile/smartphones-passwords-mcafee/>. [Accessed: 29 November 2015].
- [14] N. sultana, “The question: when will biometrics take over from passwords.” *The Guardian*, 13 April 2015, <http://www.theguardian.com/technology/2015/apr/13/biometrics-take-over-passwords-security-iphone>. [Accessed: 29 November 2015].
- [15] S. Prabhakar, S. Pankanti, and A. Jain, “Biometric recognition: security and privacy concerns,” *IEEE Security Privacy*, vol. 1, pp. 33–42, Mar 2003.
- [16] The Institute of Automation of the Chinese Academy of Sciences, “CASIA iris database.” <http://biometrics.idealtest.org/>.
- [17] J. Daugman, “How Iris Recognition Works,” *IEEE Transactions on Circuits and Systems for Video Technology*, vol. 14, pp. 21–30, Jan. 2004.
- [18] S. Fenker, E. Ortiz, and K. Bowyer, “Template aging phenomenon in iris recognition,” *IEEE Access*, vol. 1, pp. 266–274, 2013.
- [19] E. Ortiz and K. W. Bowyer, “Exploratory analysis of an operational iris recognition dataset from a CBSA border-crossing application,” in *2015 IEEE Conference on Computer Vision and Pattern Recognition Workshops*, pp. 34–41, June 2015.
- [20] K. W. Bowyer and E. Ortiz, “Critical examination of the IREX VI results,” *IET Biometrics*, vol. 4, no. 4, pp. 192–199, 2015.
- [21] I. Hickson, “Ian Hickson’s description of the eye.” <http://academia.hixie.ch/bath/eye/home.html>. [Accessed: 10 December 2015].
- [22] K. Irsch and D. L. Guyton, “Anatomy of eyes,” *Encyclopedia of Biometrics*, pp. 11–16, 2009.
- [23] J. Daugman, “Anatomy and physiology of the iris.” <http://www.cl.cam.ac.uk/~jgd1000/anatomy.html>. [Accessed: 19 November 2015].
- [24] S. Standring, *Gray’s Anatomy: The Anatomical Basis of Clinical Practice*. 41st Edition, Elsevier, 2016.
- [25] K. Hollingsworth, K. W. Bowyer, S. Lagree, S. P. Fenker, and P. J. Flynn, “Genetically identical irises have texture similarity that is not detected by iris biometrics,” *Computer Vision and Image Understanding*, vol. 115, no. 11, pp. 1493 – 1502, 2011.
- [26] A. S. Leonard Flom, “Iris recognition system,” 1985. US Patent 4641349 A.
- [27] J. G. Daugman, “Biometric personal identification system based on iris analysis,” 1994. US Patent 5291560 A.

- [28] K. W. Bowyer, "Iris recognition: From basics to research frontiers." www.cse.nd.edu/~kwb/.
- [29] J. Daugman, "Probing the uniqueness and randomness of iriscodes: Results from 200 billion iris pair comparisons," *Proceedings of the IEEE*, vol. 94, no. 11, pp. 1927–1935, 2006.
- [30] J. Matey, O. Naroditsky, K. Hanna, R. Kolczynski, D. LoIacono, S. Mangru, M. Tinker, T. Zappia, and W. Zhao, "Iris on the Move: Acquisition of Images for Iris Recognition in Less Constrained Environments," *Proceedings of the IEEE*, vol. 94, 2006.
- [31] J. Daugman, "600 million citizens of India are now enrolled with with biometric ID," *SPIE newsroom*, vol. 7, 2014.
- [32] M. D. Marsico, M. Nappi, D. Riccio, and H. Wechsler, "Mobile iris challenge evaluation (MICHE)-I, biometric iris dataset and protocols," *Pattern Recognition Letters*, vol. 57, pp. 17 – 23, 2015.
- [33] A. Martin, "NTT Docomo takes another step into a future without passwords." *Wall Street Journal, Japan*, 26 May 2015, <http://blogs.wsj.com/japanrealtime/2015/05/26/ntt-docomo-takes-another-step-into-a-future-without-passwords/>. [Accessed: 12 November 2015].
- [34] C. Boyce, A. Ross, M. Monaco, L. Hornak, and X. Li, "Multispectral iris analysis: A preliminary study51," in *Computer Vision and Pattern Recognition Biometric Workshop*, pp. 51–51, Jun. 2006.
- [35] R. Wildes, J. Asmuth, G. Green, S. Hsu, R. Kolczynski, J. Matey, and S. McBride, "A system for automated iris recognition," in *Proceedings of the Second IEEE Workshop on Applications of Computer Vision*, pp. 121–128, 1994.
- [36] W.-K. Kong and D. Zhang, "Accurate iris segmentation based on novel reflection and eyelash detection model," in *roceedings of the International Symposium on Intelligent Multimedia, Video and Speech Processing*, pp. 263–266, 2001.
- [37] C.-L. Tisse, L. Martin, L. Torres, and M. Robert, "Person identification technique using human iris recognition," in *Proc. of Vision Interface*, pp. 294–299, 2002.
- [38] L. Ma, Y. Wang, and T. Tan, "Iris recognition using circular symmetric filters," in *Proceedings of the International Conference on Pattern Recognition*, vol. 2, pp. 414–417 vol.2, 2002.
- [39] Z. He, T. Tan, Z. Sun, and X. Qiu, "Toward accurate and fast iris segmentation for iris biometrics," *Pattern Analysis and Machine Intelligence, IEEE Transactions on*, vol. 31, no. 9, pp. 1670–1684, 2009.
- [40] J. Daugman, "New methods in iris recognition," *IEEE Transactions on Systems, Man, and Cybernetics, Part B: Cybernetics*, vol. 37, no. 5, pp. 1167–1175, 2007.
- [41] S. Shah and A. Ross, "Iris segmentation using geodesic active contours," *IEEE Transactions on Information Forensics and Security*, vol. 4, no. 4, pp. 824–836, 2009.

- [42] W. Boles and B. Boashash, "A human identification technique using images of the iris and wavelet transform," *IEEE Transactions on Signal Processing*, vol. 46, no. 4, pp. 1185–1188, 1998.
- [43] S. Lim, K. Lee, O. Byeon, and T. Kim, "Efficient iris recognition through improvement of feature vector and classifier," *ETRI Journal*, vol. 23, no. 2, pp. 61–70, 2001.
- [44] B. Vijaya Kumar, C. Xie, and J. Thornton, "Iris verification using correlation filters," in *Audio- and Video-Based Biometric Person Authentication* (J. Kittler and M. Nixon, eds.), vol. 2688 of *Lecture Notes in Computer Science*, pp. 697–705, Springer Berlin Heidelberg, 2003.
- [45] S. Orandi and R. M. McCabe, "Mobile ID Device Best Practice Recommendation," *Information Access Division Information Technology Laboratory NIST*, Aug. 2009.
- [46] P. Corcoran, "Biometrics and Consumer Electronics: A Brave New World or the Road to Dystopia?," *IEEE Consumer Electronics Magazine*, vol. 2, pp. 22–33, Apr. 2013.
- [47] N. L. Clarke and S. M. Furnell, "Authentication of users on mobile telephones - A survey of attitudes and practices," *Computers and Security*, vol. 24, no. 7, pp. 519–527, 2005.
- [48] S. Trewin, C. Swart, L. Koved, J. Martino, K. Singh, and S. Ben-David, "Biometric authentication on a mobile device: A study of user effort, error and task disruption," in *Proceedings of the 28th Annual Computer Security Applications Conference*, pp. 159–168, ACM, 2012.
- [49] "Strong mobile passwords with yubikey USB token." *The Guardian Project*, <https://guardianproject.info/2012/01/04/strong-mobile-passwords-with-yubikey-usb-token/>. [Accessed: 24 November 2015].
- [50] S. Giarimi and H. Magnusson, *Investigation of user acceptance for biometric verification/identification methods in mobile units*. Department of Computer Systems Sciences, Stockholm University, Sweden, 2002.
- [51] N. Zirjawi, Z. Kurtanovic, and W. Maalej, "A survey about user requirements for biometric authentication on smartphones," in *2015 IEEE 2nd Workshop on Evolving Security and Privacy Requirements Engineering*, pp. 1–6, Aug 2015.
- [52] National Science and Technology Councils (NSTC) Subcommittee on Biometrics, "Biometrics frequently asked questions." <http://biometrics.gov/Documents/FAQ.pdf>. [Accessed: 24 November 2015].
- [53] B. Toth, "Liveness detection: Iris," *Encyclopedia of Biometrics*, pp. 931–938, 2009.
- [54] R. Rakvic, R. Broussard, L. Kennell, R. Ives, and R. Bell, "Iris acquisition device," *Encyclopedia of Biometrics*, pp. 761–769, 2009.
- [55] E. Tabassi, P. Grother, and W. Salamon, "IREX II-IQCE iris quality calibration and evaluation," *NIST Interagency report*, vol. 7820.

- [56] Working Group 3, “ISO/IEC 19794-6 Information Technology - Biometric Data Interchange Formats - Part 6: Iris image,” *JTC1 :: SC37, international standard edition*, 2005.
- [57] Working Group 3, “ISO/IEC 19794-6 Information Technology - Biometric Data Interchange Formats - Part 6: Iris image,” *JTC1 :: SC37, international standard edition*, vol. 44, no. 0, 2011.
- [58] Y. H. Li and M. Savvides, “Iris recognition, overview,” *Encyclopedia of Biometrics*, pp. 842–850, 2009.
- [59] K. W. Bowyer, K. Hollingsworth, and P. J. Flynn, “Image understanding for iris biometrics: A survey,” *Computer Vision and Image Understanding*, vol. 110, pp. 281–307, 2008.
- [60] J. Matey and L. Kennell, “Iris recognition – beyond one meter,” in *Handbook of Remote Biometrics* (M. Tistarelli, S. Li, and R. Chellappa, eds.), Advances in Pattern Recognition, pp. 23–59, Springer London, 2009.
- [61] K. Bowyer, K. Hollingsworth, and P. Flynn, “A survey of iris biometrics research: 2008–2010,” in *Handbook of Iris Recognition* (M. J. Burge and K. W. Bowyer, eds.), Advances in Computer Vision and Pattern Recognition, pp. 15–54, Springer London, 2013.
- [62] S. Z. Li, *Encyclopedia of Biometrics*, vol. 1. Springer Science & Business Media, 2015.
- [63] D. H. Cho, K. R. Park, and D. W. Rhee, “Real-time iris localization for iris recognition in cellular phone,” in *Sixth International Conference on Software Engineering, Artificial Intelligence, Networking and Parallel/Distributed Computing, 2005 and First ACIS International Workshop on Self-Assembling Wireless Networks. SNPD/SAWN 2005.*, pp. 254–259, May 2005.
- [64] Samsung, “Samsung SPH 2300.” http://samsung_moviles.index.es/subpaginas.php?title=Samsung+SPH-S2300&a=522. [Accessed: 10 December 2015].
- [65] D. ho Cho, K. R. Park, D. W. Rhee, Y. Kim, and J. Yang, “Pupil and iris localization for iris recognition in mobile phones,” in *Seventh ACIS International Conference on Software Engineering, Artificial Intelligence, Networking, and Parallel/Distributed Computing*, pp. 197–201, Jun. 2006.
- [66] D. Jeong, H.-A. Park, K. Park, and J. Kim, “Iris recognition in mobile phone based on adaptive gabor filter,” in *Advances in Biometrics* (D. Zhang and A. Jain, eds.), vol. 3832 of *Lecture Notes in Computer Science*, pp. 457–463, Springer Berlin Heidelberg, 2005.
- [67] K. Park, H.-A. Park, B. Kang, E. Lee, and D. Jeong, “A study on iris localization and recognition on mobile phones,” *EURASIP Journal on Advances in Signal Processing*, vol. 2008, no. 1, p. 281943, 2008.

- [68] K. M. Cheung, "OKI develops iris recognition for camera phones." *Reviewed.com*, Nov 2006. <http://cameras.reviewed.com/news/oki-develops-iris-recognition-for-camera-phones>. [Accessed: 24 November 2015].
- [69] S. Kurkovsky, T. Carpenter, and C. MacDonald, "Experiments with simple iris recognition for mobile phones," in *Information Technology: New Generations (ITNG), 2010 Seventh International Conference on*, pp. 1293–1294, Apr. 2010.
- [70] J.-S. Kang, "Mobile iris recognition systems: An emerging biometric technology," *Procedia Computer Science*, vol. 1, no. 1, pp. 475–484, 2010.
- [71] C. R. C. Huiqi Lu and R. C. Young, "Iris recognition on low computational power mobile devices," *Biometrics - Unique and Diverse Applications in Nature, Science, and Technology*, 2011.
- [72] L. Franceschi-Bicchierai, "How to turn your phone into a biometric scanning machine." *CNN*, April 16, 2013, <http://edition.cnn.com/2013/04/16/tech/mobile/mashable-biometric-iphone-scanner/>. [Accessed: 24 November 2015].
- [73] "Iris on mobile solution." <http://www.iritech.com/products/solutions/iris-mobile-solution>. [Accessed: 24 November 2015].
- [74] "Fujitsu develops prototype smartphone with iris authentication." *Fujitsu Press Release*, March 02, 2015, <http://www.fujitsu.com/global/about/resources/news/press-releases/2015/0302-03.html>. [Accessed: 24 November 2015].
- [75] "Delta id powers iris recognition in NTT DOCOMO and fujitsu's ARROWS NX F-04G, world's first smartphone with iris recognition." *DeltaID Press Release*, May 28, 2015, <http://www.deltaid.com/news.php>. [Accessed: 24 November 2015].
- [76] E. Allen and S. Triantaphillidou, *The manual of photography*. Taylor & Francis, 2011.
- [77] N. A. Dodgson, "Variation and extrema of human interpupillary distance," in *Proc. SPIE 5291*, pp. 36–46, 2004.
- [78] D. Ackerman, "Spatial Resolution as an Iris Quality Metric." Presented at Biometrics Consortium Conference Tampa, Florida September 28, 2011.
- [79] W. J. Smith, *Modern Optical Engineering - Third Edition*. McGraw-Hill, 2000.
- [80] J. Nakamura, "Modern Image Sensors," in *Smart Mini-Cameras* (T. V. Galstian, ed.), pp. 49–82, CRC Press, 2014.
- [81] A. Ross, R. Pasula, and L. Hornak, "Exploring multispectral iris recognition beyond 900nm," in *IEEE 3rd International Conference on Biometrics: Theory, Applications, and Systems*, pp. 1–8, Sept 2009.
- [82] H. Proença and L. A. Alexandre, "Iris segmentation methodology for non-cooperative recognition," in *IEE Proceedings- Vision, Image and Signal Processing*, vol. 153, pp. 199–205, IET, 2006.

- [83] H. Proença, “Iris recognition: A method to segment visible wavelength iris images acquired on-the-move and at-a-distance,” in *Advances in Visual Computing*, pp. 731–742, Springer, 2008.
- [84] H. Proença, “On the feasibility of the visible wavelength, at-a-distance and on-the-move iris recognition,” *IEEE Workshop on Computational Intelligence in Biometrics: Theory, Algorithms, and Applications*, 2009.
- [85] R. R. Jillela and A. Ross, “Segmenting iris images in the visible spectrum with applications in mobile biometrics,” *Pattern Recognition Letters*, no. 0, pp. –, 2014.
- [86] K. Raja, R. Raghavendra, and C. Busch, “Smartphone based robust iris recognition in visible spectrum using clustered k-means features,” in *Biometric Measurements and Systems for Security and Medical Applications (BIOMS) Proceedings, 2014 IEEE Workshop on*, pp. 15–21, Oct 2014.
- [87] K. B. Raja, R. Raghavendra, V. K. Vemuri, and C. Busch, “Smartphone based visible iris recognition using deep sparse filtering,” *Pattern Recognition Letters*, no. 0, pp. –, 2014.
- [88] M. D. Marsico, M. Nappi, and H. Proença, “Guest editorial introduction to the special executable issue on Mobile Iris CHallenge Evaluation part I (MICHE I),” *Pattern Recognition Letters*, vol. 57, pp. 1–3, 2015.
- [89] C. Rathgeb, A. Uhl, and P. Wild, *Iris Recognition: From Segmentation to Template Security*. *Advances in Information Security* 59. Springer, 2012.
- [90] R. Raghavendra, K. Raja, B. Yang, and C. Busch, “Combining iris and periocular recognition using light field camera,” in *2013 2nd IAPR Asian Conference on Pattern Recognition*, pp. 155–159, Nov 2013.
- [91] D. M. Monro, S. Rakshit, and D. Zhang, “DCT-based iris recognition,” *IEEE Transactions on Pattern Analysis and Machine Intelligence*, vol. 29, pp. 586–595, Apr. 2007.
- [92] L. Masek and P. Kovesi, *Computationally Efficient Feature Extraction and Matching Iris Recognition*. The School of Computer Science and Software Engineering, The University of Western Australia, 2003.
- [93] L. Ma, T. Tan, Y. Wang, and D. Zhang, “Personal identification based on iris texture analysis,” *IEEE Transactions on Pattern Analysis and Machine Intelligence*, vol. 25, pp. 1519–1533, Dec 2003.
- [94] J.-G. Ko, Y.-H. Gil, J.-H. Yoo, and K.-I. Chung, “A novel and efficient feature extraction method for iris recognition,” *ETRI journal*, vol. 29, no. 3, pp. 399–401, 2007.
- [95] C. Rathgeb and A. Uhl, “Secure iris recognition based on local intensity variations,” in *Image Analysis and Recognition (A. Campilho and M. Kamel, eds.)*, vol. 6112 of *Lecture Notes in Computer Science*, pp. 266–275, Springer Berlin Heidelberg, 2010.

- [96] C. Rathgeb and A. Uhl, "Context-based biometric key generation for iris," *IET Computer Vision*, vol. 5, pp. 389–397, November 2011.
- [97] P. Grother, E. Tabassi, G. Quinn, and W. Salamon, "IREX III performance of iris identification algorithms," *NIST Interagency Report*, vol. 7836, pp. 1–120, 2012.
- [98] Y. Wang, K. Streff, and S. Raman, "Smartphone security challenges," *Computer*, vol. 45, pp. 52–58, Dec 2012.
- [99] K. N. Smith, V. P. Pauca, A. Ross, T. Torgersen, and M. C. King, "Extended evaluation of simulated wavefront coding technology in iris recognition," in *International Conference on Biometrics: Theory, Applications, and Systems.*, pp. 1–7, 2007.
- [100] V. Dorairaj, N. Schmid, and G. Fahmy, "Performance evaluation of non-ideal iris based recognition system implementing global ica encoding," in *IEEE International Conference on Image Processing, 2005*, vol. 3, pp. III–285–8, Sept 2005.
- [101] S. Schuckers, N. Schmid, A. Abhyankar, V. Dorairaj, C. Boyce, and L. Hornak, "On techniques for angle compensation in nonideal iris recognition," *IEEE Transactions on Systems, Man, and Cybernetics, Part B: Cybernetics.*, vol. 37, pp. 1176–1190, Oct 2007.
- [102] M. Karakaya, D. Barstow, H. Santos-Villalobos, J. Thompson, D. Bolme, and C. Boehnen, "Gaze estimation for off-angle iris recognition based on the biometric eye model," vol. 8712, pp. 87120F–87120F–9, 2013.
- [103] P. Lee and H. Ewe, "Individual recognition based on human iris using fractal dimension approach," in *Biometric Authentication* (D. Zhang and A. Jain, eds.), vol. 3072 of *Lecture Notes in Computer Science*, pp. 467–474, Springer Berlin Heidelberg, 2004.
- [104] N. Othman, B. Dorizzi, and S. Garcia-Salicetti, "Osiris: An open source iris recognition software," *Pattern Recognition Letters*, pp. –, 2015.
- [105] R. Wildes, J. Asmuth, K. Hanna, S. Hsu, R. Kolczynski, J. Matey, and S. McBride, "Automated, non-invasive iris recognition system and method," Nov. 5 1996. US Patent 5,572,596.
- [106] J. Cambier and J. Siedlarz, "Portable authentication device and method using iris patterns," Mar. 11 2003. US Patent 6,532,298.
- [107] P. Radu, K. Sirlantzis, G. Howells, S. Hoque, and F. Deravi, "Are two eyes better than one? an experimental investigation on dual iris recognition," in *Emerging Security Technologies (EST), 2010 International Conference on*, pp. 7–12, Sept 2010.
- [108] A. Gelb and J. Clark, "Performance lessons from India's universal identification program," tech. rep., 2013.
- [109] D. Kim, H. Choi, B. Jun, M. OH, and Y. Youn, "Iris recognition combination camera having regular image capturing and iris recognition capturing modes," Jan. 23 2014. WO Patent App. PCT/KR2012/006,051.

- [110] P. Bigioi, C. Zaharia, and P. Corcoran, "Advanced hardware real time face detector," in *IEEE International Conference on Consumer Electronics.*, pp. 528–529, Jan 2012.
- [111] P. Corcoran, F. Nanu, S. Petrescu, and P. Bigioi, "Real-time eye gaze tracking for gaming design and consumer electronics systems," *IEEE Transactions on Consumer Electronics*, vol. 58, pp. 347–355, May 2012.
- [112] F. Nanu, S. Petrescu, P. Corcoran, and P. Bigioi, "Face and gaze tracking as input methods for gaming design," in *International Games Innovation Conference*, pp. 115–116, Nov 2011.
- [113] F. Nanu, C. Stan, and P. Corcoran, "Continuous autofocus based on face detection and tracking," Mar. 29 2012. US Patent App. 12/959,320.
- [114] M. Yang, Y. Wu, J. Crenshaw, B. Augustine, and R. Mareachen, "Face detection for automatic exposure control in handheld camera," in *IEEE International Conference on Computer Vision Systems*, pp. 17–17, IEEE, 2006.
- [115] M. Vatsa, R. Singh, and A. Noore, "Improving iris recognition performance using segmentation, quality enhancement, match score fusion, and indexing," *IEEE Transactions on Systems, Man, and Cybernetics, Part B: Cybernetics*, vol. 38, pp. 1021–1035, Aug 2008.
- [116] J. Daugman, "New methods in iris recognition," *IEEE Transactions on Systems, Man, and Cybernetics, Part B: Cybernetics*, vol. 37, pp. 1167–1175, Oct 2007.
- [117] S. Shah and A. Ross, "Iris segmentation using geodesic active contours," *IEEE Transactions on Information Forensics and Security*, vol. 4, pp. 824–836, Dec 2009.
- [118] H. Proença, *Towards non-cooperative biometric iris recognition*. University of Beira Interior, Portugal, 2006.
- [119] K. Hollingsworth, *Increased use of available image data decreases errors in iris biometrics*. University of Notre Dame, USA, 2010.
- [120] M. Savvides, K. Harun, V. Bhagavatula, S. Park, and Y. Li, "Computationally efficient feature extraction and matching iris recognition," Jan. 21 2010. US Patent App. 12/426,210.
- [121] C. Rathgeb and A. Uhl, "A survey on biometric cryptosystems and cancelable biometrics," *EURASIP Journal on Information Security*, vol. 2011, no. 1, 2011.
- [122] K. Xi and J. Hu, "Biometric mobile template protection: A composite feature based fingerprint fuzzy vault," in *IEEE International Conference on Communications, 2009.*, pp. 1–5, Jun. 2009.
- [123] Y. Lu, M. Higgins-Luthman, W. Livengood, and J. Harris, "Combined rgb and ir imaging sensor," 2013. US Patent 8,446,470.
- [124] OmniVision, "OmniVision's OV4682." http://www.ovt.com/download_document.php?type=sensor&sensorid=145.

- [125] B. E. Bayer, "Color imaging array," 1975. US Patent 3,971,065.
- [126] Z. Sadeghipoor, Y. Lu, and S. Susstrunk, "A novel compressive sensing approach to simultaneously acquire color and near-infrared images on a single sensor," in *2013 IEEE International Conference on Acoustics, Speech and Signal Processing.*, pp. 1646–1650, May 2013.
- [127] S. Petrescu, P. Corcoran, E. Steinberg, P. Bigioi, and A. Drimborean, "Real-time face tracking in a digital image acquisition device.," Aug. 29 2006. US7469055 B2.
- [128] R. Ramanath, W. Snyder, Y. Yoo, and M. Drew, "Color image processing pipeline," *IEEE Signal Processing Magazine*, vol. 22, pp. 34–43, Jan 2005.
- [129] P. Corcoran, P. Bigioi, and S. Thavalengal, "Feasibility and design considerations for an iris acquisition system for smartphones," in *IEEE Fourth International Conference on Consumer Electronics-Berlin*, pp. 164–167, Sept 2014.
- [130] N. Koren, "The imatest program: comparing cameras with different amounts of sharpening," vol. 6069, pp. 60690L–60690L–9, 2006.
- [131] G. Sutra, B. D. e. S. Garcia-salicetti, and N. Othman, "A biometric reference system for iris," tech. rep., 2012.
- [132] Neurotechnology, "NeuroTechnology VeriEye SDK," 2015.
- [133] Multimedia University, "MMU iris database." <http://pesona.mmu.edu.my/ccteo>.
- [134] A. Kumar and A. Passi, "Comparison and combination of iris matchers for reliable personal authentication," *Pattern Recognition*, vol. 43, no. 3, pp. 1016 – 1026, 2010.
- [135] A. Chakrabarti, W. Freeman, and T. Zickler, "Rethinking color cameras," in *IEEE International Conference on Computational Photography*, pp. 1–8, May 2014.
- [136] D. Endres and J. Schindelin, "A new metric for probability distributions," *IEEE Transactions on Information Theory*, vol. 49, pp. 1858–1860, Jul. 2003.
- [137] A. Czajka, "Pupil dynamics for iris liveness detection," *IEEE Transactions on Information Forensics and Security*, vol. 10, pp. 726–735, Apr. 2015.
- [138] K. Raja, R. Raghavendra, and C. Busch, "Video presentation attack detection in visible spectrum iris recognition using magnified phase information," *IEEE Transactions on Information Forensics and Security*, vol. 10, pp. 2048–2056, Oct 2015.
- [139] Z. Akhtar, C. Micheloni, and G. Foresti, "Biometric liveness detection: Challenges and research opportunities," *IEEE Security Privacy*, vol. 13, pp. 63–72, Sept 2015.
- [140] I. Bacivarov, M. Ionita, and P. Corcoran, "Statistical models of appearance for eye tracking and eye-blink detection and measurement," *IEEE Transactions on Consumer Electronics*, vol. 54, pp. 1312–1320, Aug. 2008.
- [141] D. A. Forsyth and J. Ponce, *Computer Vision: A Modern Approach*. Prentice Hall Professional Technical Reference, 2002.

- [142] E. Steinberg, P. Corcoran, A. V. Smith, B. M. Mehta, and M. Seth, "Digital image processing composition using face detection information," Jan. 8 2008. US Patent 7,317,815.
- [143] Working Group 3, "ISO/IEC 30107-3 Information Technology - Biometrics - Presentation Attack Detection - Part3," *JTC1 :: SC37, international standard edition*, vol. 1, no. 0, 2014.
- [144] A. Sao, B. Yegnanarayana, and B. Vijaya Kumar, "Significance of image representation for face verification," *Signal, Image and Video Processing*, vol. 1, no. 3, pp. 225–237, 2007.
- [145] S. Mandal, S. Thavalengal, and A. Sao, "Explicit and implicit employment of edge-related information in super-resolving distant faces for recognition," *Pattern Analysis and Applications*, pp. 1–18, 2015.
- [146] T. Shejin and A. Sao, "Significance of dictionary for sparse coding based face recognition," in *Proceedings of the International Conference of the Biometrics Special Interest Group (BIOSIG)*, pp. 1–6, Sept 2012.
- [147] S. Thavalengal, P. Bigioi, and P. Corcoran, "Evaluation of combined visible/nir camera for iris authentication on smartphones," in *The IEEE Conference on Computer Vision and Pattern Recognition (CVPR) Workshops*, Jun. 2015.
- [148] T. N. Cornsweet and H. D. Crane, "Accurate two-dimensional eye tracker using first and fourth purkinje images," *Journal of the Optical Society of America*, vol. 63, pp. 921–928, Aug 1973.
- [149] E. Lee, K. Park, and J. Kim, "Fake iris detection by using purkinje image," in *Advances in Biometrics* (D. Zhang and A. Jain, eds.), vol. 3832 of *Lecture Notes in Computer Science*, pp. 397–403, Springer Berlin Heidelberg, 2005.
- [150] P. Corcoran, P. Bigioi, and F. Nanu, "Detection and repair of flash-eye in handheld devices," in *2014 IEEE International Conference on Consumer Electronics*, pp. 213–216, Jan 2014.
- [151] C. Bishop, *Pattern Recognition and Machine Learning*. Springer Information Science and Statistics, 2006.
- [152] N. Ratha, J. Connell, and R. Bolle, "Enhancing security and privacy in biometrics-based authentication systems," *IBM Systems Journal*, vol. 40, no. 3, pp. 614–634, 2001.
- [153] J. Zuo, N. Ratha, and J. Connell, "Cancelable iris biometric," in *19th International Conference on Pattern Recognition, 2008.*, pp. 1–4, Dec 2008.
- [154] S. Venugopalan and M. Savvides, "How to generate spoofed irises from an iris code template," *IEEE Transactions on Information Forensics and Security*, vol. 6, no. 2, pp. 385–395, 2011.

- [155] J. Galbally, A. Ross, M. Gomez-Barrero, J. Fierrez, and J. Ortega-Garcia, "Iris image reconstruction from binary templates: An efficient probabilistic approach based on genetic algorithms," *Computer Vision and Image Understanding*, vol. 117, pp. 1512–1525, Oct. 2013.
- [156] P. Gallagher, "Smart-Phones Get Even Smarter Cameras [Future Visions]," *IEEE Consumer Electronics Magazine*, vol. 1, pp. 25–30, Jan. 2012.
- [157] G. Ward, "High dynamic range imaging," in *Color and Imaging Conference*, vol. 2001, pp. 9–16, Society for Imaging Science and Technology, 2001.
- [158] K. Hirakawa and P. M. Simon, "Single-shot high dynamic range imaging with conventional camera hardware," *International Conference on Computer Vision*, pp. 1339–1346, 2011.
- [159] Y. Bando, G. Qiu, M. Okuda, S. Daly, T. Aach, and O. C. Au, "Recent advances in high dynamic range imaging technology," in *17th IEEE International Conference on Image Processing*, pp. 3125–3128, IEEE, 2010.
- [160] S. Nayar and T. Mitsunaga, "High dynamic range imaging: spatially varying pixel exposures," in *Proceedings IEEE Conference on Computer Vision and Pattern Recognition*, vol. 1, pp. 472–479, 2000.
- [161] R. Mantiuk, G. Krawczyk, R. Mantiuk, and H.-P. Seidel, "High Dynamic Range Imaging Pipeline: Perception-Motivated Representation of Visual Content," in *Human Vision and Electronic Imaging XII*, vol. 6492, p. 649212, 2007.
- [162] X. Zhang, T. Sim, and X. Miao, "Enhancing photographs with near infra-red images," in *IEEE Conference on Computer Vision and Pattern Recognition, 2008.*, pp. 1–8, Jun. 2008.
- [163] Y. Lu, C. Fredembach, M. Vetterli, and S. Susstrunk, "Designing color filter arrays for the joint capture of visible and near-infrared images," in *16th IEEE International Conference on Image Processing (ICIP), 2009.*, pp. 3797–3800, Nov 2009.
- [164] C. Newman, "A Life Revealed." *National Geographic Magazine*, April 2002, <http://ngm.nationalgeographic.com/2002/04/afghan-girl/>. [Accessed: 14 July 2015].
- [165] J. Daugman, "How the Afghan Girl was Identified by Her Iris Patterns." <http://www.cl.cam.ac.uk/~jgd1000/afghan.html>. [Accessed: 14 July 2015].
- [166] H. Adam, H. Neven, and J. B. Steffens, "Image based multi-biometric system and method," Apr. 13 2010. US Patent 7,697,735.
- [167] T. Vuori, J. Alakarhu, E. Salmelin, and A. Partinen, "Nokia pureview oversampling technology," in *IS&T/SPIE Electronic Imaging*, pp. 86671C–86671C, International Society for Optics and Photonics, 2013.
- [168] G. Petschnigg, R. Szeliski, M. Agrawala, M. Cohen, H. Hoppe, and K. Toyama, "Digital photography with flash and no-flash image pairs," *ACM Transactions on Graphics*, vol. 23, p. 664, Aug. 2004.

- [169] P. Corcoran, P. Bigioi, E. Steinberg, and A. Pososin, "Automated in-camera detection of flash-eye defects," *IEEE Transactions on Consumer Electronics*, vol. 51, pp. 11–17, Feb. 2005.
- [170] P. Corcoran, P. Bigioi, and F. Nanu, "Advances in the detection & repair of flash-eye defects in digital images-a review of recent patents," *Recent Patents on Electrical & Electronic Engineering*, 2012.
- [171] B. Shen, I. K. Sethi, and V. Bhaskaran, "Dct domain alpha blending," in *International Conference on Image Processing, 1998.*, vol. 1, pp. 857–861, IEEE, 1998.
- [172] L. Cardoso, A. Barbosa, F. Silva, A. M. Pinheiro, and H. Proenca, "Iris biometrics: Synthesis of degraded ocular images," *IEEE Transactions on Information Forensics and Security*, vol. 8, no. 7, pp. 1115–1125, 2013.
- [173] Z. Wei, T. Tan, and Z. Sun, "Synthesis of large realistic iris databases using patch-based sampling," in *International Conference on Pattern Recognition*, pp. 1–4, 2008.
- [174] A. Lefohn, B. Budge, P. Shirley, R. Caruso, and E. Reinhard, "An ocularist's approach to human iris synthesis," *IEEE Computer Graphics and Applications*, vol. 23, no. 6, pp. 70–75, 2003.
- [175] H. Proença and L. A. Alexandre, "UBIRIS: A noisy iris image database," in *International Conference on Image Analysis and Processing*, pp. 970–977, Springer, 2005.
- [176] "BIPLab database." University of Salerno, 2015. <http://biplab.unisa.it/MICHE/database/>.
- [177] P. M. Corcoran, P. Bigioi, and F. Nanu, "Advances in the detection, repair of flash-eye defects in digital images - a review of recent patents," *Recent Patents on Electrical Engineering*, vol. 5, no. 1, pp. 30–54, 2012.

Appendix A

Performance Metrics of Biometric Systems

The section gives a brief overview of various performance metrics used in this thesis.

A.1 Functions of a General Biometric Systems

A biometric system is essentially a pattern-recognition system that recognizing individuals based on their physiological or behavioral traits [15].

Every biometric system will be performing the task of user enrollment, which registers individuals into the biometric system database. Further, depending on the application, a biometric system will typically be operating in either a *verification* or in an *identification* mode. This is depicted in the block diagram shown in Figure A.1

A.2 Biometric Performance Metrics

The main performance metrics used in this thesis are true acceptance rate (TAR), false acceptance rate (FAR), False reject rate (FRR), receiver operating characteristics curve (ROC) and equal error rate (EER).

True Positives (TP): True positives are the outcomes of the biometric verification process when the system accept, or verify true identity claims.

False Positives (FP): False positives occur when the biometric verification system accept identity claims which are not true.

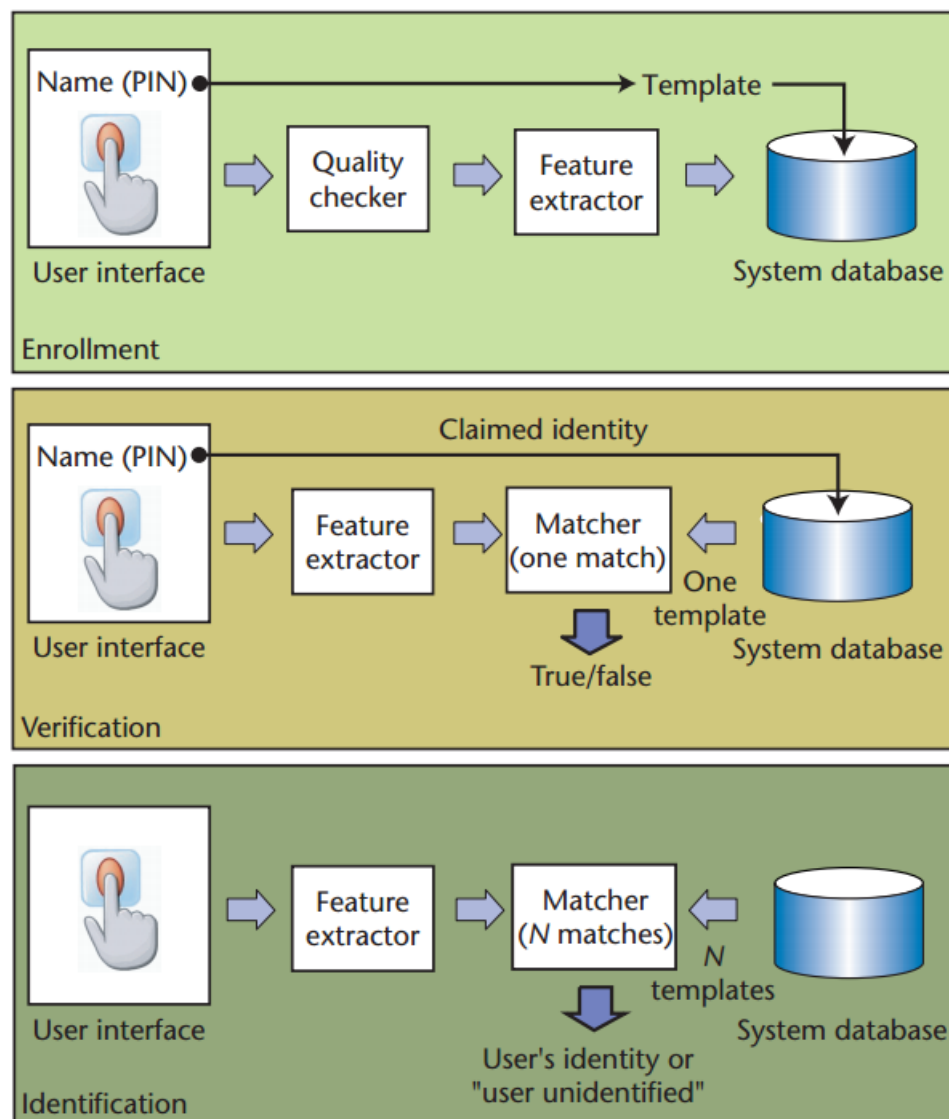


Fig. A.1 An overview of enrollment, verification, and identification tasks of a biometric system [15]. Copyright ©2003, IEEE

True Negatives (TN): When the biometric verification system reject identity claims and the claims are not true, the system outputs are called true negatives.

False Negatives (FN): False negatives occurs when the system reject true identity claims.

TP, FP, TN and FN are depicted in Figure A.2

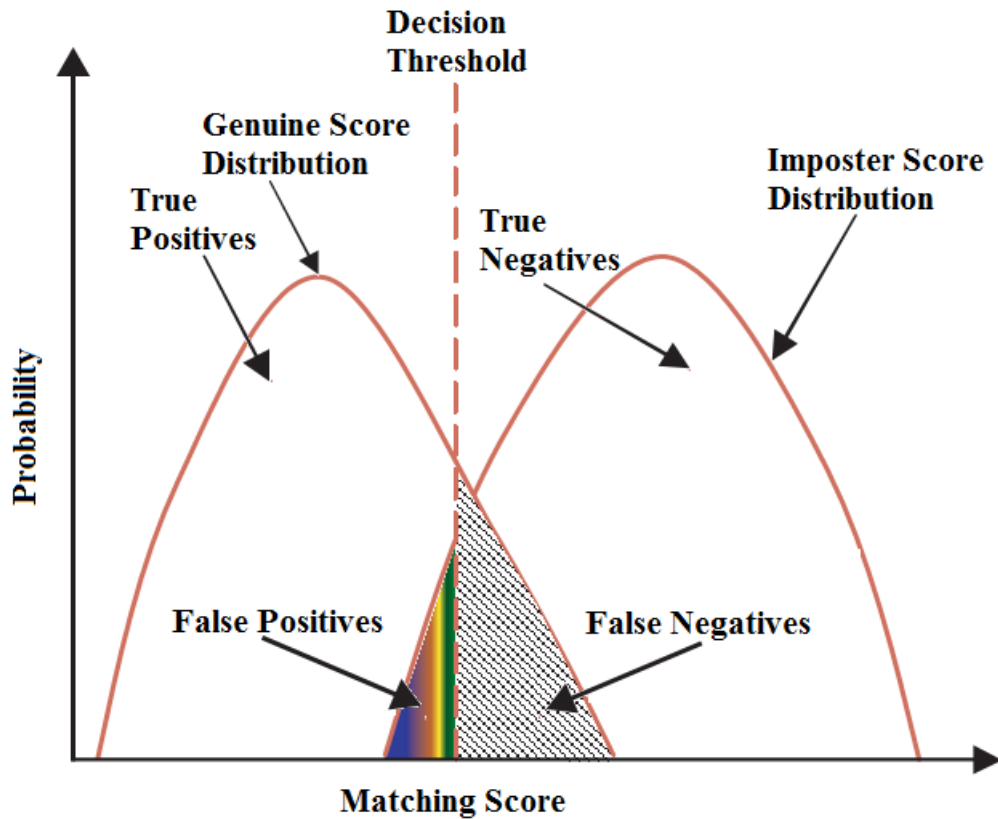


Fig. A.2 An overview of the outcome of a biometric verification system. Image is adapted from [15]. Copyright ©2003, IEEE

True Acceptance Rate (TAR): True acceptance rate, also known as *sensitivity* is the proportion of true positives to the total true claims. That is,

$$TAR = \frac{TP}{TP + FN} \quad (\text{A.1})$$

False Acceptance Rate (FAR): False acceptance rate, also is the proportion of false positives to the total false claims.

$$FAR = \frac{FP}{FP + TN} \quad (\text{A.2})$$

False Rejection Rate (FRR): False rejection rate can be defined as

$$FRR = 1 - TAR \quad (\text{A.3})$$

$$= \frac{FN}{FN + TN} \quad (\text{A.4})$$

Receiver Operating Characteristics curve (ROC): Receiver Operating Characteristics curve (ROC) is a graphical plot that illustrates the performance of the biometric authentication system as its decision threshold is varied. x-axis of the ROC represents FAR and y-axis represents TAR. An ROC can be depicted as in Figure A.3

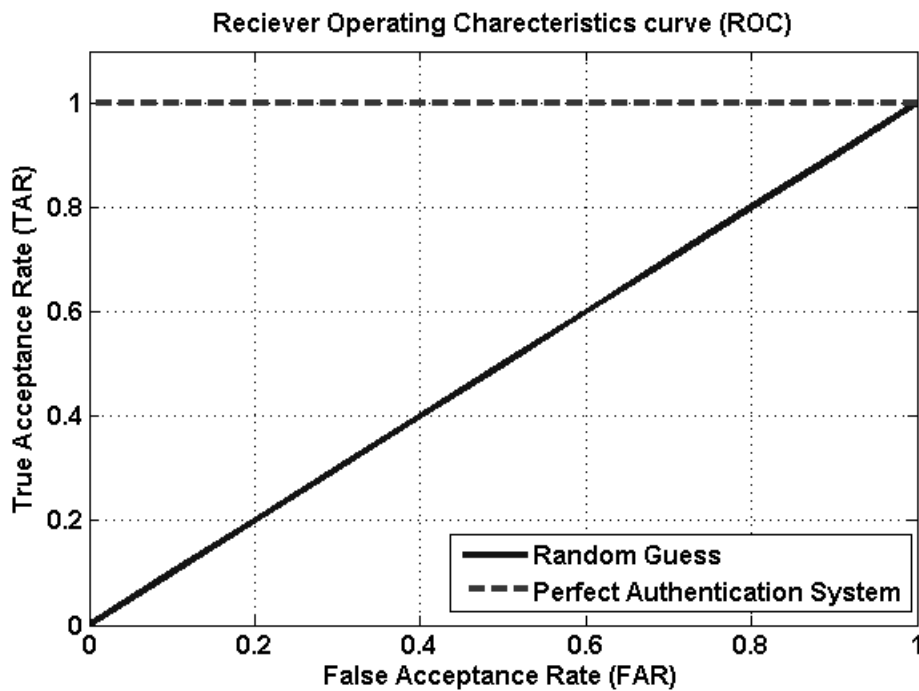


Fig. A.3 Receiver operating characteristics curve

Equal Error Rate (EER): Equal error rate (EER) is the rate at which FAR is equal to FRR. EER can be easily obtained from the ROC curves. The performance of two biometric verification systems can be compared by comparing their EER. The system with lowest EER is the better performing system.

A.3 Performance Evaluation of Liveness Detection System

The performance of a liveness detection system is measured based on two error rates:

Normal Presentation Classification Error Rate (NPCER): NPCER is the proportion of live users incorrectly classified as presentation attacks by the liveness detection system.

Attack Presentation Classification Error Rate (APCER): APCER is the proportion of presentation attacks incorrectly classified as live users.